AN ABSTRACT OF THE THESIS OF

Chang-Seop Ri for the degree of Doctor of Philosophy in Chemistry presented on November 28, 1990.

Title: Surface Structural Studies of The Titanium/Chlorine System.

Redacted for privacy

Abstracted approved: _____

Philip R. Watson

The atomic structure of the adsorption site involved in the $TiCl_3$-catalyzed Ziegler-Natta polymerization of olefin is still not known. In this thesis I have followed two approaches towards providing useful information for a better understanding of these sites.

The $TiCl_3$ single crystals, as an example of a real Ziegler-Natta catalyst, have been prepared in a gradient furnace specially designed for this study. They were then gold-plated in a vacuum deposition apparatus, especially designed for this purpose, to protect the crystal from moisture. The $TiCl_3$ crystal then was mounted in a special manner that can allow this friable crystal to be attached to the sample holder of the manipulator for the UHV studies. Auger spectra were taken for various conditions of the $TiCl_3$ to test this series of experimental

procedures. LEED experiments were also attempted to reveal the surface structure of $TiCl_3$ under the various experimental conditions.

The chlorine covered Ti(0001) surface was prepared as a model catalyst for the study of Ziegler-Natta catalysis. The Diffuse LEED technique for surface structural determination has been applied to this disordered, low coverage phase of Cl on Ti(0001). An in situ molecular chlorine source, which is a solid state electrochemical cell, was employed for dosing of chlorine for the first time in DLEED study. The diffuse scattering intensities have been measured by a TV-computer method using an image intensifier camera. The measured diffuse intensities were manipulated by a computer program developed for this study on a personal computer.

A detailed multiple scattering analysis was carried out using the DLEED program of Van Hove. The Pendry R-factor was used for theory-experiment comparison between the experimental data and model calculations. From an analysis of two sets of data, the favored adsorption sites as well as the bond lengths were derived. In addition, the relative occupation of the two favored adsorption sites was found.

Surface Structural Studies of The Titanium/Chlorine System

by

Chang-Seop Ri

A THESIS

submitted to

Oregon State University

in partial fulfillment of

the requirements for the

degree of

Doctor of Philosophy

Completed November 28, 1990

Commencement June 1991

APPROVED:

Redacted for privacy

Associate Professor of Chemistry in charge of major

Redacted for privacy

Chairman of Department of Chemistry

Redacted for privacy

Dean of Graduate School

Date thesis is presented November 28, 1990

Typed by researcher for Chang-Seop Ri

ACKNOWLEDGEMENT

I appreciate the kind help and guidances of my advisor, Prof. Philip R. Watson. Without his support and care, this work could not have been completed.

A number of people in my group helped me, physically or mentally, in the process of this research. I would like to thank John Mischenko III and Scott Mokler for their guidance, Glenn Tinseth and Valerie Marty for their help and kindness.

I also thank to my Korean friends, Hyunik Shin and Hoh-gyu Hahn, for their encouragement and friendship.

In addition, I dedicate this work to my mother and father to whom I owe everything. I do so in appreciation of their countless love for me.

Finally, I thank Kyung Hee, my friend, colleague, and lovely wife. She has been so nice in everything, encouraging my academic motivation, always by my side. I love you Kyung Hee! I also thank Narae, my five-year old daughter who has been a good girl for the period of my thesis work. I hope she will be a nice lady in the future too.

TABLE OF CONTENTS

LIST OF FIGURES

LIST OF TABLES

SURFACE STRUCTURAL STUDIES OF THE TITANIUM/CHLORINE SYSTEM

I. INTRODUCTION

Polymers have become essential materials in many products and devices and occupy a major part of our modern life. These materials are being used in applications ranging from the production of toys to the manufacturing of the space shuttle. The history of these versatile materials is relatively short. In the late 1930's, a free-radical method [1] for polymerizing olefins was developed by Imperial Chemical Industries. The process involved pressures from 1500 to 3000 atm with temperatures up to 300°C and produced highly branched, low density polyethylene. Industrial production of polyethylene began in earnest during the Second World War, one of the early applications being for submarine cables.

In contrast to this high pressure and moderate temperature (150-230°C) process, Karl Ziegler discovered that certain transition metal complexes catalyze the polymerization of ethylene at room temperature and atmospheric pressure.

The discovery of the Ziegler catalyst was the culmination of many years of basic research in the field of organometallic chemistry by Ziegler and his coworkers. The initial observation in 1952 was the discovery of an anomalous effect of colloidal nickel on the Aufbau

reaction. While attempting to understand the "nickel effect", other transition metal compounds, e.g., zirconium acetyl acetonate, were substituted for colloidal nickel. Instead of low molecular weight hydrocarbons, high molecular weight linear polyethylene was formed exclusively, in high yields.

Giulio Natta then extended the work to the stereospecific polymerization of propylene and higher α-olefins [2]. By 1955 he had developed a procedure for the polymerization of α-olefins using titanium chloride. As a result of extensive, highly original, and profound synthetic and structural investigations conducted under Giulio Natta's direction, the basic principles of stereoregulation and stereoregularity were unequivocally established. Catalysts of this type, which came to be known as Ziegler-Natta catalysts, can polymerize alkenes and dienes with very high activity and selectivity, under a wide range of conditions. In 1963, Ziegler and Natta were jointly awarded the Nobel Prize.

Ziegler-Natta catalysts are generally formed by combining under an inert atmosphere a metal alkyl or hydride, which is an activator, with a transition metal salt [3]. But this activator is not necessary for polymerization. In the Ziegler-Natta polymerization process, $TiCl_3$ has been used as a catalyst. Usually colloidal particles of α-$TiCl_3$ are dispersed into the

hydrocarbon solvent, and then ethylene or propylene gas is bubbled through the mixture [4]. The polymer forms rapidly around the finely dispersed particles, entraining the catalyst and masking the initial stages of the reaction.

Based on the commercially used catalyst, $TiCl_3/AlR_3$, Cossee and Arlman [5-7] proposed a mechanism in 1964 for a typical Ziegler-Natta system [Fig. 1.1]. The titanium was determined to have an alkyl group as an initial ligand. This configuration indicates that a vacant site exists, revealing an active center. It is to this active center that the α-olefin (eg. ethylene) coordinates with titanium. This mechanism is still the most widely accepted version. However the fundamental question about the nature of the active sites still remains unsolved. In order to solve this question, the atomic structure of titanium/chlorine surfaces should be understood precisely to identify active sites.

Titanium trichloride exists in four crystalline modifications α-,β-,γ-,δ- [8]. The α-, β-, and δ-$TiCl_3$ forms all have layer structures made up of closed-packed anionic planes with the metal atoms occupying two thirds of the octahedral holes in between every other plane [9,10]. In α-$TiCl_3$ [Fig. 1.2] the anion packing is hexagonal, while in γ-$TiCl_3$ it is face centered cubic. δ-$TiCl_3$ is believed to have a less ordered structure with

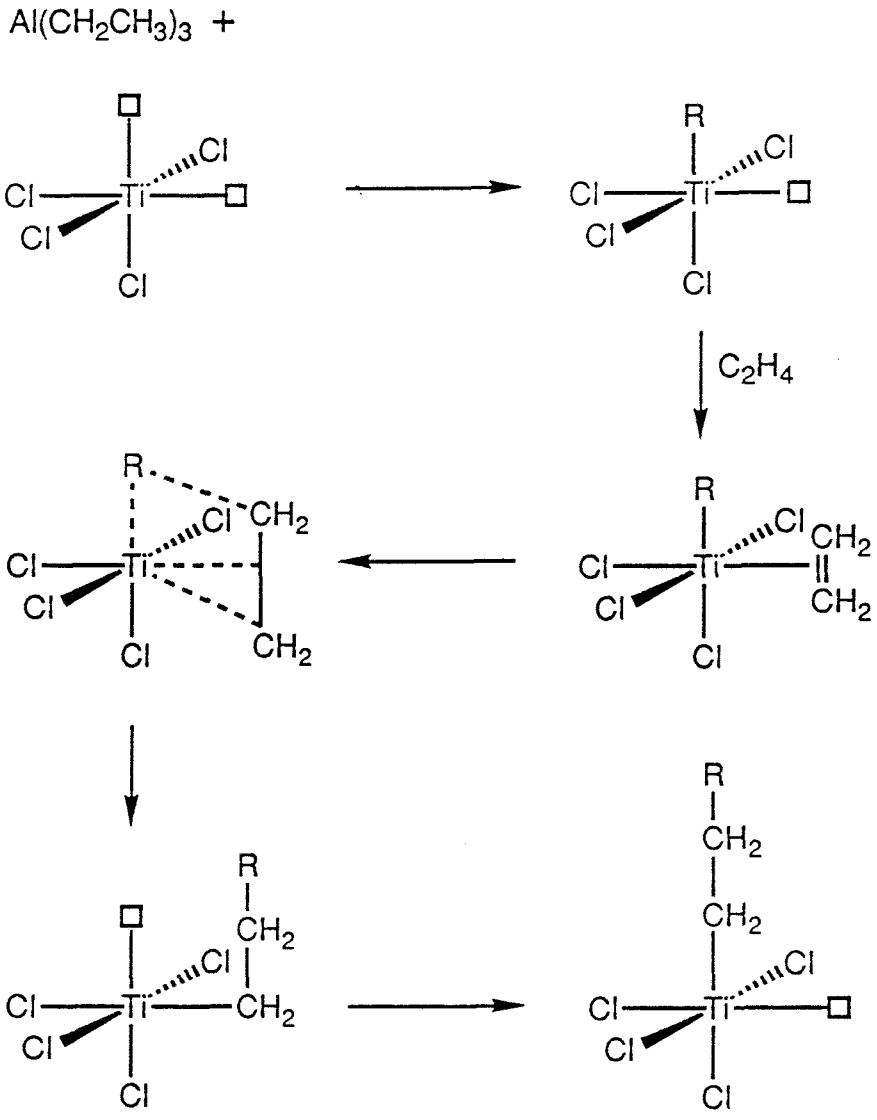

Figure 1.1 Cossee-Arlman mechanism for Ziegler-Natta polymerization.

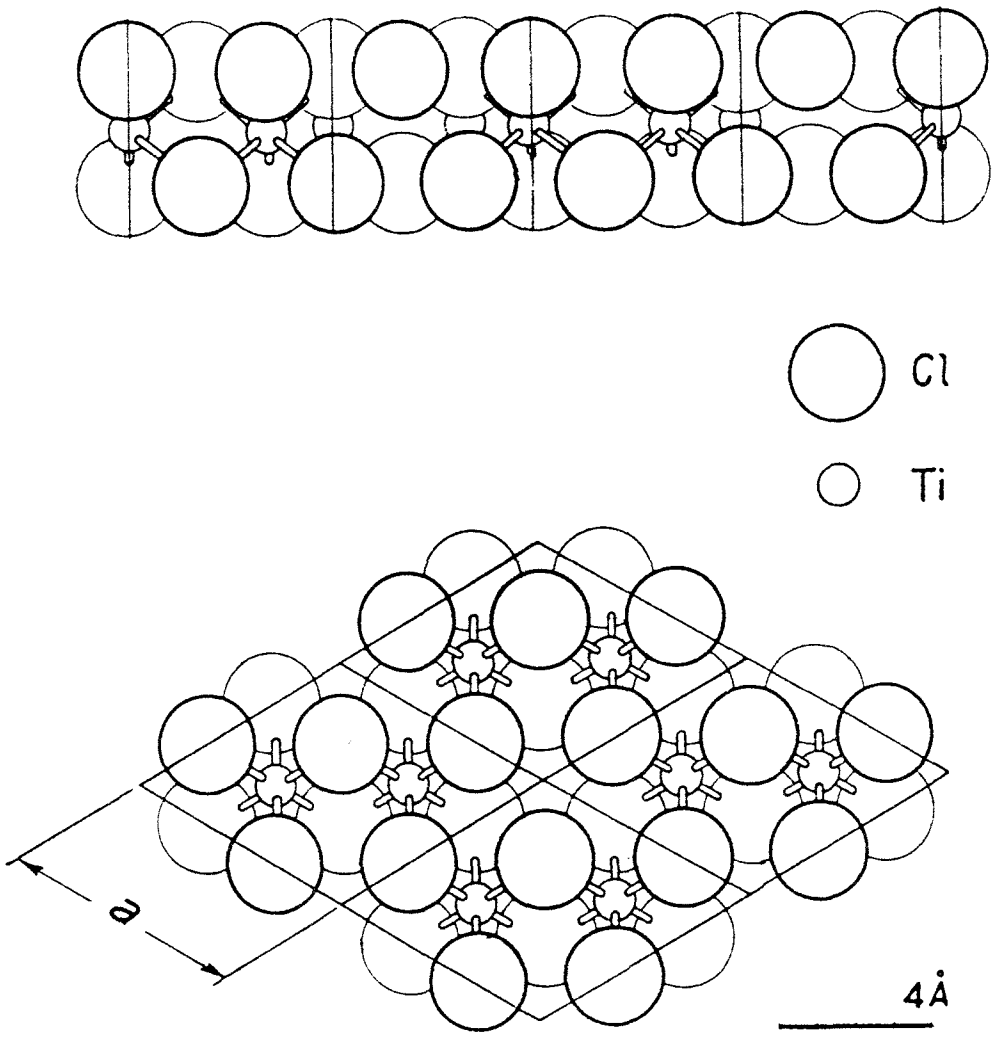

Figure 1.2 Stereochemical model of the structural layer which characterizes α-$TiCl_3$.

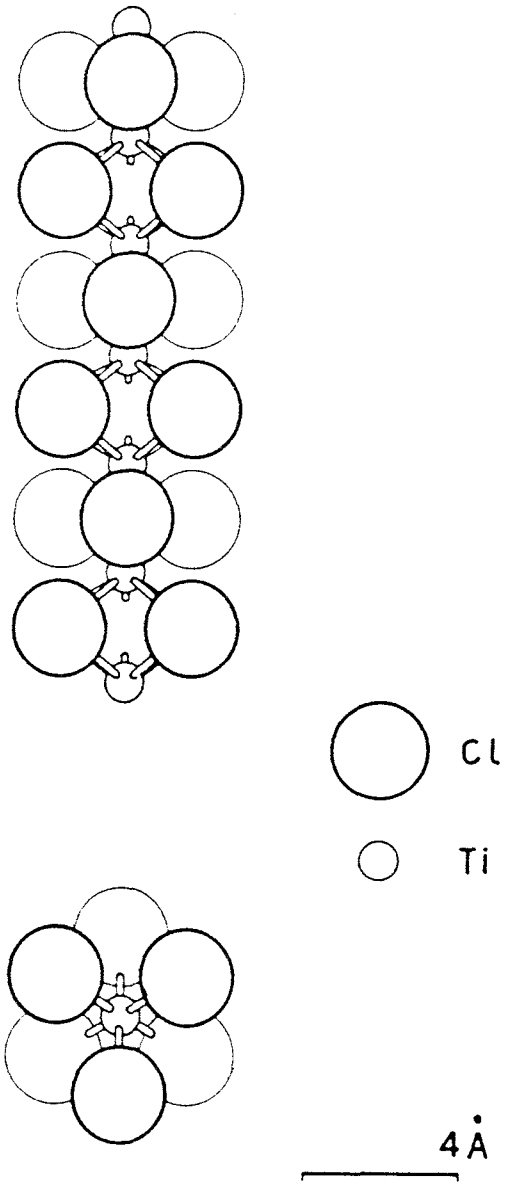

Figure 1.3 Stereochemical model of the structural layer which characterizes the chain structure (β-$TiCl_3$).

a mixture of hexagonal and face centered cubic packing. All of these forms are violet in color, whereas β-$TiCl_3$ is brown. Unlike the others it has a chain structure [Fig. 1.3] with titanium ions stacked above each other in between every pair of planes. One-third of the octahedral holes are occupied between each pair of planes. The α-form is the most widely used and studied.

In such an ionic lattice the principle of electroneutrality requires that a crystal of finite dimensions must have anion vacancies, or possibly positive holes, to achieve a balance of anionic charges. Arlman [5] has shown that the energetically most favorable location for such chloride vacancies is at the edges of elementary (0001) sheets. A plane made up of edges of these elementary sheets, often referred to as a "lateral face", would contain a high number of chloride vacancies. A typical example is the $(10\bar{1}0)$ face of α-$TiCl_3$; this face is normal to the (0001) sheets and contains one chloride vacancy per titanium atom. Depending upon the arrangement of these vacancies, four different surface structures are possible. Also these chlorine vacancies are thought to have some relationship with active sites, but so far the exact nature of the active sites on the $TiCl_3$ crystal has not been elucidated although much work has been done on this topic. There are two ways to approach this question.

One way is to work with the $TiCl_3$ crystal itself.

This way is rather traditional, is direct and has the advantage that we can study the real catalyst. The disadvantage is that $TiCl_3$ crystals are very hard to work with because they are only commercially available as very small crystallites and are very water sensitive. The $TiCl_3$ layers are weakly held together by van der Waals forces. These characteristic properties make $TiCl_3$ crystals difficult to use in UHV studies, given that UHV compatibility is essential to surface structural determination. Therefore, samples need to be of a suitably large size and strength in order to endure mounting and handling procedures. Special procedures are needed to grow crystals and special techniques are necessary to handle them in order to overcome the above mentioned difficulties. These methods are described in chapter III.

The other way to investigate such active sites is to use an indirect method, ie. working with an appropriate model catalyst system. This strategy can be used to simulate a $TiCl_3$ surface under ultra high vacuum (UHV) conditions, directly forming a chlorine layer on the Ti single crystal surface. Models are then employed as substitutes in place of the real catalyst. Although the model surface may not perfectly mimic the true catalyst, this is a common approach due to the convenience and stability of the simulated sample. This model catalyst

also has an advantage in that adsorbates can be isolated on a surface of known symmetry. In this thesis I have employed both methods to help to understand the surface structures present in the titanium/chlorine system.

Studies of titanium trichloride and Ziegler-Natta catalysts using physical methods sensitive to bulk properties, such as X-ray diffraction, are fairly common [8, 11-14]. For example, many workers have tried to correlate catalyst activity with the titanium oxidation state as measured by titration or electron spin resonance (ESR) [11, 15]. Unfortunately, the results of these studies seem to be catalyst-specific; such experiments have implicated oxidation states from 2 to 4 as responsible for polymerization activity [11, 14]. These results are tainted by the fact that techniques used are not specific to the surface sites where reaction occurs. There is a report of an XPS [16] study on various catalysts that attempted to correlate the total amount of surface titanium with activity for propylene polymerization. Any differences in oxidation state for any of the samples relative to $TiCl_4$ could not be detected in this study, possibly due to oxidation during transfer of the samples into the spectrometer. Another XPS study [17], performed on solid $TiCl_4$, describes in passing a Cl $^2P_{3/2}$ binding state in α-$TiCl_3$ but without reference as to how this was determined. Neither of these studies could

reveal the chemical nature of the titanium atoms at the surface of $TiCl_3$.

On the other hand, there are several reports concerning chlorine adsorption on Ti metal [18-21]. Smith studied chlorine adsorption on Ti(0001) by Auger spectroscopy and ellipsometry [19]. He found adsorption to be non-activated and that more than one monolayer of chlorine could adsorb, but did not propose a structure. Recently, Cox and his coworkers [21] reported an experiment which was done on a surface of Ti foil. They found $TiCl_3$ forms upon exposure to the chlorine gas. This was in agreement with Kahn's [18] conclusions. Cox et al. [21] argue that, although $TiCl_2$ might be expected to be the thermodynamically favored product under the conditions of their experiments, the equilibrium situation is not reached, and $TiCl_3$ is the major halide species formed. Despite these studies on the titanium/chlorine system, the atomic structure of the titanium-chlorine surface has not been revealed in detail.

We might hope to obtain useful information concerning the surface structure of the titanium/chlorine system using surface sensitive techniques such as Low Energy Electron Diffraction (LEED) or Auger Electron Spectroscopy (AES). Both of these methods employ electrons to probe a sample and are sensitive to only the first few atomic layers of the solid.

In the LEED method, intensity-voltage or I-V measurements are combined with dynamical calculations. A comparison of their degree of agreement is then based on a statistical correlation factor (R-factor). So far, interpretation of experimental data has been limited to well-ordered surfaces, and is confined to systems with long-range order [22-24]. When the surface is disordered in some way, electrons are scattered out of the discrete beams which characterize diffraction from an ordered surface. Adsorbates without long range order have not been accessible to LEED until recently. The titanium/chlorine surface is one of these kinds of disordered systems, this is due to the high electronegativity of chlorine and high reactivity of the Ti surface. There is an earlier report from this lab of a LEED study [25] on the Ti(0001) surface, which reveals no ordered LEED patterns unless a high- coverage surface was annealed to a temperature of 620°C. The resulting (16x16) pattern was interpreted as due to a coincidence lattice on the Ti substrate, with the Cl unit mesh vectors aligned with those of Ti(0001).

Five years ago, Pendry and coworkers [26] proposed a scheme which makes use of the diffusely scattered intensity to determine the structure of the disordered adsorbate system (DLEED, diffuse LEED). Since the first diffuse scattering intensities of disordered oxygen

adsorbed on W(100) [27] were measured by Heinz in 1985, several efforts have been reported to measure the diffuse scattering intensities and identify the surface adsorption geometry. Most of these investigations have been performed on well known systems to test the DLEED technique, as well as for the examination of the geometry upon disordering.

It is the main purpose of this study to develop the DLEED technique to identify the atomic structure of disordered chlorine adsorbed on the Ti(0001) surface. These DLEED experiments on clean and chlorine-covered surfaces were all carried out on the well characterized (0001) surface of titanium single crystals cleaned *in situ* by ion bombardment and annealing (IBA) techniques. The experimental results were collected using standard surface science techniques under UHV conditions. These techniques allow us to investigate surface structure and composition.

By understanding the atomic structure of titanium/ chlorine surfaces, we hope to contribute to a better understanding of the mechanism of Ziegler-Natta catalysis.

II. THEORETICAL BACKGROUND

A. Ultra high vacuum (UHV) condition

In this study I have used a number of surface sensitive techniques. In this section I provide a brief theoretical background to each one and a discussion of the need for ultrahigh vacuum (UHV) in surface science studies. Recent surface studies have required ultra vacuum conditions which has been defined as the region of pressure below 10^{-9} torr. If we want to study a surface property, the surface composition should be kept constant over the period of experiment. This requires that the arrival of the reactive species from the surrounding phase must be restrained as much as possible, and that in the gas phase only a several percentage of an atomic layer should land on the surface. The implications of this criterion can be evaluated from simple kinetic theory of gases.

The rate of arrival of reactive species from a number of gas molecules n in a given volume and with an average velocity $\bar{u}$ is

$$R = \frac{1}{4}\left(\frac{n}{V}\right)\bar{u} \qquad (2\text{-}1)$$

where $\bar{u}$ has a relationship with the root mean square velocity u_{rms}

$$\bar{u} = \left(\frac{8}{3\pi}\right)^{1/2} u_{rms} \qquad (2\text{-}2)$$

From the Maxwell-Boltzman distribution expression, u_{rms} is determined by the absolute temperature T and Boltzman's constant k_B by

$$u_{rms} = (3k_BT/m)^{1/2} \qquad (2\text{-}3)$$

and the pressure P is defined as

$$P = (n/V)k_BT \qquad (2\text{-}4)$$

Finally, we can express the rate of arrival [28] as

$$R = P/(2\pi mk_BT)^{1/2} \qquad (2\text{-}5)$$

If this form is expressed in torr for pressure, then at room temperature (298K) the collision rate is

$$R_{298} = 2x10^{21}\ P/(m)^{1/2} \qquad (2\text{-}6)$$

Now a typical metal surface has about 10^{15} surface sites/cm^2. For a gas of mass 28 (e.g. N_2 gas), and assuming unit sticking coefficient, the rate of adsorption is

$$R_{ad} = 3.8x10^{20}\ P \text{ molecules } cm^{-2}s^{-1}torr^{-1} \qquad (2\text{-}7)$$

$$= (3.8x10^{20})/10^{15}\ P$$

$$= 3.8x10^{5}\ P \text{ surface layers } s^{-1}\ torr^{-1} \qquad (2\text{-}8)$$

If we consider the time of an experiment to be not less than 100 minutes, this requires that

$$3.8\times10^{5}\ P\times100 < 1 \qquad (2\text{-}9)$$

i.e. for such a system the working pressure P should be less than about 1.0×10^{-9} torr. In other words, at 10^{-9} torr the period of an experiment is limited on the order of an hour. This means that a pressure of 10^{-9} torr or lower is required for a good experiment in surface science. Ultra high vacuum is a requirement for many experiments that involve either the reaction between a surface and a gas or the properties of the surface itself.

Although we can buy vacuum pumps capable of operating in the 10^{-10} torr range, the baking procedure for the entire system is another requirement for attainment of UHV, effectively obtained by baking the whole chamber at a temperature for an extended period of time. The gas adsorbed on the metal is rapidly desorbed, then pumped at a much high pressure during the time the chamber is baked at high temperature. The total throughput of desorbed gas is increased during this period by a large factor. Then when the system is cooled back down to room temperature, most of the easily desorbed gas has been removed from the surfaces; the outgassing rate is decreased by many factors of 10. This reduces the gas load on the pumps and thus allows a lower pressure to be achieved. Usually a

stainless steel chamber with its instrumentation is enclosed and baked to 110°- 130°C for about 72 hours or so. Obviously this means that all the components in the vacuum chamber should be stable and have low vapor pressures at 130°C.

In addition, another requirement for the UHV experiments is that all components must be non-magnetic, as many surface techniques involve low energy electrons which are easily deflected by weak electrostatic and magnetic fields. Also many materials acceptable in "high vacuum" ($< 10^{-6}$ torr), such as many adhesives and plastics, are not acceptable in UHV. Fabrication methods compatible with these requirement are now well established, involving the use of stainless steel and refractory metals with ceramics for electrical and thermal insulation. Modern chambers are constructed of non-magnetic stainless steel or mu metal (a ferrous alloy with high magnetic permeability). Vacuum seals between flanges are usually made using copper gaskets pinched between steel knife-edges, although annealed rings of pure gold wire or indium strips compressed between mirror-polished flats are still sometimes used.

In UHV studies most experiments have been concerned with the adsorption of atoms and molecules on the surface, and thus this requires us to define some of the terms and units used in these studies. One way of defining the

coverage of a surface at the monolayer level i.e. of a single component atomic or molecular layer, is in terms of the coverage of a two-dimensional close-packed layer that takes into account the atomic or molecular size. Such a definition is frequently used in studies of polycrystalline surfaces. However on surfaces of well defined crystallography, it is generally more convenient to use a definition that a monolayer of adsorbed atoms or molecules involving a number density equal to that of a single atomic layer of the substrate material parallel to the surface. In the absence of reconstruction, this is the same as the number density of atoms in the top atomic layer of the substrate. Frequently, saturation of a particular adsorbate species occurs at a coverage of less than one monolayer, so the definition implies nothing about the maximum possible coverage which depends on the adsorption system under study.

The second definition concerning adsorption studies is for a unit of exposure. The unit which is firmly established in the literature is the Langmuir(L), with 1 L= 10^{-6} torr sec exposure. A disadvantage of this unit is that the actual number of atoms or molecules arriving at a surface for 1L of exposure actually depends on the molecular weight of the gaseous species and its temperature.

Although this Langmuir unit is not an SI unit, it has

a big advantage of experimental convenience, as most surface studies are carried out using an ion gauge to measure pressure in torr and a stopwatch to measure in seconds. The SI scale is a convenient unit to characterize the exposures needed to produce certain adsorption states on a surface, and can be communicated to other experimentalists working on the same adsorption system.

B. Auger electron spectroscopy (AES)

If a core electron is ejected from an atom by a primary electron beam, the resulting ion is in a highly excited state. A number of possible processes may contribute to reducing the excitation. One of these is emission of a secondary electron, this process being known as the Auger effect. The other is emission of a photon. Auger emission is caused when one electron drops from a higher level into a core vacancy, the energy liberated leading to the ejection of a second, or Auger, electron. The Auger process is illustrated in Figure 2.1. The energy of the secondary electron is analyzed, not the primary electron. In the case of photon emission, we have (ignoring relaxation)

$$h\nu = E_1 - E_2 \qquad (2\text{-}10)$$

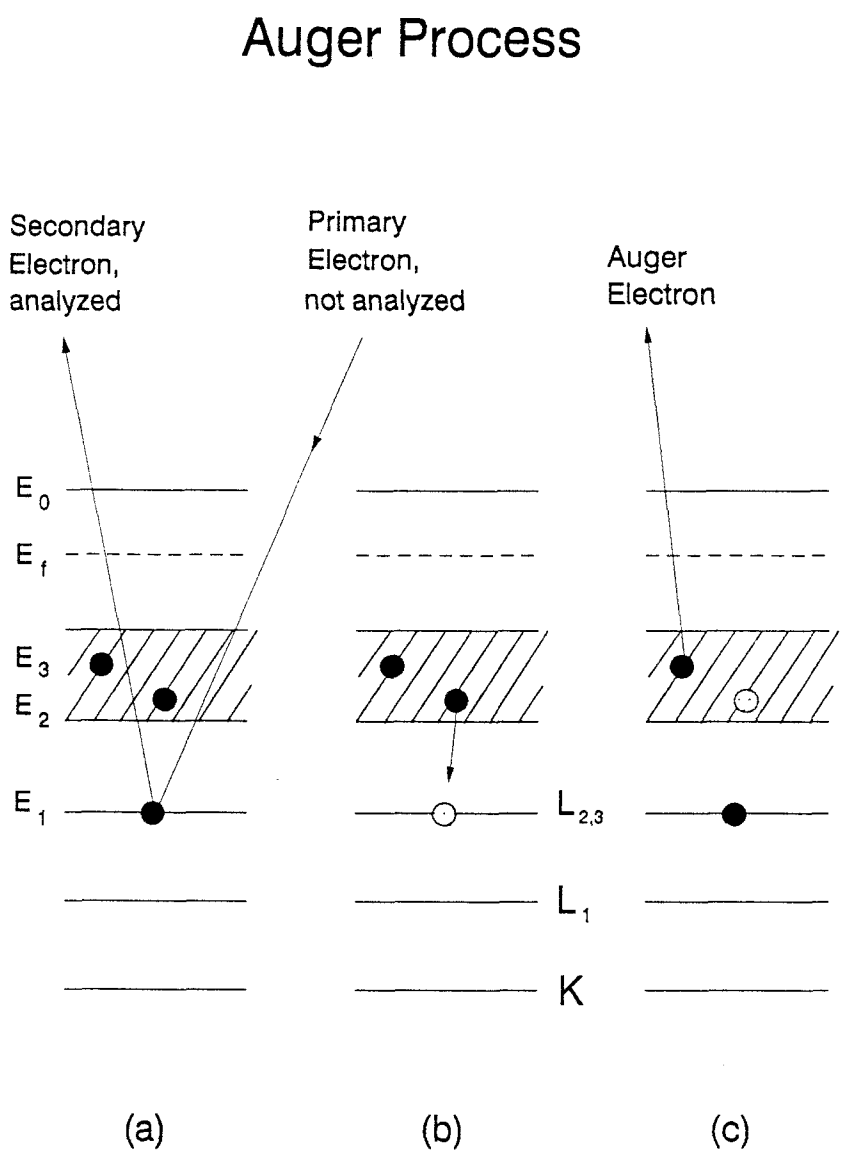

Figure 2.1 Diagram of the Auger process.

where E_1 is the electron energy at lower level, E_2 for the higher level, and in the case of Auger electron emission

$$K.E. = E_1 - E_2 - E_3 \qquad (2.11)$$

In each case the emitted particle is characteristic of some combination of atomic energy levels of the emitter and so forms the basis of a core level spectroscopy. Thus, Auger electron emission is an efficient means of filling core holes of low binding energy, giving rise to relatively low kinetic energy Auger electrons of short mean-free-path. The kinetic energy of an Auger electron is characteristic of the energy levels of the atom and independent of the energy of the exciting radiation. Therefore, its detection outside the solid provides a surface sensitive probe of the chemical composition. There are two main applications of Auger Electron Spectroscopy (AES).

The first application is in cleaning of the metal surface, prior to adsorption experiments. Carbon is a very common impurity on metal surfaces, but its KLL spectrum is readily recorded. AES has a sensitivity of about 1 % of a monolayer, therefore the progress of cleaning procedures, used to remove carbon and other impurities, can be monitored until impurity peaks are absent. This ensures the initial cleanliness of the surface.

The second application of AES is the measurement of the amount of gas adsorbed on a surface layer. For this purpose the peak to peak height of the AES derivative curve is a convenient measure of surface concentration, although calibration by some other technique, such as flash desorption, is often required.

C. Low energy electron diffraction (LEED)

Many properties of solids are intimately related to the special symmetry of these materials. While a solid surface is intrinsically an imperfection of the crystalline bulk, terminating the three-dimensional periodicity of the structure, this region retains two-dimensional periodicity parallel to the surface. This periodicity is an important factor in determining some of the properties of the surface. Therefore, a proper understanding of surface crystallography is very important for a general understanding of many surface effects. For this purpose, Low Energy Electron Diffraction (LEED) has proved to be the best technique, providing useful information on the structure of the surface, and also yielding information on the electronic properties of the surface.

The electron diffraction technique was perfected with the aid of extensive experience from conventional

diffraction methods on the bulk crystals. A diffraction experiment designed for crystal structure analysis requires a probe with de Broglie wavelength less than typical interatomic spacings, say about 1 Å. In order to fulfill this requirement, electrons must have kinetic energy $E = (h/\lambda)^2 \cong 150$ eV. Electrons of this energy also have a very short mean free path in matter. This fortunate coincidence forms the basis for low energy electron diffraction (LEED) from solid surfaces. Electrons with energies in the range of 20-500 eV that are elastically backscattered from a crystal surface form a diffraction pattern which is the Fourier transform of the surface atom arrangement. The first experiment was performed by Davisson and Germer in 1927 [29], they discovered that when firing electrons with energies lying between 15 and 200 eV at a crystal of nickel, the angular variations in the reflected flux were consistent with electron diffraction.

The LEED pattern appears as an image of the surface *reciprocal* net when viewed along the surface normal at a proper distance from the crystal. The distance between adjacent points in a reciprocal lattice is inversely proportional to the distance between points in the corresponding direction of the direct lattice. For a purely planar lattice mesh the periodic repeat distance is infinite in the z-direction. The reciprocal lattice

points along the surface normal are therefore infinitely dense. Nonetheless, translational invariance in two dimensions ensures that diffraction occurs if the two-dimensional Laué conditions [30] are satisfied,

$$(\mathbf{k}_i - \mathbf{k}_f) \cdot \mathbf{a}_s = 2\pi m \qquad (2\text{-}12)$$

and

$$(\mathbf{k}_i - \mathbf{k}_f) \cdot \mathbf{b}_s = 2\pi n \qquad (2\text{-}13)$$

where $\mathbf{k}_i$ and $\mathbf{k}_f$ are the wave vectors of the incident and scattered electron, respectively, and m and n are integers.

The Laué conditions [30] can be illustrated well using the Ewald construction [31, Figure 2.2]. A reciprocal lattice rod passes through every point of the surface reciprocal net, $\mathbf{g}_s = h\mathbf{A}_s + k\mathbf{B}_s$. The magnitude of the electron wave vector sets the radius of the sphere and the diffraction condition is satisfied for every beam that emerges in a direction along which the sphere intersects a reciprocal lattice rod. As in three dimensions, the beams are indexed by the reciprocal lattice vector that produces the diffraction. The beam spots are labelled with the appropriate $\mathbf{g}_s$.

A knowledge of the surface structure has become one of the most important pieces of information needed for the understanding of a surface. In recent years, LEED has proved to be the best established method for the determination of the geometrical structure of the surface and adsorbate layers. Its similarities to X-ray

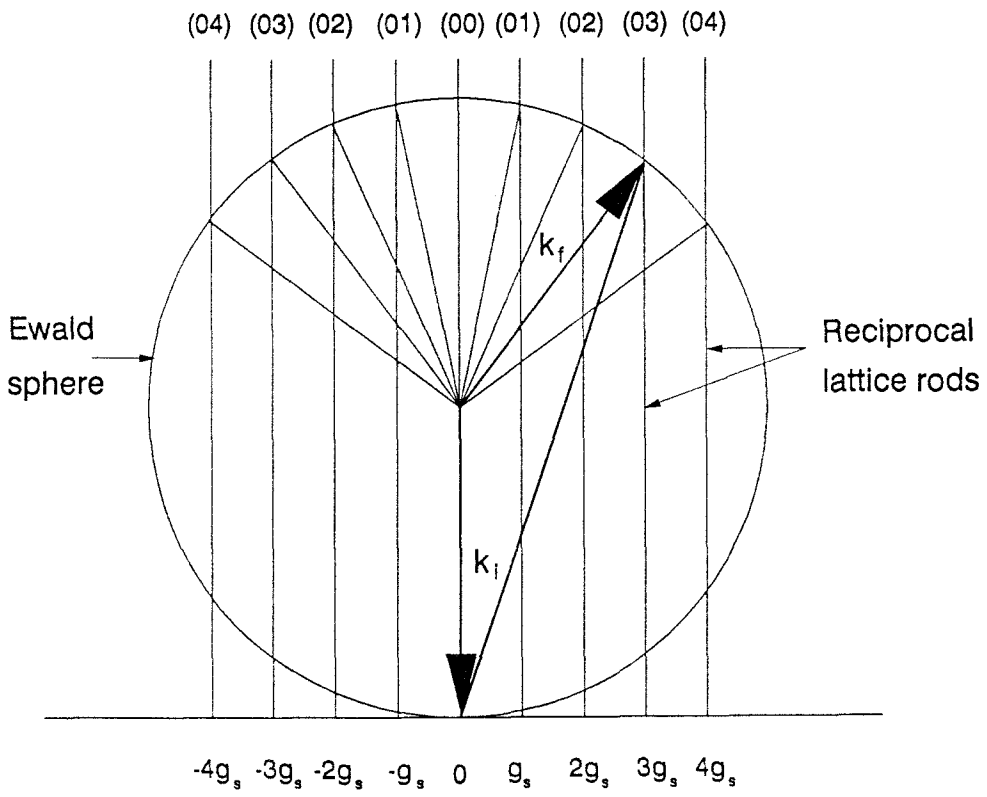

Figure 2.2 The Ewald construction for an electron incident normal to the surface. Nine backscattered beams are shown.

diffraction have led to its adoption as the basis for the new science of "Surface Crystallography". LEED techniques can reveal the atomic arrangement at the surface within 0.05 Å. Although numerous other techniques have been recently proposed which may provide information concerning the geometrical arrangement of atoms at a crystal surface, none have been studied as widely as LEED, and it is LEED which has usually provided the information by which other techniques are judged.

In the LEED technique, an I-V plot, the experimental record of the intensity of a scattered beam as a function of the electron energy, is used in an iterative procedure to determine the geometrical arrangement of surface atoms [32]. First, an arrangement of atom is postulated that is consistent with the symmetry of the LEED pattern. Next, the intensities of a number of diffracted beams are calculated as a function of the incident electron energy. This is accomplished by solving the equation for the electron wave function within the first few atomic layers. Finally, the resulting I-V curves are compared with experimental curves based on a reliability, or R-factor. The process is continued using a refined geometry until satisfactory agreement with experiment is obtained. This procedure involves significant computational work, but the results can predict the atomic arrangement within 0.05 Å at the surface. This useful technique still however has

some limitations for surface structural studies.

D. Diffuse LEED

1. Introduction

Since the formation of a LEED pattern is a diffraction phenomena, surface structural determination by LEED has been limited to well ordered surfaces with long range order [24]. Particularly, we are faced with the restriction to studying adsorbates at discrete coverages corresponding to the ordered overlayers. However, many important surface structures are inevitably disordered. When disordered adsorbates are present on the surface, electrons are scattered out of the discrete beams that characterize diffraction from an ordered surface, and conventional LEED theory fails. In addition, for low coverage structures not only is disorder frequently observed, but any ordered structures that are formed will have a very large unit cell. In this type of situation conventional LEED is inappropriate because of the computational difficulty of handling large unit cells. The same problem of large unit cells arises with saturation coverages of large molecules adsorbed on a substrate [33].

In these cases, the contribution of diffuse

scattering becomes dominant over regular LEED spots. Diffuse intensities as appearing in a normal LEED experiment in which disordered adsorption occurs, contain a lot of structural information, namely that of the adsorption sites of the molecules. Theoretical treatments [34,35] for disordered adsorption of a lattice gas where the local atomic arrangement is the same for each adsorbed molecule or atom, have shown that structural information can be obtained from the DLEED intensity. Here the molecule-substrate interaction is the dominant and chemically significant quantity. By contrast, the molecule-molecule interactions (responsible for any ordering) are relatively weak and chemically a minor part.

In this study, where we consider a disordered adsorbate on a nearly perfect substrate, each electron contributing to the diffuse LEED pattern has scattered at least once from an adsorbate atom and therefore the diffuse intensities have contained within their pattern information about the local environment of the adsorbate. In this, there is an analogy with surface extended X-ray adsorption fine structure (SEXAFS) experiments [34,36-38] which have been so successful in the study of local structure at surfaces. Actually, according to recent theory [34,38], the main process of a diffuse LEED experiment, is precisely a SEXAFS event but one in which the electron has been introduced by an electron gun rather

than by ejection of a core electron. In fact, it even has some advantages over SEXAFS, partly because of the additional information present in the diffuse scattering, but much more importantly for the following reasons. SEXAFS has a serious limitation in that there is one and only one data set available for the system. Thus in SEXAFS, information about the surrounding atoms decreases rapidly with the distance of the adjacent atom from the adsorbate. In a really complex unit cell, there is just not enough data to resolve the structure. On the other hand, using the DLEED method, more data can be collected at will simply by changing the energy or angle of incidence. Then, on observing the new diffuse pattern, a larger quantity of structural data becomes available for analysis. Also DLEED can be used in the case of large molecules adsorbed at surfaces and for the monitoring of adsorbate structures as a continuous function of coverage. This also allows for the examination of the surface migration of adsorbates or highly reactive adsorbates which can not be made to order.

The great advantage of diffuse LEED is that it is insensitive to the long range order of the surface. The diffuse LEED intensity is a local probe of the surface geometry surrounding the adsorbed atom, whereas conventional LEED is concerned with measuring the sharp Bragg spots resulting from a well ordered surface.

2. Diffuse intensities

Since calculated intensities cannot be compared directly to measured intensities, current theories are complicated. The present theory avoids consideration of the contributions caused by the thermal movement of atoms. However, surface phonons significantly contribute to the quasi elastic background which can not be separated from the elastic signal when conventional LEED optics are used. This is because the cut off energy for the suppressor ground has to be some electron volts below the primary beam energy. It was shown both experimentally [39] and theoretically [40] that at low coverages phonon contributions originate mainly from substrate phonons. We can cancel this background intensity out by a simple subtraction of the diffuse intensity map of the clean surface which can be measured separately. This is also true for contributions from surface defects of the substrate. Basically, the subtraction procedure has the effect of taking the derivative of the scattered intensity I with respect to the coverage θ, (ie. $I'=dI/d\theta$) instead of using the simple intensity I. It is understood that both I and I' are functions of the momentum $K_{\parallel}$ parallel to the surface, as well as of the primary electron energy E. Thus $I=I(K_{\parallel},E)$ and $I'(K_{\parallel},E)$. For multiple adsorbates positioned in equivalent adsorption sites, the total

signal is

$$I'(K_{\parallel},E) = I_{o}(K_{\parallel},E).S(K_{\parallel}-K_{\parallel,in}) \qquad (3.1)$$

where S is the structure factor for consideration of interference contributions from different adsorbates. If the electron beam is averaged over many different lattice gas configurations, S could be more or less structureless. Fortunately, S is independent of energy, i.e. its derivative with respect to energy for fixed $K_{\parallel}$ vanishes, dS/dE=0. Thus we can completely dispense with S by the use of the logarithmic derivative of I', defined below as L:

$$L = \frac{dI'/dE}{I'} = \frac{dI_{o}'/dE}{I_{o}'} \qquad (3.2)$$

The interactions between the adatoms that are the possible results of nonideal disordered adatom arrangement, and which lead to special variations of S, are significant. Removing the unknown S requires one to have I' at two neighboring energies, then $dI'/dE \cong (I'(E+\Delta E) - I'(E))/\Delta E$. We should think that obtaining I' at an additional energy would require two additional measurements, one for the adsorbate and one for the clean surface. Actually for the construction of L, four sets of data need to be measured. The use of L is the same as taking the second derivative, I'' of intensities, $I'' = d^{2}I/dE.d\theta$. However the order of the derivative increases,

the influence of noise has a considerable affect on the original intensity maps, resulting in a high signal-to-noise ratio.

3. Y-function

The use of the logarithmic derivative may be dangerous if I' happens to be so small that it can not be accurately measured. Then L might take on artificially high values, leading to wrong conclusions. Therefore it is better to replace large values of L by the physical maximum value that L can take. It is known from experience in conventional LEED that the energy half width of an I-V curve is approximately $2V_{oi}$, with V_{oi} being the part of optical potential describing the electron attenuation. For a triangularly shaped peak the slope would be

$$(dI/dE) = I_{peak}/2V_{oi} \qquad (3\text{-}3)$$

leading to the logarithmic derivative

$$L = (dI/dE)/I_{peak} = 1/2V_{oi} \qquad (3\text{-}4)$$

For a realistic shape, the maximum slope should be twice as large ($L_{max} = 1/V_{oi}$) and it is therefore reasonable to limit L to this value by using the Y-function [41] as follows.

$$Y(E,K_{\|}) = \frac{L(E,K_{\|})}{1 + L(E,K_{\|})^2 . V_{oi}^2} \qquad (3.3)$$

In this case V_{oi} is the imaginary part of the inner potential (often taken to be about V_{oi}=4 eV), which is used in order to avoid divergencies for small values of I. This Y-function has its maximum for $L=1/V_{oi}$. The use of the Y-function removes an adsorbate structure factor and the finite coverage effect.

4. R-factor

To compare experimental and theoretical Y-functions [41,42], the Pendry R-factor(R_p) was used.

$$R_p = \frac{\Sigma_{K_{\|}} (Y_e(E,K_{\|}) - Y_t(E,K_{\|}))^2}{\Sigma_{K_{\|}} (Y_e(E,K_{\|})^2 - Y_t(E,K_{\|})^2)} \qquad (3.4)$$

where Y_e is the experimentally generated Y-functions and Y_t is the theoretically calculated Y-functions. The summation extends over all points of measurements. i.e. over all parallel components $K_{\|}$ for which diffuse intensities were measured. An average over energies has to be taken for different energy sets in DLEED, while a total R_p factor as averaged over all beams results in

normal LEED. R corresponds to the mean square deviation of the Y-function. For diffuse intensities, the R-factor is the particularly appropriate measurement, since the Y-functions are the proper quantities needed to compare theory and experiment.

5. Survey of the previous DLEED studies

Although the number of publications which deal with LEED techniques or discuss results of LEED studies for surface structural studies run into the thousands, a search of the literature reveals that the corresponding experiments using the diffuse LEED technique are very rare, probably due to the short history of this new technique which is still being developed. Pendry and Saldin [34] developed in 1984 a formulation which allows the calculation of diffuse intensities emerging from a single adatom on a crystalline substrate, but it was only recently that the first diffuse intensity measurements were performed by Heinz and his coworkers [42]. They applied Pendry's theory to disordered oxygen on a W(100) surface to determine the surface adsorption geometry and employed a computer controlled TV method [43,44] to measure the diffuse intensities. They also used oxygen adsorbed at a low temperature of about 120 K in order to reduce the thermal diffuse background and to avoid

ordering of the adatoms. Experimental measurements and theoretical calculations for the Y functions were performed for the two energies of 46 and 48 eV relative to the muffin-tin zero. From this first application of the DLEED technique to disordered oxygen on W(100), they had reported that (1) the phonon background does not seem to interfere with the experiment-theory comparison, if the sample is cooled to liquid nitrogen temperature; (2) use of the Y-function for experiment-theory comparison eliminates spurious correlations between adatoms which are not taken into account in the theory; (3) the method shows good sensitivity to surface geometry comparable with that in conventional LEED experiments on ordered surfaces; (4) R-factors obtained at the optimum geometry were very low; (5) oxygen sits in the four-fold hollow sites on a tungsten(100) surface at 0.55 ± 0.1 Å above the last tungsten layer.

There is a report [45] by Ibach and Lehwald in 1986 that measured elastic diffuse and inelastic electron scattering from surface with disordered oxygen adsorbed on the Ni(100) surface. They measured phonon spectra with a recently developed version of the double-pass electron spectrometer using cylindrical deflectors. The author found that (1) the elastic diffuse intensity rises linearly with coverage when the adsorbate is a lattice gas and that; (2) the integrated intensity of phonon events

shows practically no change for coverages up to 20% of a monolayer and that; (3) as a result, the elastic diffuse intensity arising from the disordered adsorbed species can be experimentally determined with low resolution instruments such as a Video-LEED camera, by measuring the total (elastic and inelastic) diffuse intensity of the adsorbate covered surface, and then subtracting out the contribution of the clean surface.

Another study on the Ni(100)/O system, that focused on the test for reliability by varying the instrumental as well as the physical parameters of measurement. This was reported by Starke et al [46]. The authors reported that; (1) they were able to detect the low level signals with sufficient accuracy and resolution by employing a fast, sensitive and momentum resolving technique such as a video camera based system; (2) the subtraction of the clean substrate signal to cancel the phonon and defect contributions to diffuse intensities is essential; (3) the Y-function allows one to get rid of the structure factor and to concentrate on the local adsorption structure of a single adatom or molecule. The Y-function is independent of coverage in the range of moderate coverages (below θ=0.25) and in addition, the use of the Y-function allows for a high signal-to-noise ratio.

On the other hand, a theoretical study for the phonon contribution was reported by Andres et al in 1988 [47].

They evaluated the contribution to the diffuse LEED pattern due to thermal vibrations by using a linear version of the new tensor LEED technique, which was originally developed to treat the changes in conventional LEED I/V spectra produced by static displacements [48,49]. They employed basically a perturbative method in which a complete LEED calculation for an unperturbed reference surface was used as the starting point. This theory was applied to two previously studied systems. A system of disordered oxygen adsorbed on both a W(100) and a Ni(100) surface were studied by varying the energy of the incoming beam, the temperature, and the incoming and outgoing beam angles. Their report was contributed to show that the theory is broadly in agreement with the previous experimental work [45]. It also permitted the use of a more flexible of theory to extend investigations over a wide range of energies and scattering angles.

There were recently several reports investigating local adsorption geometry using DLEED [50-53]. Illing et al [50] studied carbon dioxide adsorption on Ni(110) using DLEED combined with X-ray photoemission and NEXAFS techniques. They measured diffuse intensities at two energies, 70 and 75 eV with respect to the Fermi energy, where the scattered intensity was relatively high. They admitted CO_2 gas while maintaining a crystal temperature of 130 K. In addition a CO_2 exposure of 10^{-7} mbar s was

used. This was done to minimize multiple scattering between adsorbates molecules by using low temperature and coverage. They also used the Y-function and employed the Pendry R-factor for theory-experiment comparison. They found that R_p-factor analysis can distinguish only between structures whose R-factor deviates by more than 20% from the minimum. Their R-factor analysis favored the coexistence, with no clear preferential azimuthal orientation, of molecules aligned along each principle azimuthal direction (<100> and <110>) also equal numbers of molecules on top sites appeared to be more likely than those on hollow, or bridge sites. This DLEED analysis was in agreement with the NEXAFS results. They could not yet reliably determine the magnitudes and sign of the bond angles.

A DLEED study that completely determined local bonding geometries in a disordered molecular overlayer together with the relative occupation of different coexisting adsoption sites, was reported for the first time by Blackman et al in 1988 [52]. They used a fast, sensitive "digital" or electron counting LEED apparatus which was recently developed by the authors on the disordered CO/Pt(111) system. Their apparatus uses hemispherical grids for energy selection, two microchannel plates as the amplification stage, and a wedge-and-strip position sensitive detector to collect the electrons. It

allows a reduction in beam current down to less than 1 pA. This largely eliminates electron stimulated desorption or decomposition of in the overlayer during the experiment. Digital LEED did not show any significant background noise and is only limited by statistical noise with a signal to noise ratio determined by the counting time. They have for the first time applied an extension of the beam set neglect theory [53] to a disordered system. This is more efficient than the three step theory, which will be explained in chapter V [34,42]. Only a minimal loss of structural accuracy occurs when using the beam set neglect theory[38]. They followed Pendry's method for the comparison of theory and experiment and applied the Pendry R-factor to the Y-function of the intensity rather than to the intensity itself [42]. From the R_p factor analysis, they found a clear minimum near the spacings $d_{\perp,top}$=1.85 Å and $d_{\perp,bridge}$= 1.55 Å, the values determined earlier for the ordered c(4x2) structure. Using the site mix dependence analysis, they got a sharp minimum at 88±5 % top site and 12±5 % bridge site occupation. Subtraction of the clean surface diffuse intensity did not cause any significant effect in their result.

Most recently, Piercy et al [51] studied adsorption geometry of disordered carbon monoxide adsorbed on the Ru(001) surface. They used a multi channel, angle resolved, energy dispersive electron analyzer to measure

diffuse intensities. The incident beam was off normal and diffuse intensities were measured in the plane of incidence, for different azimuthal angles of incidence, and for different beam energies. The DLEED program of Saldin and Pendry was employed to carry out a detailed multiple scattering analysis. Three different absolute CO coverages of 5%, 10%, and 20% a monolayer at temperatures of T=120 and 330 K were tried to test the diffuse LEED technique for structural determinations. For 10% of a monolayer the comparison with theory was best when Y functions were used, while for the 5% coverage relative intensities could be successfully analyzed directly. For 20% of a monolayer the analysis was disturbed by partial ordering. Piercy et al found that the favored adsoption structure has CO linearly bonded to the on top site with a perpendicular Ru-C distance of 2.0 ± 0.15 Å, which is in close agreement with the ordered $\sqrt{3}$ structure at θ=1/3.

We know from these studies that all of the authors previously mentioned have performed both a test of the DLEED technique as well as an examination of the geometry of the system upon disordering. By choosing a well known system having a known structure in the ordered state, some of them have tried to compare their DLEED analysis with other surface sensitive techniques. All of them used a gaseous source as an adsorbate because it can be easily introduced through leak valves. This avoids the

difficulties associated with moving the sample. The measurement of diffuse scattering intensities should be carried out with the covered sample in an identical position with that of the clean sample, This is a necessary procedure for the elimination of phonon and defect contributions.

These studies show that, (1) a fast, sensitive, momentum resolving and computer based technique with a video camera is required to successfully carry out diffuse intensity measurements, (2) low coverages of less than 20% of a monolayer are required to minimize multiple scattering between adsorbates molecules, (3) the use of the Y function, the logarithmic derivative of intensity with respect to energy, cancels the influence of many instrumental parameters as well as that of coverage, and (4) the results of the R factor analysis in the DLEED technique are in close agreement with other surface sensitive techniques.

III. PREPARATION AND CHARACTERIZATION OF $TiCl_3$ CRYSTALS

A. Growth of single crystals

1. General description of apparatus

Sublimation and recrystallization of $TiCl_3$ crystals were carried out in a gradient furnace shown in Figure 3.1. The hot region in a gradient furnace is the sublimation portion, and the cold region the condensing portion. Each portion of the furnace consisted of a ceramic tube wound with nichrome wire for resistance heating. Two different sets of heating wires were regulated by separate Variacs. The temperature profile of the furnace was calibrated and is shown in Figure 3.2. The outside of the furnace was wrapped with insulating material to prevent the loss of heat and shorting out of the circuit.

2. Preparation of $TiCl_3$ single crystal

Anhydrous, hydrogen-reduced, non activated, powdered $TiCl_3$ (Alpha Products) was used in growing $TiCl_3$ single crystals. A specially prepared pyrex tube, which can withstand a high temperature, was employed to grow $TiCl_3$ crystals. This sample tube is shown in Figure 3.3. The

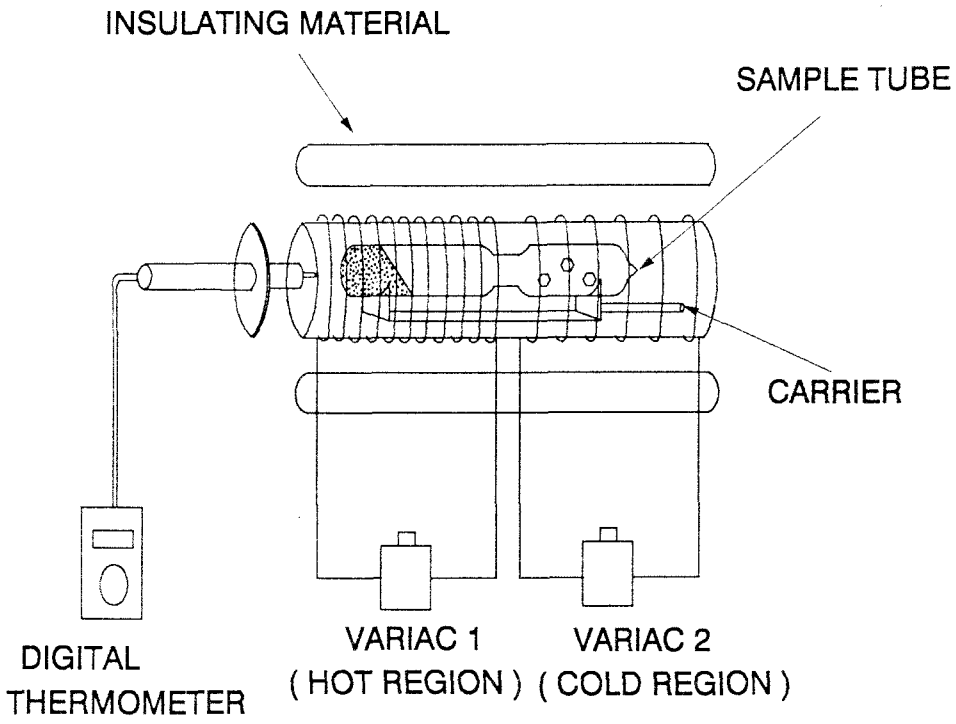

Figure 3.1. The schematic diagram of the gradient furnace used in growing $TiCl_3$.

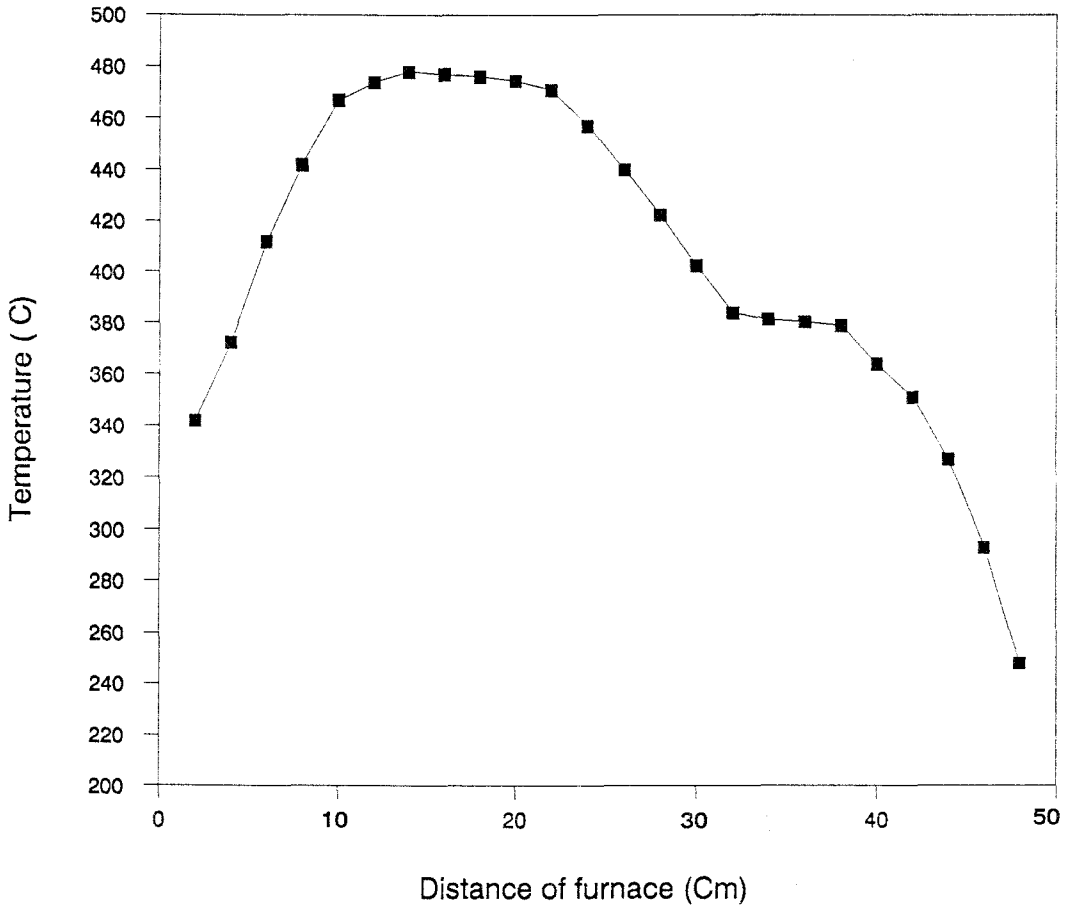

Figure 3.2. Temperature calibration curve of the gradient furnace

middle portion of sample tube is designed to be thinner than other portions, since this portion is broken to remove the crystals. The sample tubes had been stored in the drying oven at 130°C and heated with a hot air gun before use. $TiCl_3$ powder was introduced into this sample tube. All manipulations of $TiCl_3$ were carried out under a Argon atmosphere in a dry box. The sample tube was vacuum sealed by an oxygen/acetylene torch and placed in the hot region of the furnace. The tube was transported to the inside of the furnace by means of a stainless steel carrier, and both sides of the furnace were plugged with insulating materials. The subliming portion of the tube was maintained at 480 to 495°C, and the condensing portion, at 380 to 390°C [54]. The vapor pressure is estimated to be about 2×10^{-4} torr. Temperatures of the 2 regions in the furnace were checked periodically using the thermocouple (chromel/alumel) with which the furnace was equipped.

$TiCl_3$ single crystal leaflets, which are 5 to 10 mm in diameter and violet in color, formed in about 5 days. The growing period was terminated by removing the sample tube from the furnace. In the dry box, the grown single crystals were removed from the tubes by breaking the tube and moved to a vacuum deposition apparatus. The rest of the crystals were placed in small, open sample bottles. These small bottles were placed in a desiccator which

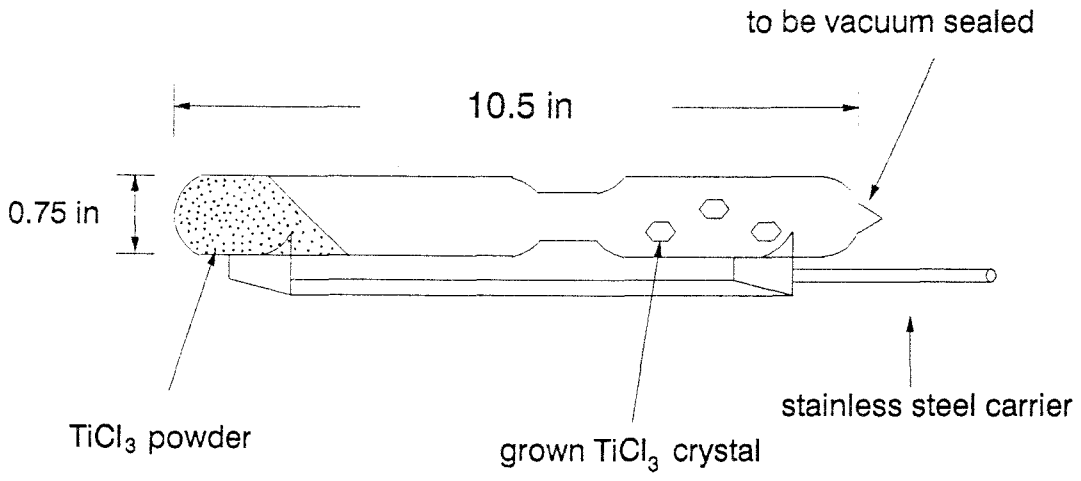

Figure 3.3. The pyrex sample tube used in growing $TiCl_3$ single crystals.

contained calcium chloride. This desiccator was tightly capped and stored in the dry box for the next use.

B. Gold-plating on the $TiCl_3$ crystal

1. General description of apparatus

$TiCl_3$ is a very friable solid which is very difficult to work with, since it is very brittle and water-sensitive. It requires the use of some special handling techniques to prevent it from coming in contact with water vapor in the air until it is attached to the manipulator of the UHV chamber where it is to be studied. A vacuum deposition technique [55] was employed to protect the freshly made single crystal from moisture in the air. The idea of this technique is to form an inert layer, in this case gold, on the crystal by vacuum deposition. The deposition apparatus used in this study was simply designed for gold-plating and made from pyrex [Figure 3.4]. In this glass cell, tungsten ribbon was used as a heating template to vaporize gold. The ribbon was spot welded to the top of a tungsten welding rod, which is connected to the variac for the application of voltage, and a gold wire (0.005" Dia.) was coiled around the tungsten ribbon to be vaporized.

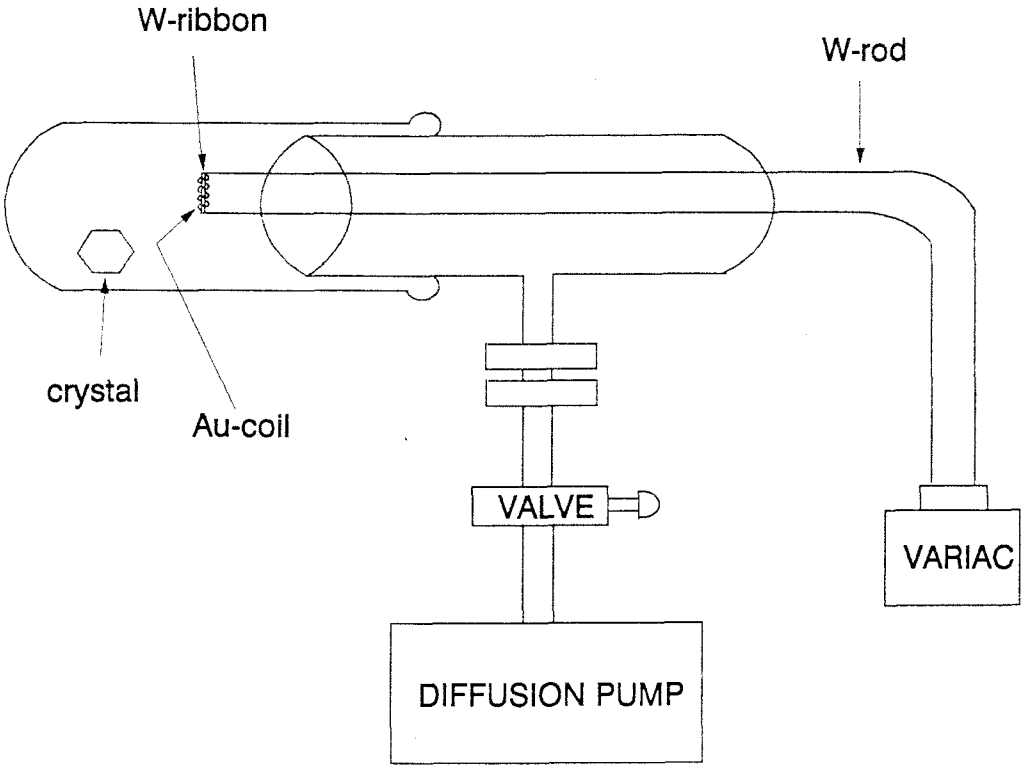

Figure 3.4. The vacuum glass apparartus used in gold-plating.

2. Gold-plating

The freshly-grown $TiCl_3$ crystal was moved to the glass deposition cell in a dry box, and then the cell was connected to a diffusion pump. The pressure in the vacuum cell was maintained to $2x10^{-4}$ torr, and 12 V of alternating current (AC) was applied. The gold wire was heated and easily vaporized by the application of about 12 V AC and deposited on the $TiCl_3$ single crystal. A thin gold layer, deep yellow in color, was successfully formed on the $TiCl_3$ crystal. It did not take more than 2 minutes after which gold plating was terminated in this simple and handy glass apparatus. Gold plated $TiCl_3$ crystals were placed in a small sample bottle and the bottle was stored in a desiccator.

C. Mounting of the gold plated crystal

Since the as grown $TiCl_3$ crystal was so fragile, the crystal could not be clipped to the sample holder of the UHV chamber directly, as is a normal metal sample. Thus a special design was required to mount this brittle crystal. This design is shown in Figure 3.5. A molybdenum plate was employed as a template to be clipped to the manipulator. A thin indium film then was sandwiched in between the $TiCl_3$ crystal and the molybdenum plate. The

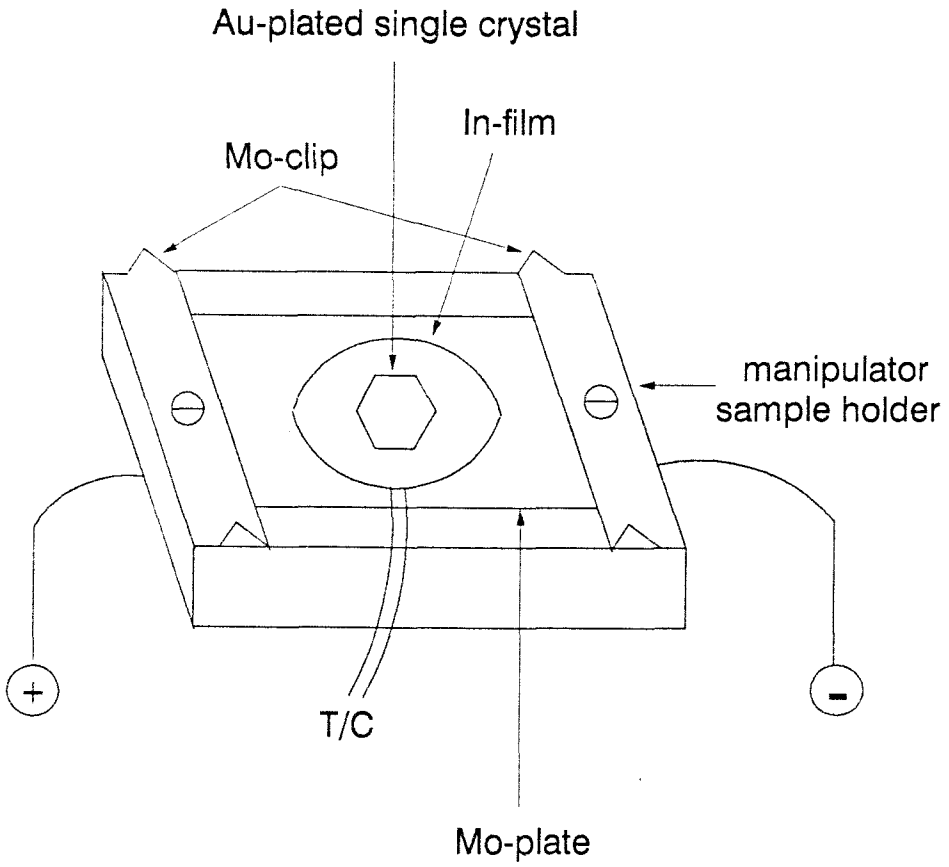

Figure 3.5. Mounting of the gold plated $TiCl_3$ single crystal on In/Mo template.

indium ball was melted and allowed to spread out on the Mo plate which was heated on a hot plate in a dry box, Then the gold plated $TiCl_3$ crystal was put on the melted indium. This process did not cause any loss from the $TiCl_3$ crystal, since the melting point of indium (m.p. 176°C) is lower than the sublimation temperature of the $TiCl_3$ crystal (s.t. 486°C). The molybdenum plate with the $TiCl_3$ crystal attached was then clipped to the sample holder which is attached to the manipulator. Voltages could be applied for heating and temperature was checked using a thermocouple (chromel/alumel) which was placed in between the molybdenum plate and the sample holder. The manipulator with sample holder was set up in the UHV chamber for the surface structural studies.

D. Auger spectra of gold plated and clean $TiCl_3$ crystals

The Auger spectrum was recorded for both the gold plated $TiCl_3$ crystal and the clean $TiCl_3$ crystal after the gold layer was removed by argon ion sputtering. The Ar ion beam energy was set to 1 kV, with a current of 2.0 μA, and $5x10^{-5}$ torr of Ar pressure was employed. These spectra are shown in Figure 3.6. For the gold plated surface, Auger peaks which are characteristic of gold appeared at 150, 160, 184, and 239, eV and the indium peak appeared at 404ev. Carbon and oxygen are also found at

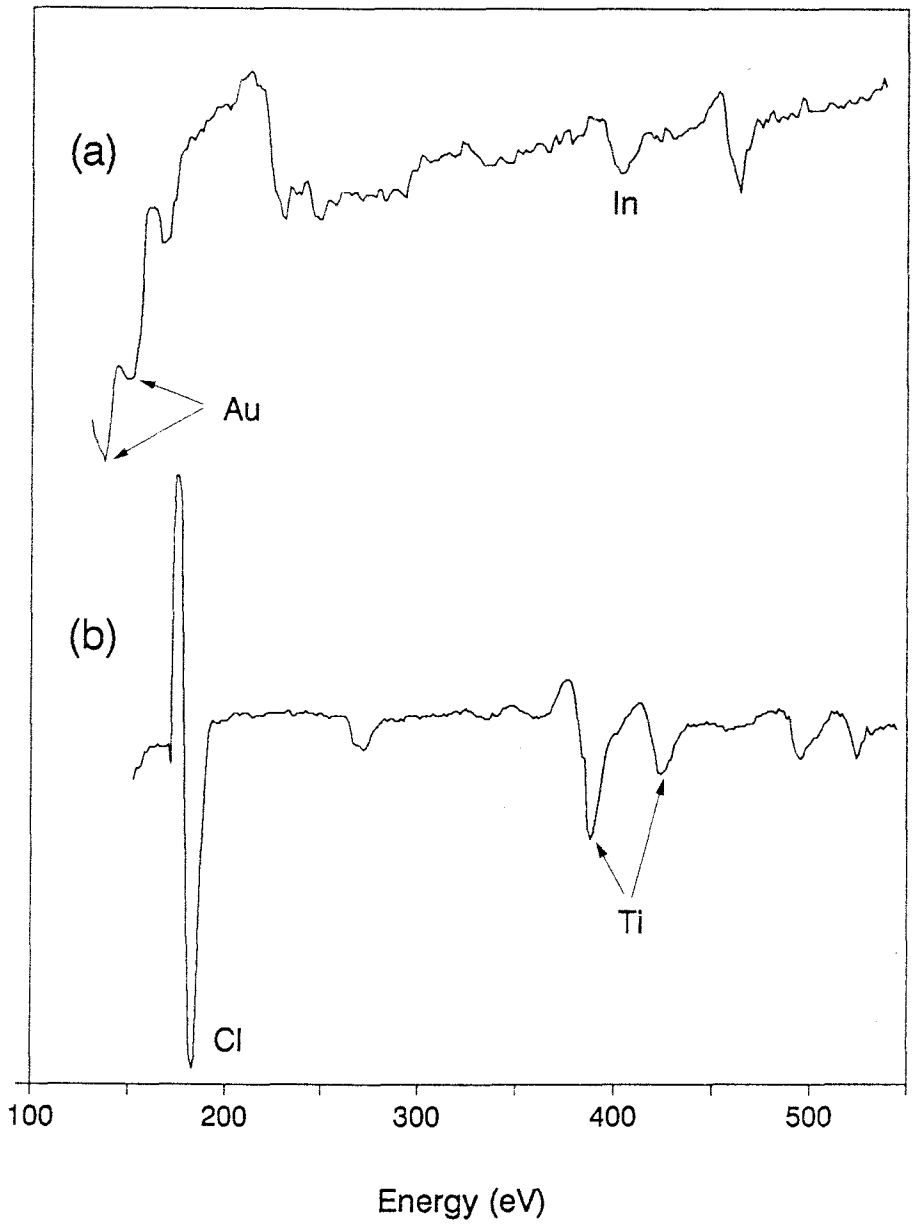

Figure 3.6 Auger spectra of $TiCl_3$ crystal (a) gold-plated (b) clean.

273 and 513 eV respectively on the gold plated surfaces of $TiCl_3$. Titanium and chlorine peaks were not observed, which indicates that the gold-layer was thick enough to prevent the escape of Auger electrons from the $TiCl_3$ crystal. Then the gold layer was removed by repeated Ar^+ ion bombardment. The Auger spectrum for the clean $TiCl_3$ surface after removal of the gold layer is shown in the bottom of Figure 3.6. Gold peaks were not found on the spectrum any more and sharp titanium and chlorine peaks appeared at 388, 419 and 273 eV respectively.

E. LEED pattern of the clean $TiCl_3$ crystal

We attempted to observe the LEED pattern after following the cleaning procedures described in the previous section. The $TiCl_3$ crystal was annealed to repair the surface damaged caused by the repeated Ar^+ bombardment. The annealing of the crystal was carried out both with and without the application of a chlorine flux to saturate the surface with chlorine while heating at 165°C overnight. After annealing the LEED pattern. was checked. Unfortunately, a good LEED pattern was not observed except for an increase in the diffuse scattered background. This diffused LEED pattern might be influenced by the following two reasons; a damaged surface by Ar ion beam during removal of the gold layer which

would result in disordered crystal surface; low annealing temperature which was not sufficiently high to repair the damaged surface. The annealing temperature could not be raised up above 165°C because of the low melting point (176°C) and high volatility of the indium, even though a good annealing temperature was thought to be higher than this. Actually a small indium peak was found in the Auger spectrum of a $TiCl_3$ crystal that had been annealed overnight. This indicated that some indium may have evaporated. Despite repeated annealing under various conditions, we could not obtain a sharp LEED pattern. These results, the failure of the regular LEED technique on the real catalyst ($TiCl_3$ crystal), required us to employ another technique which allows surface structural studies on the disordered surface.

The following chapters describe some of the relevant experimental procedures and calculations in the Diffuse LEED technique.

IV. EXPERIMENTAL PROCEDURE

A. Experimental set-up

1. General description of equipments

The experiments were carried out in a standard stainless steel UHV chamber, equipped with nine ion pumps in the lower portion along with a titanium sublimation pump (TSP). The UHV system was initially rough pumped by employing a liquid nitrogen cooled sorption pump or by using an oil diffusion pump in some cases. The UHV chamber was equipped with four grid LEED optics which also functioned as an Auger spectrometer which will be discussed later. In addition, the chamber was equipped with a quadruple mass spectrometer (Dycor M 200), an Ar ion sputter gun and a nude ionization gauge for pressure measurement. The LEED optics and vacuum chamber were enclosed by two sets of Helmoltz coils to minimize magnetic fields near the crystal. These coils were adjusted until there was no significant deflection of the specularly reflected beam over the energy range used for DLEED experiments. A diagram of the UHV chamber showing the locations of the various devices which were used in the experiments is illustrated in Figure 4.1. The manipulator is a high precision manipulator allowing x,y,

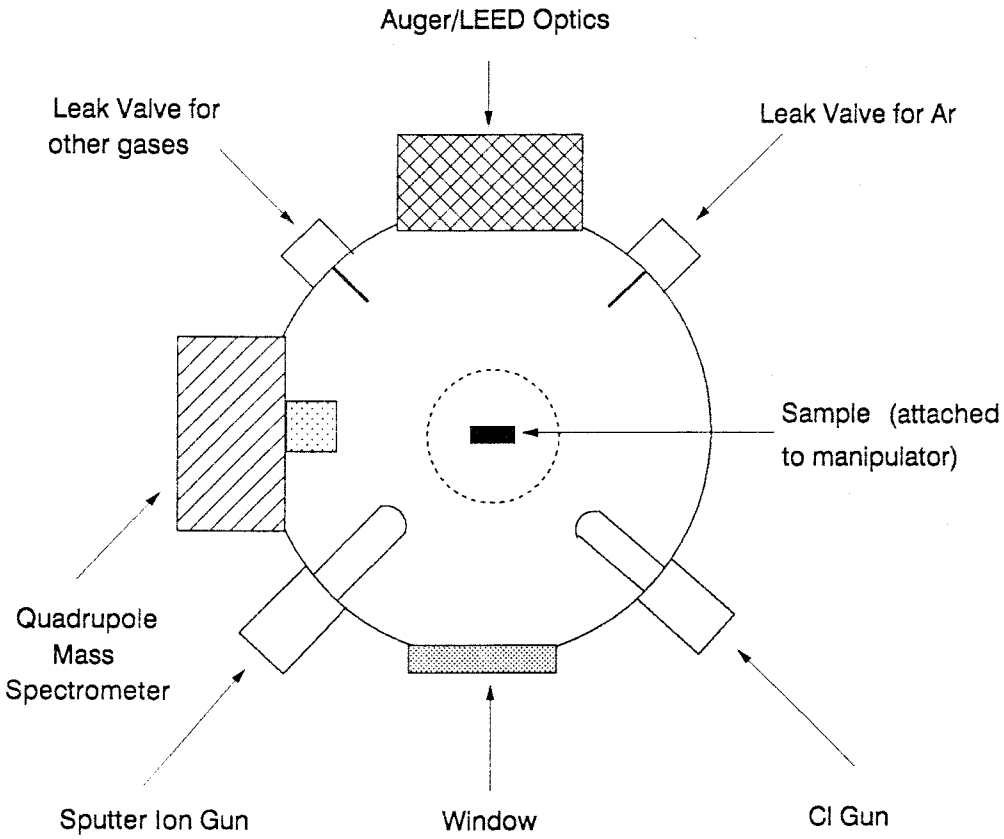

Figure 4.1 Diagram of UHV chamber used in the experiments

and z translations, tilt and azimuthal adjustments (Vacuum Generators, United Kingdom). The chamber was initially evacuated using the roughing pumps until a pressure of about $1x10^{-5}$ torr was obtained and Then the ion pumps and the TSP were started.

While running the ion pumps and the TSP, the whole chamber system was baked out for several days to achieve UHV. The baking process was described in the previous UHV section. When the period of bake out was terminated, the ovens were removed from the chamber. At this time the chamber was still warm, and all of the filaments which were to be used for experiments were degassed by heating them to their operating temperature, usually for 5 minutes. This process included the ion gun, the electron gun, vacuum gauge and mass spectrometer filaments as well as additional heating elements attached to the sample. The degassing job was done while the chamber was still warm so that any desorbed gases were not re-adsorbed onto the walls of the chamber. The base pressure of the chamber was maintained at below $2x10^{-10}$ torr.

2. LEED system

The essential requirements for a LEED experiment are an electron source or gun, a sample manipulator and a means of displaying or recording the diffracted beam

intensities. The intensity of the electron beams diffracted from the crystal surface may be measured directly, for example by collecting an electron beam in a Faraday cup, or indirectly by causing the electrons to impinge on a screen coated with a phosphorescent material and then measuring the brightness of the resulting spots of light. The latter method has the advantage of producing a pattern which can be viewed by eye. The most common form of a LEED apparatus comprises a hemispherical phosphorescent screen with a fixed electron gun aligned along the central axis of the screen. The crystal sample is positioned at the center of radius of the hemispherical screen. With this arrangement, diffraction beams emerging from the surface of the crystal travel radially towards the screen. The standard LEED system is illustrated in Figure 4.2.

The diffraction pattern is usually viewed from behind the crystal, so the observer can see only a projection of the pattern that forms on the screen. Consequently the screen is not constructed to form a hemisphere, and the angle subtended by the screen at the crystal is set at 60° about the central axis.

The screen is metallic and coated with a phosphorescent material. It is biased to 3-6 kV, so that the approaching electrons are accelerated sharply to the surface coating. Electrons which impinge on the screen

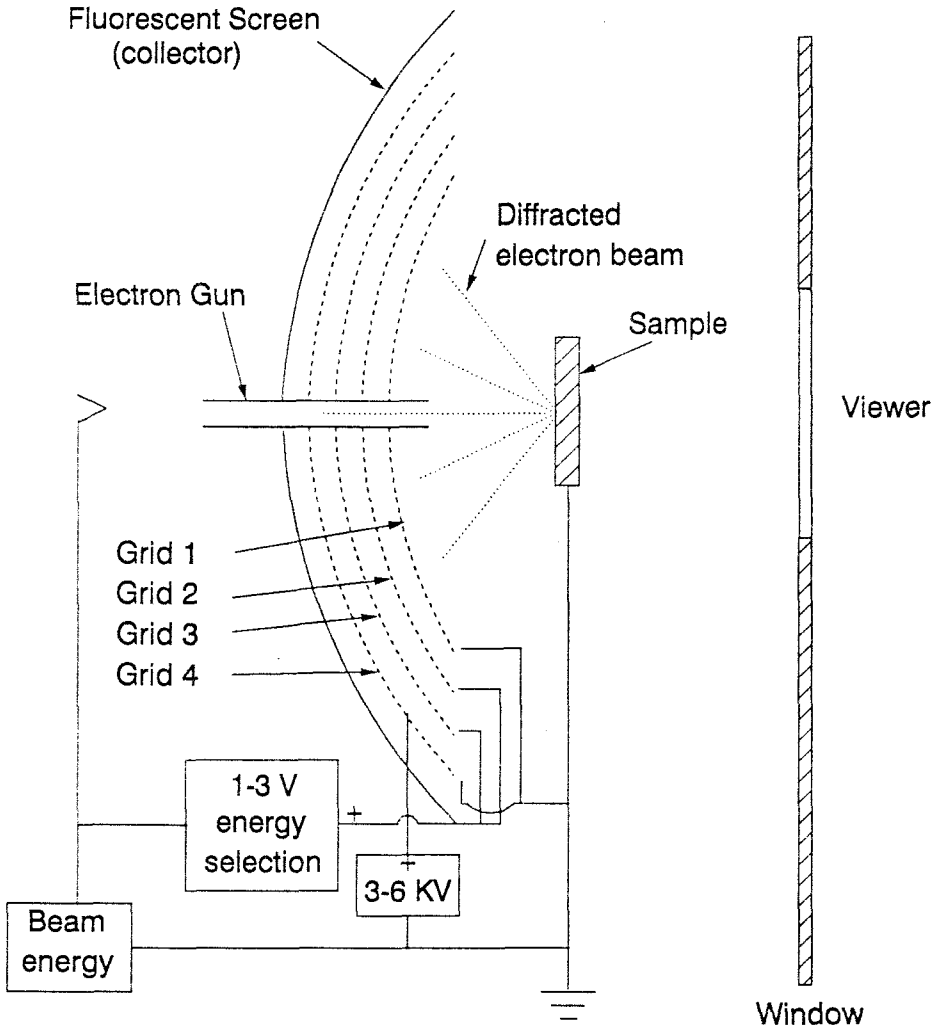

Figure 4.2 Schematic diagram of a standard LEED system.

create a glow proportional to the beam intensity. The metallic nature of the screen is necessary to permit the incident electrons to be conducted away, avoiding undesirable charging The grid nearest the sample (the first grid) is grounded so that the diffracted beams follow linear trajectories in field free space. Since the screen does not subtend an angle of 90 degree about the normal to the sample surface, not all emergent beams appear on the screen. The next grid away from the sample (the second grid) is maintained at a potential a few volts below the incident electron beam. This way it acts as an energy election grid; electrons which have lost more than a few volts, and can not therefore be part of the "elastic" diffraction process, have insufficient energy to pass this grid, and so can not reach the phosphorescent screen.

In a four grid optics system, the second and third grids are linked together to improve their energy selection characteristics, and the fourth grid is grounded, to isolate the phosphorescent screen potential from the energy selection potential. For the purpose of the LEED experiment, two grids are sufficient, but the four grid system provides more accurate energy selection. This is an advantage when the system is used for AES.

3. Auger system

As discussed in chapter II.A, electron bombardment of a surface leads to the emission of secondary Auger electron that have kinetic energy characteristic of a particular element. Since the Auger process is weak, it leads to an electron current which is trivial compared with the total current of secondary electrons. The quantitative detection of Auger electrons against this background emission, whose amplitude may vary considerably with energy, therefore poses a problem. This can be overcome by employing the technique of phase sensitive detection (PSD). A consequence of using PSD is that the Auger peaks are recorded as the first derivative of the original curves.

The Auger system used in this study was of the four grid LEED optics type. This grid arrangement may also be used as a retarding field analyzer (RFA), for obtaining Auger spectra. A diagram of the RFA configuration is shown in Figure 4.3. When an RFA was used for taking Auger spectra, the grid system was set up with the sample. Grids 1 and 4 were grounded and grids 2 and 3 functioned as repeller grids to allow only electrons with energies greater than the applied potential to pass through to the collector. The DC potential was applied to these grids and scanned over the voltage range of interest. This

RFA SYSTEM FOR AUGER SPECTROSCOPY

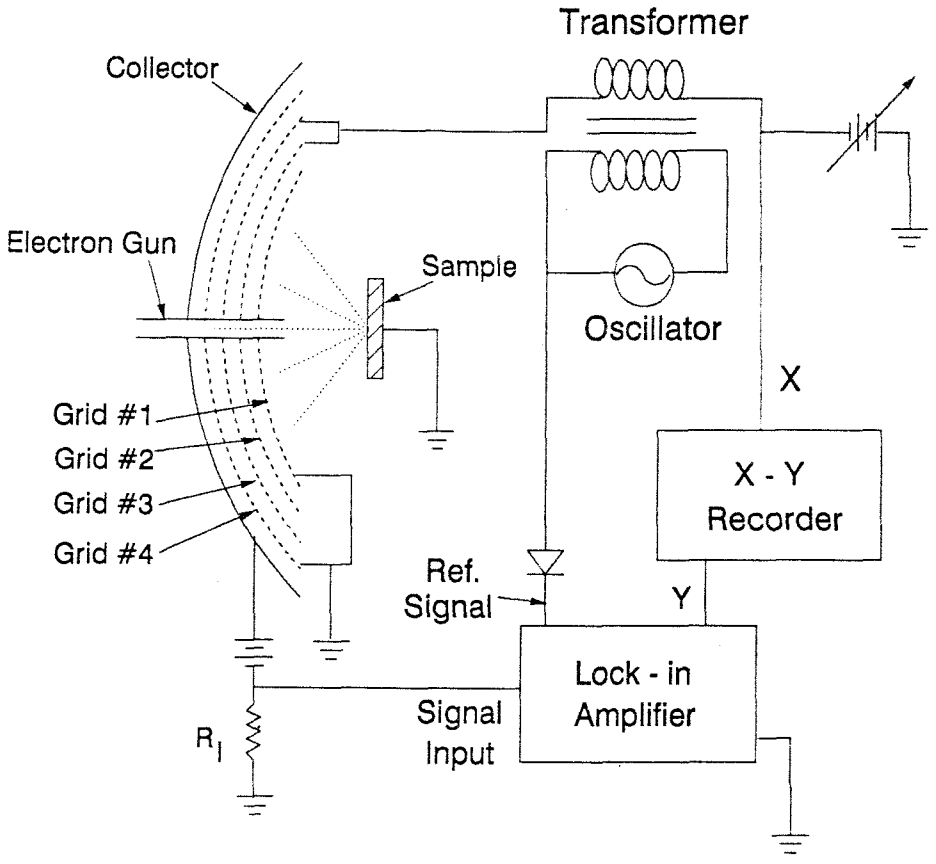

Figure 4.3 Diagram of grid optics and an RFA configuration set up for taking Auger spectra.

signal was monitored on the X channel of an X-Y recorder. When the spectrum was scanned, the Auger signal was displayed as a second derivative of the collector current, which is the first derivative of the Auger electron distribution (described in chapter II.A). Auger spectra collected using a Varian model 891-2145 electron gun control module at a beam energy of 1 kV and a beam current of 20.0 μA.

B. Preparation of Sample

1. Crystal orientation

The sample of titanium single crystal with the (0001) face exposed was cut from a titanium single crystal rod, which is 99.999 % pure and 1 inch long (Materials Research Corporation, Orangeburg, New York). The sample crystal was oriented using the Laué back reflection technique [56,57].

Before the Laué photo was taken, the expected Laué pattern for the (0001) surface of the hexagonal closed packed titanium single crystal was simulated using a computer program. The program was originally written to be suitable for the IBM mainframe computer by E. Preuss [58], but was modified for the Vax by Dr. P.R. Watson. The computer program, actually the O.S.U. version of

Preuss' program, allows one to calculate the possible positions and corresponding intensities of all Laué spots which will occur in the various Laué patterns. The theoretical positions and intensities of the Laué spots in the Laué pattern for the Ti(0001) surface were calculated by the computer program. The calculated data from the Vax was transfered into the Personal Computer and plotted to give the Laué pattern. Figure 4.4 is a Laué reflection diagram of the Ti(0001) surface which as simulated by the computer program.

The plotting program was written in the Quick Basic language and listed in Appendix 1. The program draws filled circles for the expected Laué spots, makes the sizes of the circle proportional to the diffracted intensities, and describes the film distance, lattice parameters and angles. Also the plotting program skips the Laué spots which have relatively low intensities and the same symmetry in order to avoid overlapping. The HP 7440A plotter was used to plot the simulated pattern.

The Laué reflection photo was taken using an X-ray spectrometer (Philips). The sample crystal rod of 6 mm diameter was glued on the top of an aluminum rod which was installed in a goniometer. The distance between the sample crystal and the film (Polaroid T-57, 4x5 in., U.S.A.) was kept to 3 cm. The angle of the crystal which is oriented to the (0001) plane was gradually adjusted

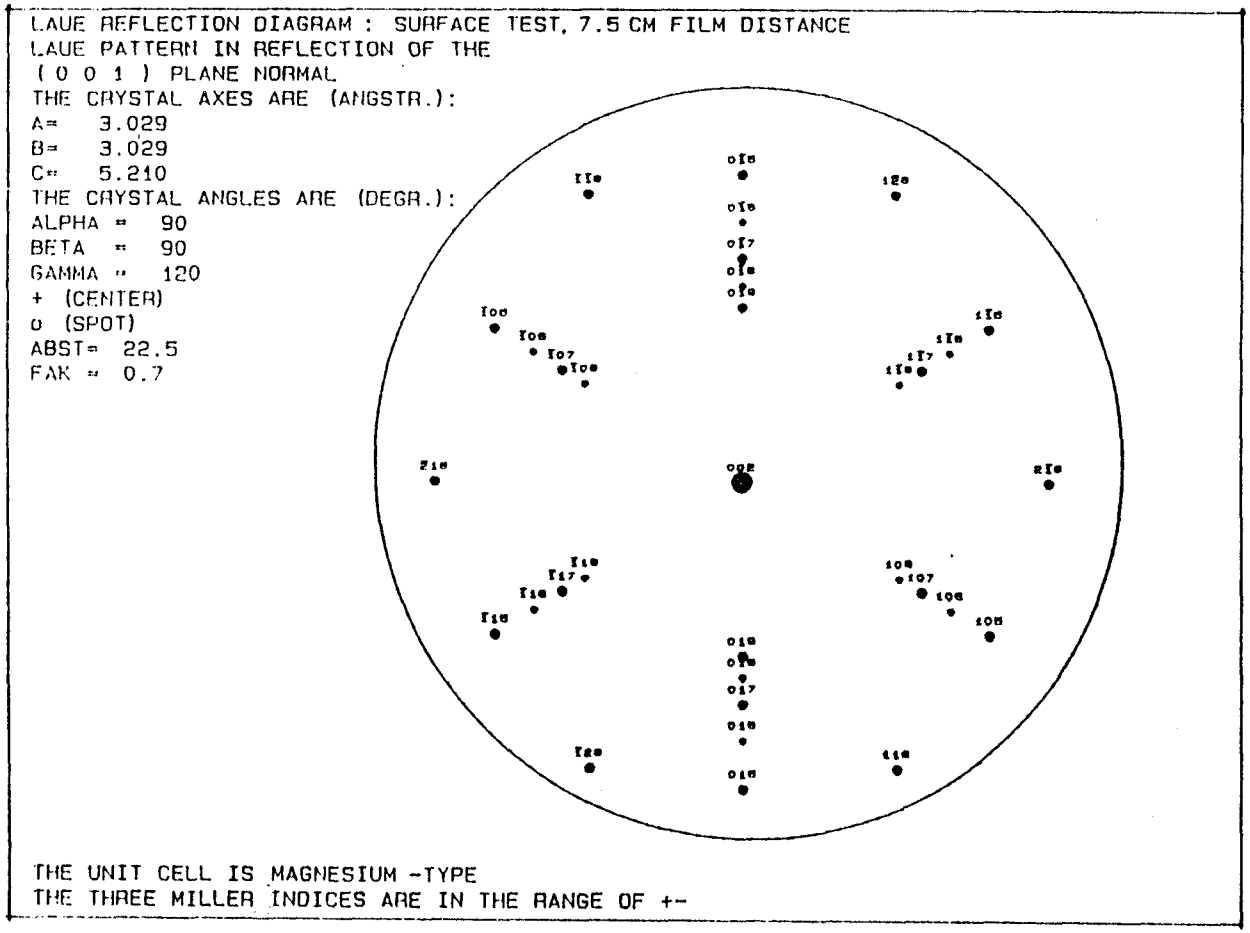

Figure 4.4 Simulated Laué pattern for the Ti(0001) surface.

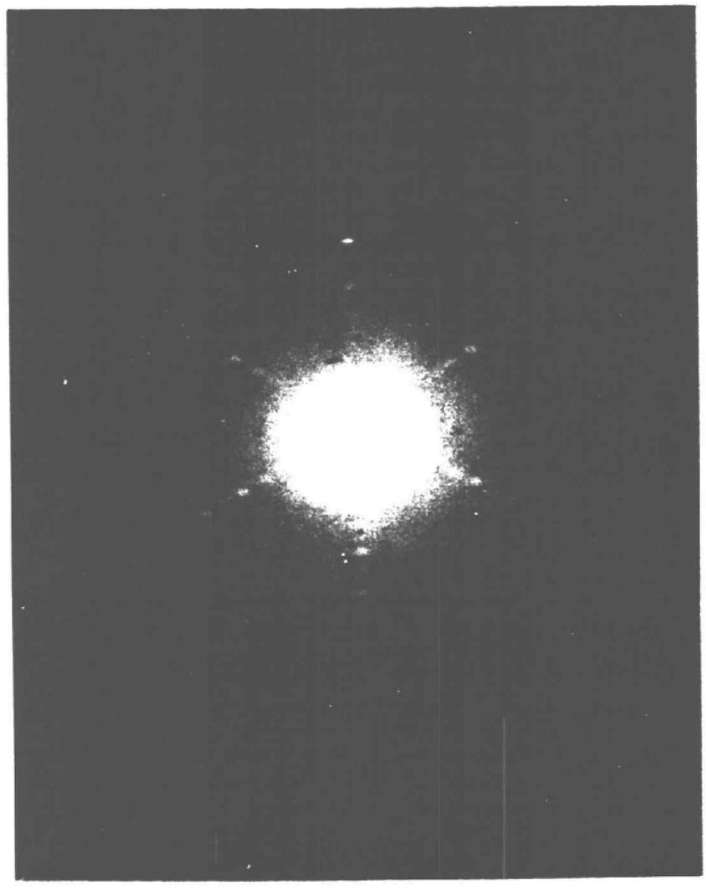

Figure 4.5 The Laué photo for the Ti(0001) surface which is taken by Laué back-reflection technique.

with the aid of Greninger net. The film was exposed for about 100 minutes, with a voltage of 31 kV and a current of 18 mA. The Laué reflection photo for the Ti(0001) plane is shown in Figure 4.5. The sample crystal was cut to a thin slice by wire saw.

2. Polishing

Standard metallographic polishing methods [59] were employed to prepare the sample crystal. A disk shaped single crystal of titanium with a diameter of 5.7 cm and a thickness of 0.43 mm was mounted in Acrylic plastic with the oriented face exposed on the one side. The sample surface was then polished using gradually smaller particle size polishing compounds which were dispersed in water and subsequently applied to the polishing clothes attached to a polishing wheel. Commercial polishing compounds and clothes were used (Buehler,LTD., IL, U.S.A.). Various particle sizes of polishing compound from 12 microns down to 0.05 microns were used and the polishing compounds were composed of either silicon carbide or aluminum oxide. The aluminum oxides were the finer particle size compounds.

As the sample surface was polished down, the particle size becomes smaller and smaller and thus the Ti surface flows out producing a disordered layer of metal. An acid etching solution was applied to get rid of this

layer while the polishing was performed with the finest compound.

The etching solution for rough polishing was prepared by mixing 250 ml of distilled water, 22 ml of 70% HNO_3 and 3 ml of 48% HF. The etching solution for fine polishing was prepared by mixing 200 ml of distilled water, 30 ml of 70% HNO_3, 3 mL of 38% HF and 20 mL of H_2O_2. By using the acid etching solution during or after the polishing operation, the surface damage on the crystal was removed. Also the etching solution speeds the removal of fresh surface from the face of the crystal. The removal of the distorted upper layer of metal turned out to be essential for obtaining a good LEED pattern. After the polishing was done, the sample crystal mounted in Acrylic plastic was separated from the plastic by soaking in acetone overnight. By applying these procedures, a mirror finished surface on the sample was obtained.

The polished crystal was next cleaned in a series of solvents which can get rid of any organic materials which may have accumulated [60]. Then the crystal was carefully sonicated in an ultrasonic cleaner using a laboratory detergent. After rinsing the crystal with distilled water, sonication was continued using a solvent series of acetone, methanol, and trichloroethylene.

3. Mounting

In order to mount the sample to the sample holder in a manner which allows for heating and cooling, a tantalum heating wire was spot welded around the outside edge of the disk shaped crystal. In addition, a thermocouple (chromel-alumel) was spot welded to the unpolished back side of the sample. The ends of the heating wire were also spot welded to the electrical posts on the manipulator arm. A drawing of the sample holder used in this study is shown in Figure 4.6.

The output which the power supply can support was 70 A at about 7 volts. One heating lead was connected directly to the chamber by means of a grounding strap so that the negative side of the heating power supply was operated at ground potential. This way of grounding prevented the sample from charging when an electron or Ar ion beam was impinging on the crystal. This arrangement permitted the use of a programmable temperature controller to linearly vary the heating rate, monitor the sample temperature and main constant elevated temperatures. The sample was cooled down by means of an electrically isolated copper cooling lead which was attached to a liquid nitrogen feed through. The end of the cooling lead was connected to one of the terminals of sample to which the tantalum heating wire was welded. Liquid nitrogen

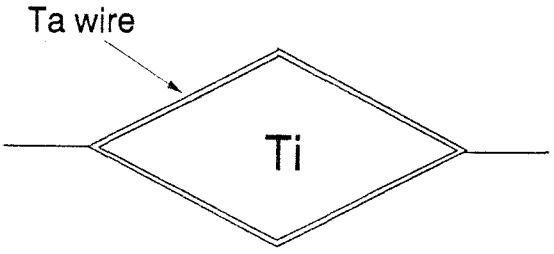

(a)

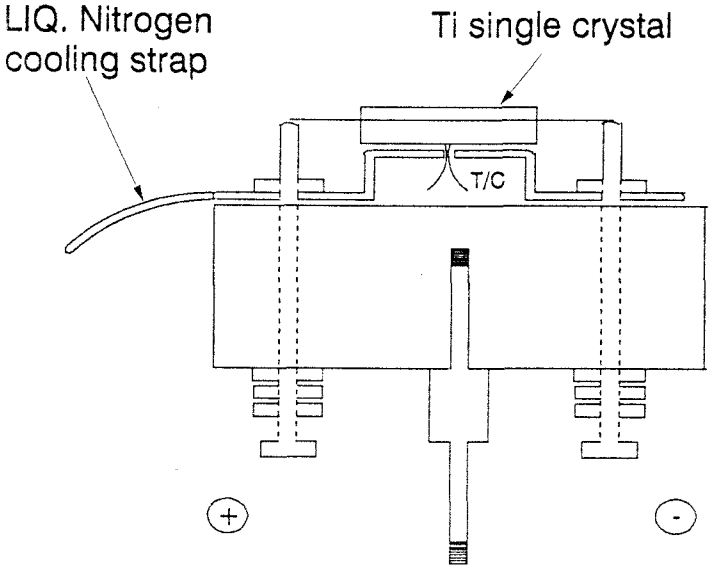

(b)

Figure 4.6 Schematic diagram of the sample holder which is used to attach the titanium single crystal sample (a) top view (b) side view.

cooling enables one to achieve the temperature of about 130 K.

C. Cleaning of the sample

Although the sample crystal was cleaned by etching followed by sonicating, the sample surface which is set up in the vacuum chamber is still dirty, covered with various gas molecules, adsorbed organic molecules and strong oxide layer. This is to be expected since the sample has been exposed to the Acrylic plastic, organic solvents and air. Also the sample surface was damaged by successive polishing steps which may result in poor LEED patterns. Therefore *in-situ* cleaning has to be performed on the sample surface to be studied. In general, there are two ways that have been extensively used.

The first is the use of Ar ion bombardment of a surface, which removes the impurity layers of the surface by sputtering. This technique is effective in the removal of many atomic layers of a surface and even though an impurity species is often far less effectively sputtered than the substrate it can be removed eventually. One disadvantage of ion bombardment, typically at energies of 0.5-5.0 kV, is that the surface is left in a heavily damaged state, usually with embedded Ar atoms. The surface must be annealed to reconstruct the order. This

in itself can create problems. For example, dilute impurity species in the bulk of a solid can preferentially segregate to the free surface and if a clean sample surface is heated, the diffusion rates of impurities are increased and further segregation can occur. This then requires requires another ion bombardment followed by annealing and so on. Despite these disadvantages, the Ar ion bombardment is the primary cleaning method used for metal surfaces.

The second popular cleaning method is chemical cleaning. Chemical cleaning involves the introduction of gases into the vacuum system at low pressures (-10^{-6} torr or less) which can react with impurities on a surface to produce weakly bound species, which can be thermally desorbed. This method is mainly used for the removal of carbon from refractory metals such as Mo and W which can be cleaned of most other impurities by heating alone. Exposing such a metal surface to oxygen produces CO which when desorbed, results in the removal of C, from an oxidized surface. The oxidized surface can then be cleaned by heating alone.

In this study, Ar ion bombardment was used to perform *in-situ* cleaning. Ar pressures of $5x10^{-5}$ torr and a sample temperature of 600°C was employed. The Ar ion beam energy and the sample current were set to 1 kV and 2.5 μA respectively. Usually Ar ion bombardments were carried

out for about 30 minutes, then the chamber was pumped down. The final ion bombardment of the cycle was performed at room temperature. Many cycles of this procedure eventually produced a surface free of impurities except for carbon. The main impurity contained in the Ti crystal turned out to be sulfur which segregates from the bulk of the sample to the surface during heating. Another was carbon which usually results from adsorption of background CO onto the sample surface. This carbon was subsequently removed by flashing to 600°C for a period of one or two minutes as described elsewhere [61]. The flash to 600°C followed by one minute of annealing allows the surface damaged by the Ar ion beam, to heal itself. Any CO or other adsorbed gases are desorbed and heating drives carbidic carbon into the bulk of the sample.

It is known that the phase transition temperature of bulk titanium is 885°C [62]. The sample was therefore never heated above 750°C in order to avoid the possible damage to the crystal. It took several weeks before a the high quality of crystal surface was obtained by the repeated cycles of Ar ion bombardment and annealing. The cleanliness of the sample was checked using the Auger spectrum and the sharpness of the LEED pattern. All the experiments were carried out as soon as possible after cleaning to avoid contamination.

D. Chlorine gun and dosing

A molecular chlorine source, a so called "chlorine gun", was constructed and installed in the vacuum chamber for the purpose of chlorine dosing to the sample surface [63]. The great advantage of this solid state electrochemical cell is its ability to provide a high dosing level without a corresponding increase in the chamber background pressure. This aspect of the chlorine gun minimize the corrosion of the vacuum chamber and other installed equipment, and reduces wall adsorption effects. A diagram of the electrochemical cell used as a chlorine source is shown in Figure 4.7.

The basis of the chlorine gun is the electrochemical cell $Ag/AgCl/Cl_2/Pt$, in which silver chloride is electrolyzed to silver and molecular chlorine. This involves the electric field induced motions of Ag^+ ions through defects in the AgCl lattice. It was necessary to heat the cell to 330 K in order to increase the mobility of Ag^+ ions in the AgCl, thereby lowering the cell resistance. The cell consists of a pellet composed of 96% AgCl and 4% $CdCl_2$, used to increase the conductivity of the cell. The pellet is encased in a pyrex tube and assembled onto an eight-pin UHV flange. The cell electrodes consist of a silver wire cathode and a platinum mesh anode fused to opposite ends of the pellet by heating

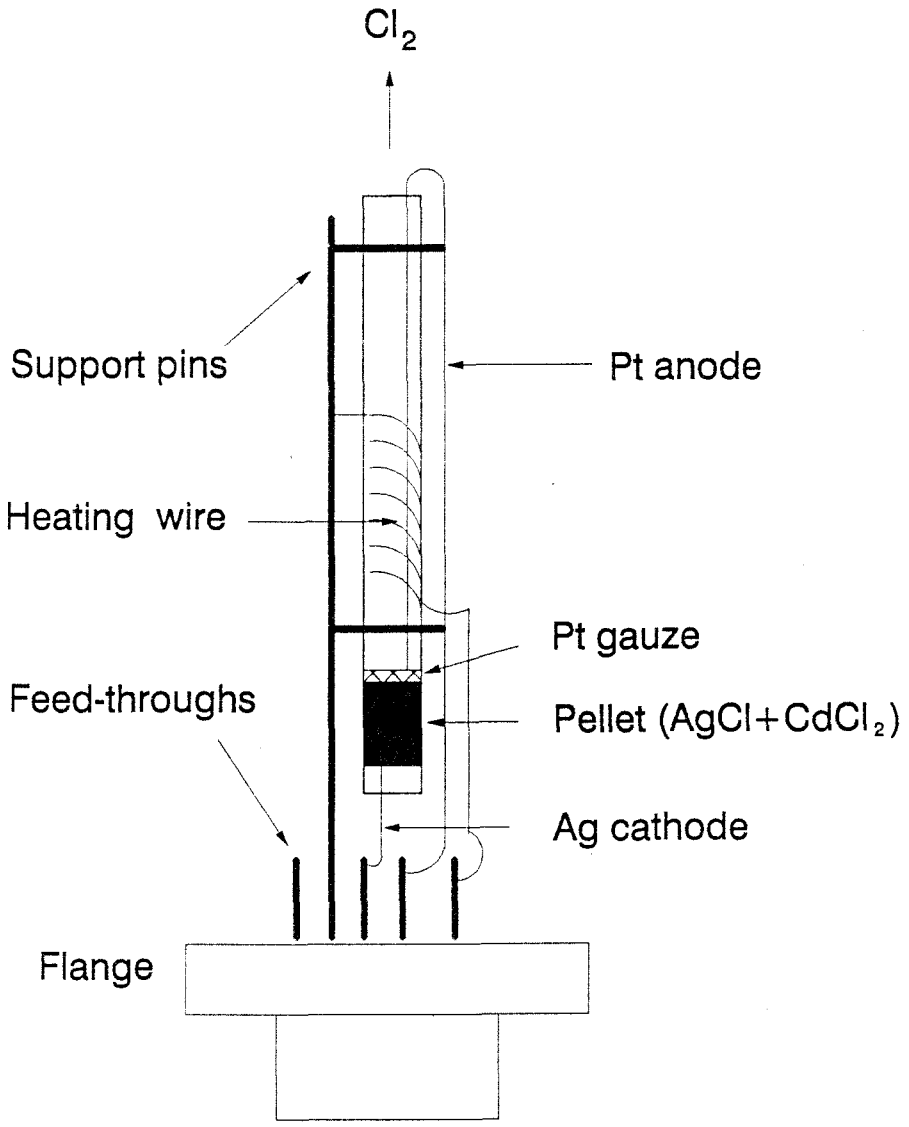

Figure 4.7 The solid state electrochemical source of chlorine.

the tube to near the melting point of the AgCl. The pellet-electrode composite was made by the mechanical pressing instead of completely melting the AgCl. The pyrex tube was wrapped with nichrome wire for heating. During the pressing operation, a thermocouple was incorporated into the pellet, and spot welded to the appropriate pin of the feed through. The Ag wire cathode was also connected to the feed through by using a barrel connector.

Ideally based on Faraday's law, it was calculated that the passage of about 80μC of charge through the cell should result in monolayer coverage with chlorine atoms for a 0.5 cm^2 sample. A constant unit sticking coefficient was assumed without any losses to the gun. Experimentally testing, it was found that a monolayer coverage of chlorine came from a Cl_2 dose equivalent to the passage of roughly 5000-6000 μC (1.7-2.0 % efficiency) of charge through the cell, given a constant unit sticking coefficient.

E. Camera set-up and measurements of DLEED intensities

As previously mentioned in chapter II.3, a fast and sensitive data acquisition system is very important since for long measuring times residual gas adsorption may occur and contribute to the diffuse background. Moreover, high

speed data collection is important because a large amount of data is expected. On the other hand, the diffuse intensities are usually weak compared to the normal LEED beam intensities and therefore the detector used must be of high sensitivity. Obviously high energy resolution also would be a desirable property in order to avoid electrons being scattered inelastically by surface phonons. This requirement, however, can be omitted as the phonon influence can be canceled out by the subtraction of the clean surface signal. These requirements can be satisfied by employing a video based TV computer method, which originally was used for conventional LEED experiments [42,64] but was recently modified to cover the area of diffuse LEED [28].

In this study, the diffuse LEED intensities were measured by the TV computer method using an image intensifier camera in order to collect the weak diffuse intensities. The TV computer system consists of a low-light video camera (image intensifier, Cohu 5000 series), a video monitor, a video data acquisition card (Coreco, Oculus 200 + image analysis software) including a fast video memory, and a processing computer which controls data acquisition, data handling, and the production of 3-D plots. A VCR can be used to permanently record the images. A low light video camera was employed in order to be sensitive to the relatively weak diffuse intensity

signals. This was used after a warm up of at least 12 hours in a completely dark place. A schematic diagram of the TV computer system is shown in Figure 4.8.

The video camera views the diffuse LEED pattern from outside the UHV chamber, and converts the DLEED pattern into electric signals which are passed to the video card for display on the monitor. The computer can access the position and intensity of any of the (512x480) pixels in the image using software written by Dr. Scott Mokler and built around subroutines supplied by Coreco. For this experiment a windowing function was used to isolate the region of interest for the DLEED data.

For the DLEED data collection, the diffuse intensity map including 4 LEED spots, the (0,0), (1,0), (0,1) and (-1,1), covering a total of 180 x 360 = 64800 data pixels. Video images of the electronic window defined above were averaged (16 times) using the averaging function of the image analyzer (Oculus 200). Then the whole screen data file was saved to the hard drive. The saved data files of images were transfered to floppy disks for long term storage. The primary beam current was limited to 5 μA in order to avoid camera damage at the high intensity regions of the substrate spots. During the time which the video camera was on, the TSP was turned off to prevent a possible accident which may result in damage to the low light video camera. Data were taken at a low temperature

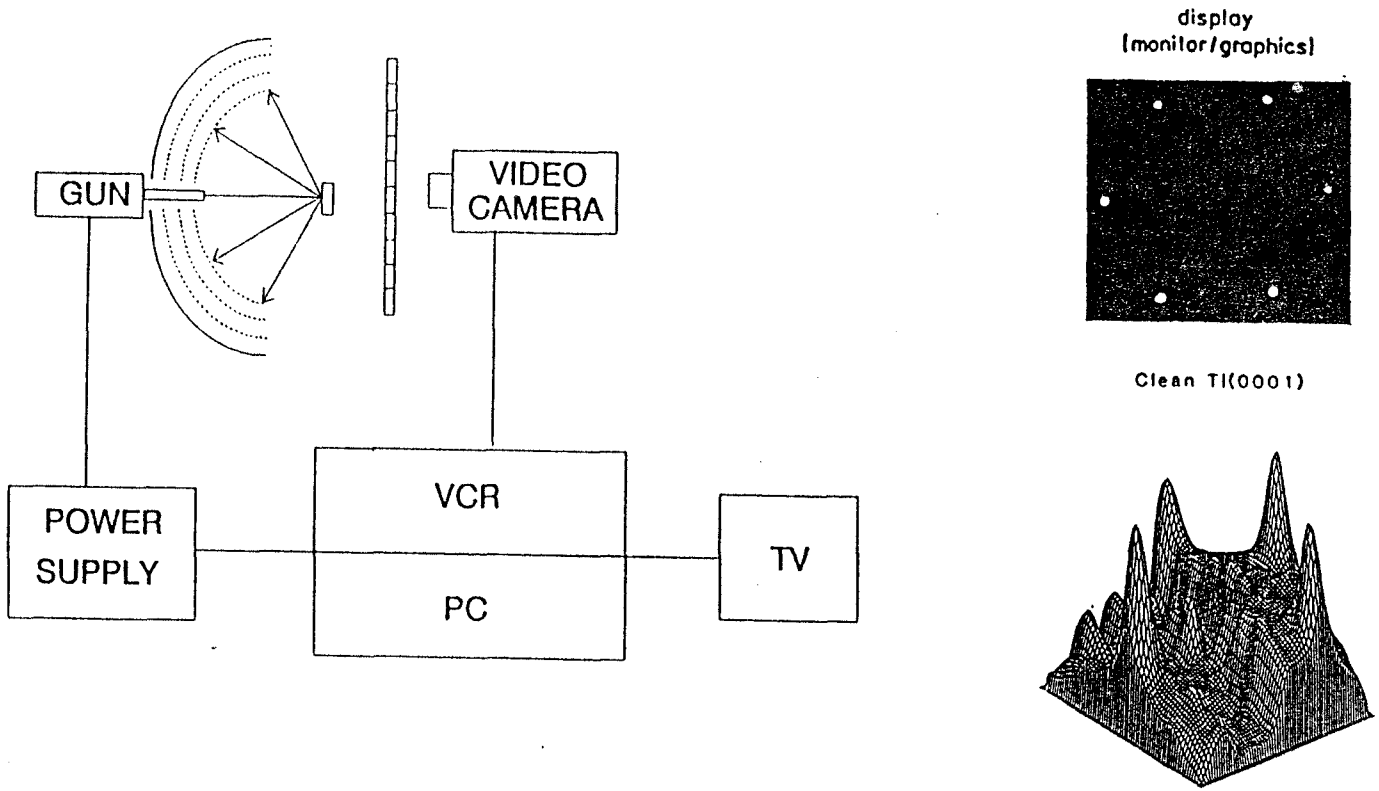

Figure 4.8 A schematic diagram of the experimental set-up for DLEED measurements

of about 170°K in order to reduce thermal diffuse scattering which would contribute to diffuse intensities. Another set of data was taken at room temperature to estimate the degree of thermal diffuse scattering. The contribution of phonons, mainly from substrate phonons as well as from the grids and from surface defect structures, was cancelled by simple subtraction of the diffuse intensity map of the clean surface which was measured separately.

All measurements were taken at normal incidence to the primary electron beam. The primary current was about 0.5 μA and the acceleration voltage onto the screen was about 3-4 kV. The diffuse intensities were measured in the range of 70 to 110 eV at 4 eV intervals.

Three sets of coverages of chlorine i.e. 10%, 20%, 40% were chosen. The coverages were produced by passing current to the electrochemical cell for the time, based on the uptake curve of chlorine on the Ti(0001) surface necessary to give the desired amount of Cl. Two sets of data corresponding to different settings of the gain control of the video camera were obtained.

F. Image processing

The digitized screen images, which were stored on the hard drive could be redisplayed on a video monitor. The

disordered diffuse LEED pattern had some amount of noise structure that was not removed by the 16 times averaging procedure. It was, in fact, due to the four grids of the LEED optics which are designed to repel the inelastically scattered electrons.

In order to manipulate the experimental data taken from the windowed part of the screen to an appropriate form which can be compared with theory, a series of manipulation procedures were carried out on the digitized pattern. A diagram depicting these procedures is illustrated in Figure 4.9.

The experimental data is first reduced in size for two reasons. First, the calculations are sufficiently complex that they are carried out on a sparse grid of about 100 points, so there is little point in having large numbers of experimental points. Secondly, the 3-D plotting program employed (Surfer, Golden software, Co) to visualize the data is limited to a 100x100 grid. This reduction procedure yields a grid of a convenient size, but may result in deformation in the shape of 3-D plot (in which case, the plots needs smoothing). The digitized experimental DLEED pattern was reduced to two different sizes of grid. The first was a 30x60 grid using a 6x6 matrix sampling method (1/36 reduction). The second was a 45x90 grid using a 4x4 matrix sampling method (1/16 reduction). The 45x90 grid file was used for the theory-

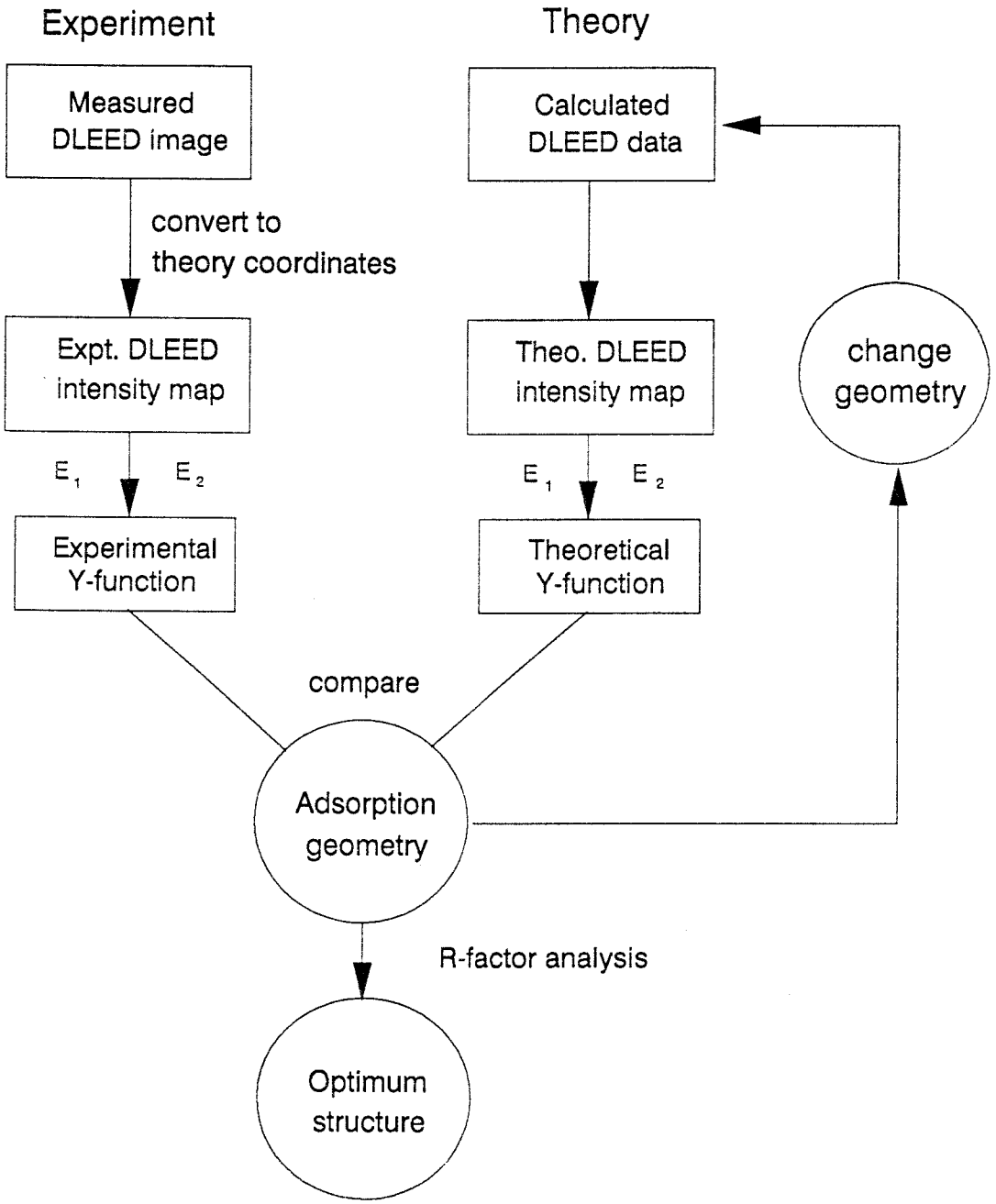

Figure 4.9 Schematic diagram of the procedures of DLEED analysis.

experiment comparison.

The second step in manipulating the experimental data is coding of screen x,y coordinates for the 3-D plot. This associates all the intensity pixel values of the grid with x,y and z coordinates in a manner that can be accepted by the Surfer program. This step allows the data file to be visualized as a 3-D plot; an example is shown in Figure 4.8.

The third step is the conversion of x,y and z screen coordinates to the k space values that are appropriate to the diffraction pattern; we convert the x,y coordinates of the plot file to k-space values via a set of conversion coefficients. These conversion coefficients are dependent on the electron energy and the grid size, and are derived from the following geometrical relationship between regular LEED spots of the clean sample surface based on 60 degree real space.

A diagram of a typical LEED pattern is shown in Figure 4.10.

$$K_x = a(X-X_{oo}) + b(Y-Y_{oo}) \qquad (4\text{-}9)$$

$$K_y = c(X-X_{oo}) + d(Y-Y_{oo}) \qquad (4\text{-}10)$$

where K_x and K_y are K-space values and a,b,c and d are the conversion coefficients. X and Y are the real space coordinates of the regular LEED spots and X_{oo} and Y_{oo} are the real space coordinates of the (00) specular spot in the center of the pattern. Two sets of the conversion

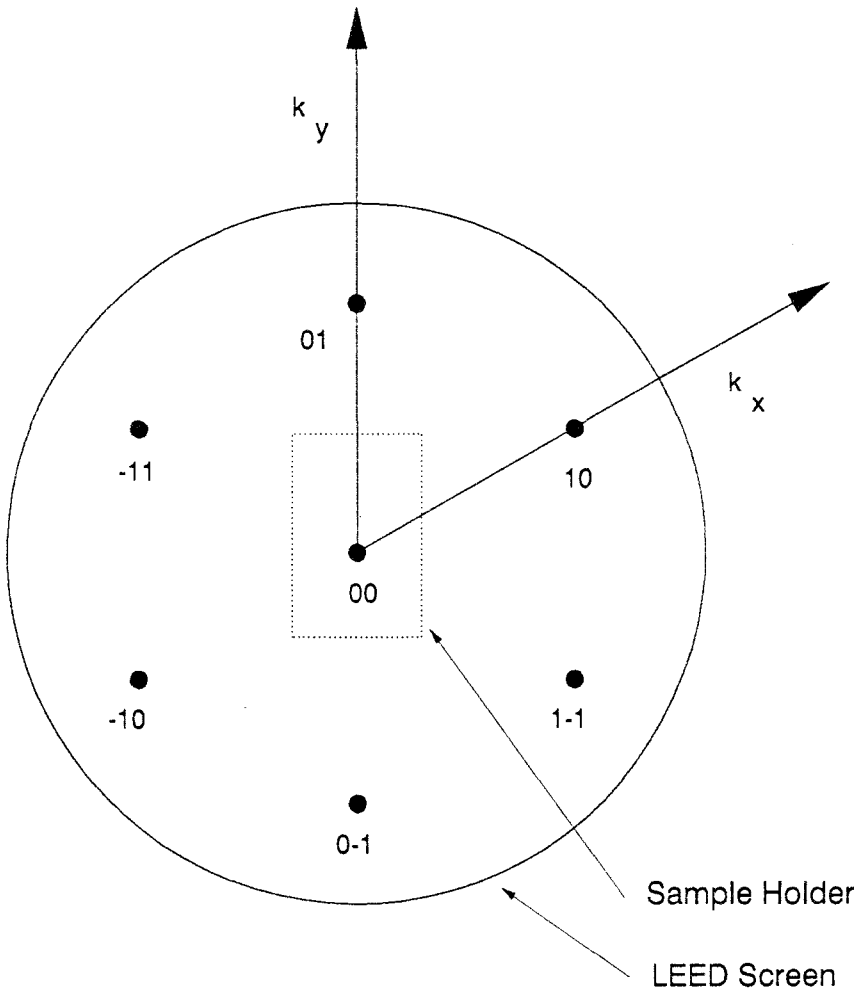

Figure 4.10 Diagram of the LEED pattern for the clean Ti(0001) surface.

coefficients as a function of electron beam energy and different grid size were derived and summarized in Table 4.1.

The fourth step is the matching of the experimental and theoretical data. This procedure first picks the closest experimental data points in a given size of circle in k-space with respect to each theoretical data point and then averages the diffuse LEED intensities in each circle (Figure 4.11). This procedure makes the experimental data set have the same format as the theoretical data set. At this stage, the procedure allows the experimental data to be plotted in a 3-D plot, coordinated with K-space.

The fifth step is the calculation of the Y function. As shown earlier in chapter II.3, it is known that the Y function, the logarithmic derivative of the diffuse intensity with respect to electron energy, is a good parameter for theory-experiment comparisons. The experimental data that was matched to equivalent k-space points where the calculations were performed is needed to calculate Y functions. The calculated Y function was then loaded to the Surfer program which produces a grid file written in binary code, for a 3-D plot or contour map. It took about 15 minutes to generate a grid file on the personal computer (Leading Edge model D2 with 80286 processor, 10 MHz speed, 80287 math co-processor installed). Noise in the experimental data was removed

Table 4.1 Conversion coefficients of k-space as a function of electron energy.

Size		30x60	45x90
Electron energy (eV)	Coeff.		
78	a	0.0007588	-0.0004502
	b	0.04414	0.02852
	c	-0.04533	-0.03112
	d	-0.02328	-0.01490
82	a	0.0003054	-0.0007258
	b	0.04344	0.02945
	c	-0.04604	-0.03179
	d	-0.02258	-0.01527
86	a		-0.0002604
	b		0.02955
	c		-0.03512
	d		-0.01631
90	a		-0.001055
	b		0.02991
	c		-0.03083
	d		-0.01733
94	a		-0.001332
	b		0.03071
	c		-0.03412
	d		-0.01607

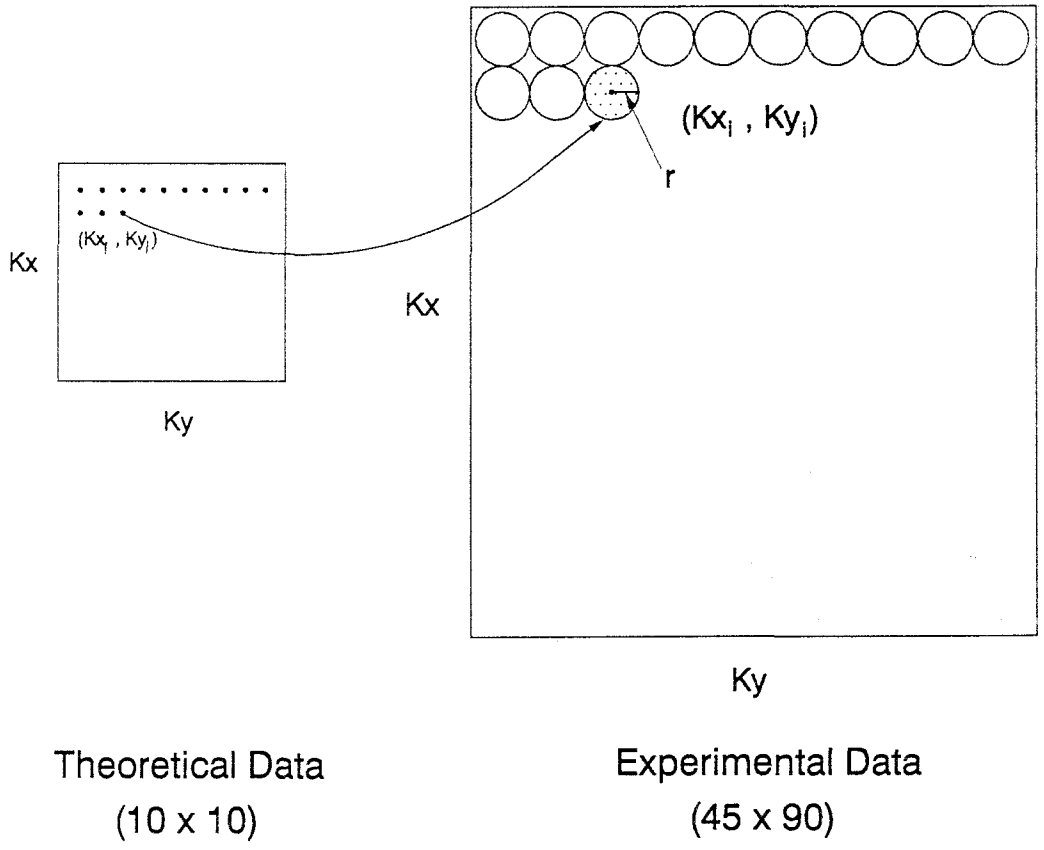

Figure 4.11 Matching of the experimental and theoretical data

using the matrix smoothing function in Surfer.

The final step was to match the smoothed experimental Y functions (Y_{ex}) with the equivalent theoretical Y functions (Y_{th}) to permit a theory-experiment comparison. The data are compared via the Pendry R-factor (R_p) defined in chapter II.3. All of these procedures were accomplished using the computer program which was written in Quick Basic for the personal computer and is listed in Appendix 2.

V. DLEED CALCULATION

In order to determine adsorption site and structural parameters, the experimental data should be modeled using a theory which describes diffuse electron scattering from a disordered adsorbate at low coverage. Diffuse LEED scattering theory differs from both conventional LEED and X-ray scattering. In X-ray scattering, the intensity of each Laué spot is determined by the product of an atomic scattering factor and a simple geometric structure factor. The positions of atoms within the unit cell are varied until the geometrical factors predict the correct intensity for each beam. The simplicity of this process is due to the fact that X-rays interact very weakly with matter. Each photon is backscattered after a single encounter with a lattice ion. Another result of this single scattering or kinematic scattering is that the spot intensities are independent of both the incident beam energy and the azimuthal angle of incidence. But neither of these are true in LEED calculations.

Structural determination from LEED is complicated by the fact that every electron undergoes multiple elastic scattering within the first few layers of the crystal surface. The main features of a LEED pattern (sharpness, streaking of beam spots and distribution of diffuse scattering) are governed by a kinematic structure factor

which depends only on the nature of the long-range ordering. This structure factor modulates a separable form factor representing the electron scattering (including multiple scattering) by atom clusters. The size of the form factor is determined by the electronic mean free path. This form factor includes all the short range structural information such as layer spacings, bond lengths, and bond angles. A multiple scattering theory of diffuse LEED should calculate the probability that an electron scatters at least once from an adsorbate displaying disorder. In general, two approaches have been used to calculate the resultant diffuse intensities for a given local geometry.

The first method is the "three step theory" which was developed by Saldin and Pendry [65,66]. In this method, the dynamic calculation of the diffuse scattering amplitude is separated into three steps in order to include multiple scattering of the low energy electrons [38]. First the wave function of the electron incident upon an adsorbed molecule is calculated using standard methods of multiple scattering theory. This involves the effects of reflection from the ordered substrate. This step generates the total incident wavefield which can be calculated by simple LEED theory for perfect, clean surfaces. In the second step, all scattering paths which start with the first encounter with the molecule and end

with the last encounter are included. In this step conventional LEED theory cannot be used because the presence of the molecule breaks the translational symmetry of the surface. This part of the calculation resembles the theory of SEXAFS [67] because it involves a spherical outgoing wave being backscattered by the atoms surrounding the adsorbate. A cluster calculation is used in this step. The cluster need only contain a finite number of atoms because inelastic events prevent the electron from escaping from a cluster that is more than a few angstroms from the scattering site. Finally in the third step, the diffusely scattered wave propagates away from the surface into the vacuum including possible LEED reflection from the substrate. This step is a time reversed calculation. Of the three steps, the second is least important since it is of at least third order in multiple scattering, and its contribution is generally weak. In addition, it is relatively time consuming to compute since it is evaluated in a spherical wave representation.

The second method is an extension of the beam set neglect method which was developed by Van Hove, Lin and Somorjai [53] and previously applied to ordered LEED calculations for systems with large unit cells [68]. This approach is based on the familiar concept of beam sets [69]. It effectively neglects certain beam sets from the weak and time consuming second step of the three step

method. The first and third steps are then efficiently combined and computed in a plane wave representation in a method analogous to a standard ordered LEED calculation. The calculation is limited to the integer order beam set generated by the ordered substrate and a fractional order beam set containing the exit direction and all shifted copies of it generated by the addition of a member of the integer order beam set. Then the overlayer scattering matrix is calculated which allows full intra-molecular multiple scattering, but neglects inter-molecular scattering paths. Consequently, only third and higher order multiple scattering events are neglected. The accuracy of this procedure has been demonstrated by comparison with the three step theory and was found to produce virtually identical results [38].

In this study, the program package which was developed by Van Hove and recently modified by Wander is used to calculate the diffuse intensities for a given local adsorption geometry. As the experimental data was collected, the diffuse intensities were calculated at several energies , from 78 to 94, every 4 eV, for the construction of the Y-function. The calculated Y-functions were then compared with the experimental Y-functions using the Pendry R-factor as a measure of the goodness of fit between the two data sets.

The inner potential was also considered in order to

avoid a further problem which may result in a poor fit. In conventional LEED, this parameter can be determined by fitting the theoretical and experimental curves by rigidly shifting the calculated I(V) curves with respect to the energy axis. In this DLEED study, several sets of calculations involving neighboring energies at 4 eV spacing with respect to the energy at which the experimental data collected, were performed. These calculations were compared with the experimental data in terms of R factors in order to solve the inner potential energy problem.

Four sets of calculations obtained at a series of neighboring energies were compared with the experimental data. The Pendry R factor analysis for the four sets of calculations and the experimental data favored the identical energy as indicated in the experimental data. Thus, there were no indicated discrepancies in inner potential between the calculations and the experimental data.

The titanium phase shifts were taken from Van Hove et al. [70] and are available in the OSU Van Hove-Tong LEED package The relativistic chlorine phase shifts were obtained from Norman [71] and are listed in Appendix 3. The atomic phase shifts up to l=6 were included.

VI. RESULTS AND DISCUSSION

A. Auger data

1. Auger spectra of Ti(0001) surfaces

It is necessary to be able to distinguish the differences between the Auger spectra of dirty, clean, and chlorine-covered titanium surfaces. Auger spectra measured for contaminated and clean Ti(0001) surfaces are shown in Figure 6.1. Significant amounts of carbon, sulfur and chlorine impurities are shown for the initial Auger spectrum of the sample [Figure 6.1a]. These impurities have characteristic peaks at 271, 154 and 183 eV respectively. As described in chapter IV.D, these impurities were reduced to levels of C, S, and O contamination of the order of 1% [Figure 6.1b] by many cycles of Ar^+ ion sputtering at high temperatures (650°C) and thermal flashes to 700°C for about 20 second. Since the clean Ti surface is very reactive, thermal flashing followed by annealing needs to be repeated in every hour to remove impurities re-adsorbed on the surface.

Typical Auger spectra for the chlorine saturated Ti(0001) surface, obtained after by a chlorine dose of 5000 μC is shown in Figure 6.2. In that figure a huge chlorine peak appears at 183 eV. A small amount of carbon

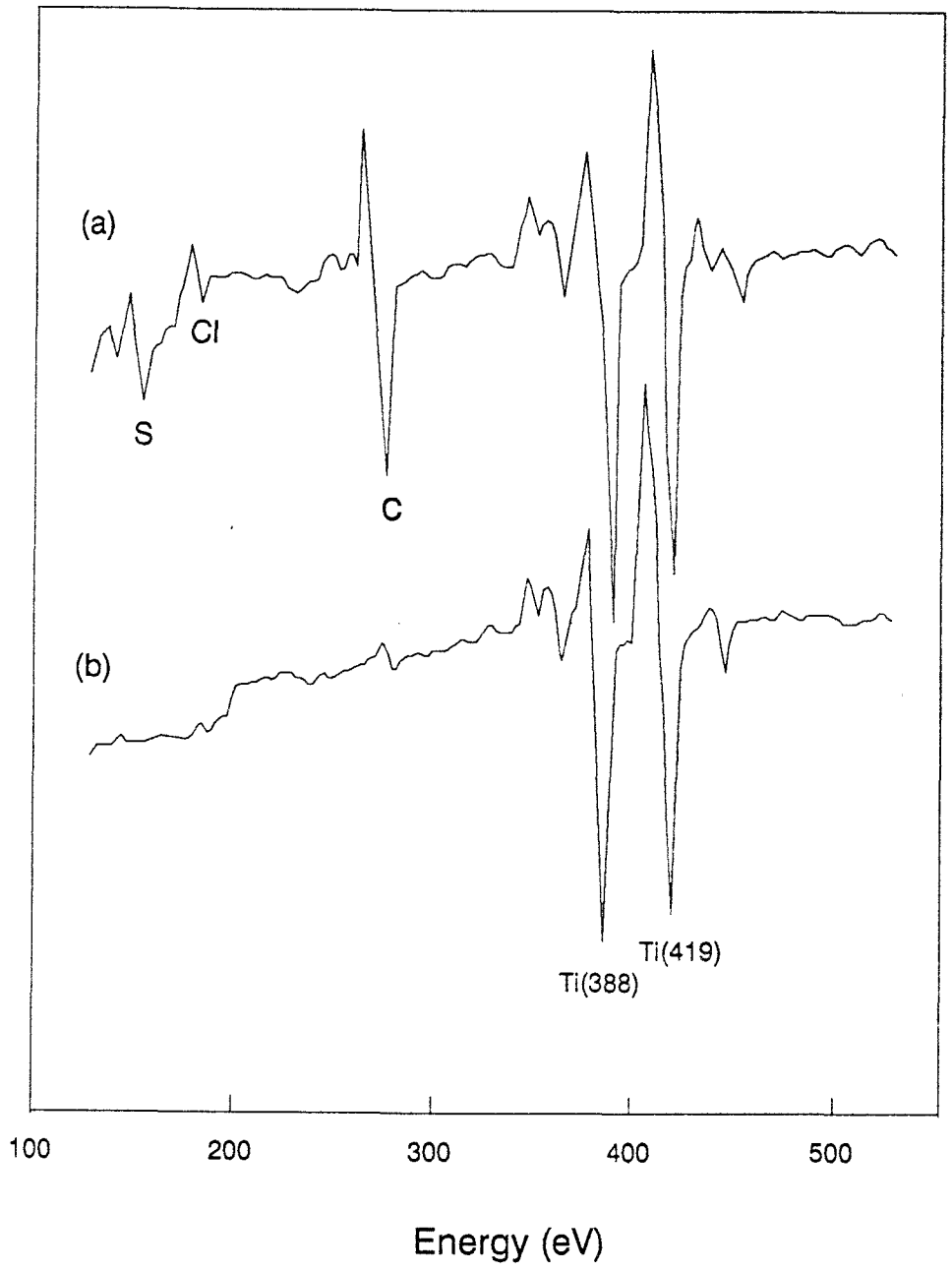

Figure 6.1 Auger electron spectra (1 keV,20 μA) of the Ti(0001) surface (a) dirty, (b) clean.

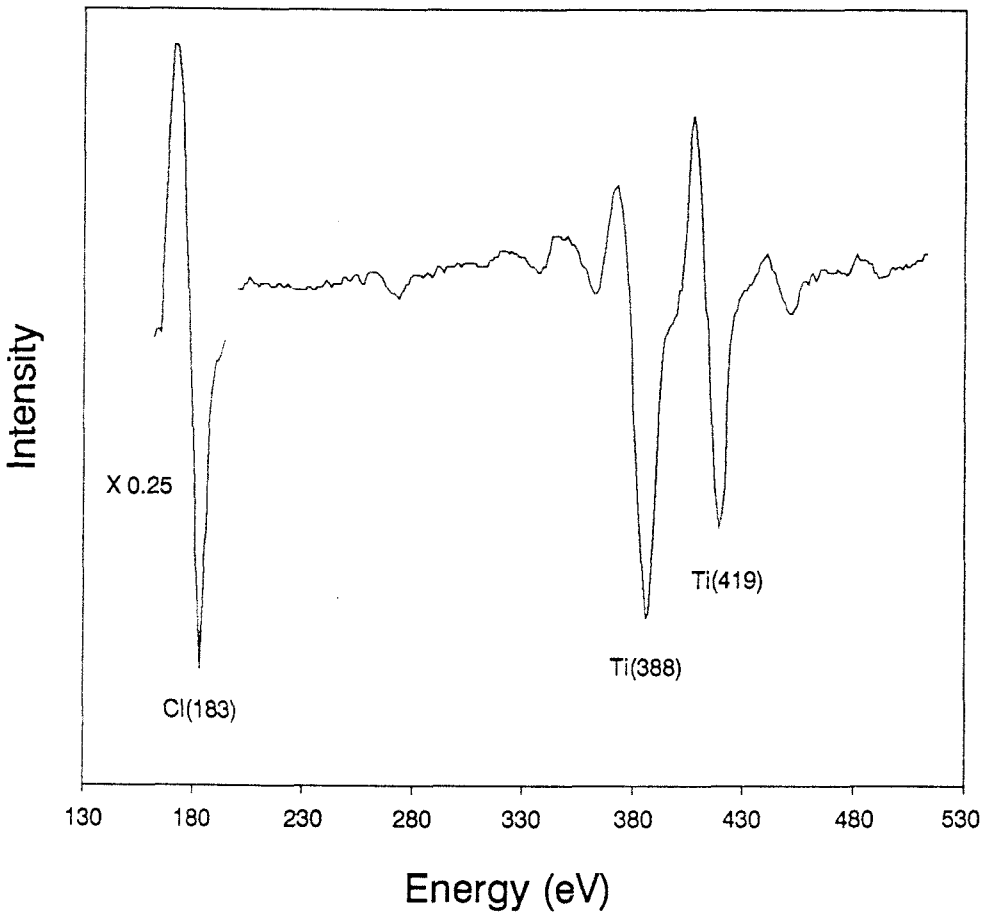

Figure 6.2 Auger electron spectra (1 keV, 20 μA) of the Ti(0001) surface saturated with chlorine.

still appeared in the spectrum, which is thought to be due to CO uptake, upon cooling.

2. Chlorine uptake on Ti(0001) surface

The Ti(0001) surface was dosed with chlorine by using the solid state electrochemical source described in Figure 4.7. The dose of chlorine was measured in microcoulombs of cell current, based on Faraday's law, not Langmuir. The chlorine source was warmed up overnight to 50°C before it was used. The electrochemical cell usually maintained a constant cell current, at a level of 10 μA, during the period of operation. The exposure time was measured in seconds by stopwatch. The resulting dose of chlorine was measured in units of microcoulombs by taking the product of time in seconds and microamperes of cell current.

The uptake curve of chlorine on the Ti(0001) surface was determined by measuring the change in the Cl(183) Auger peak height after successive doses with chlorine were applied to the surface. This plot is shown in Figure 6.3. The Auger spectrum shows that the chlorine Auger signal increases rapidly and saturates smoothly at about 2000 μC. At saturation exposure, a value for the ratio of Auger signals of Cl(183)/Ti(388) was found to be 7.12 ± 0.2 which reasonably agrees with the value of 9.1 of Smith [72] measured using a similar retarding field analyzer.

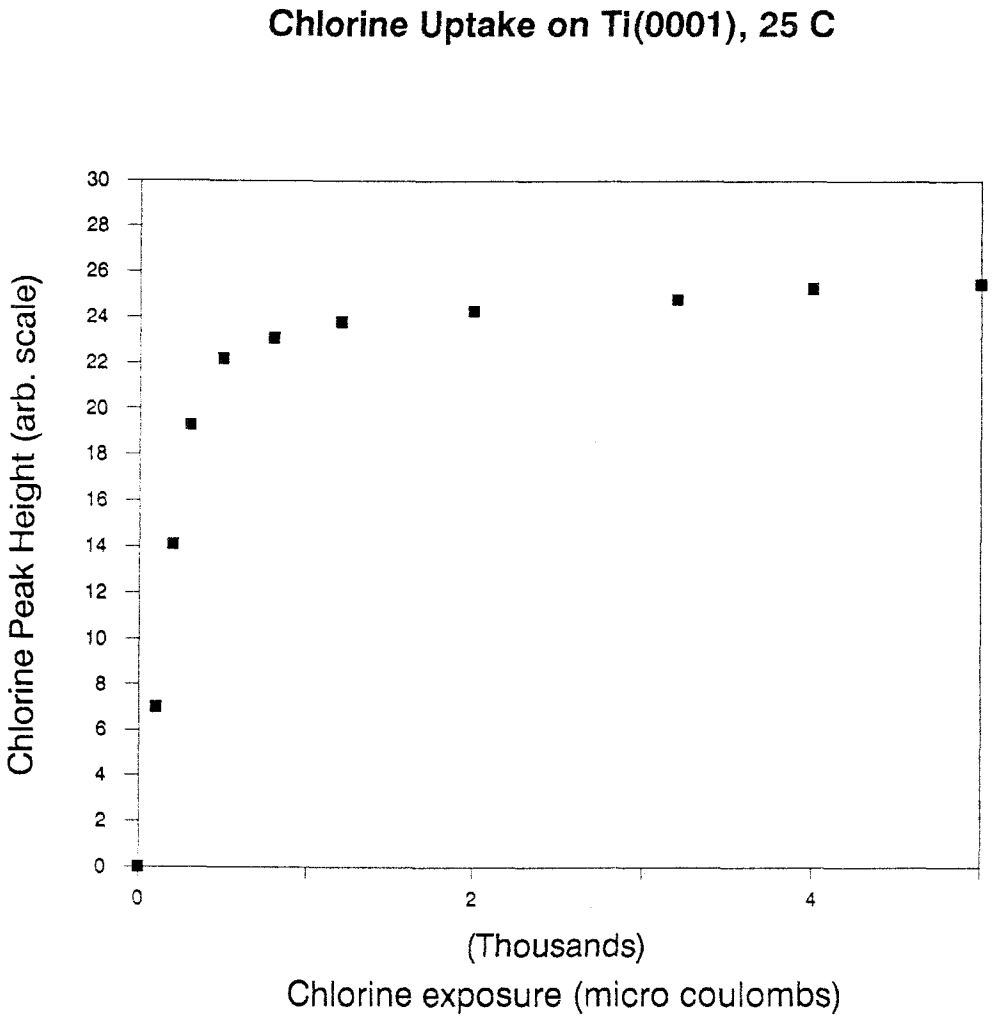

Figure 6.3 Chlorine uptake on Ti(0001) surface at 25°C.

Usually for halogen adsorption on a metal surface, a high sticking coefficient, close to unity has been assumed [73]. The amount of cell current required for the saturation was close to that which was expected (1600-2000 μC) for the adsorption of a monolayer of chlorine assuming unity for the sticking coefficient.

B. LEED results

After sample cleaning, the typical six-fold symmetric diffraction pattern for the Ti(0001) surface was observed (Figure 6.4a). The LEED patterns observed after the passage of 250 μC of charge passed through the Cl dosing cell, did not show any change from the hexagonal pattern of the clean Ti(0001) surface [Figure 6.4b]. This corresponded to a Cl coverage of about 20 % of a monolayer based on the curve of Fig. 6.3. It was observed that the only diffuse background increased on the chlorine covered Ti(0001) surface, in comparison with a clean surface. This is in agreement with the results of a previous study reported by other researchers [69] in which no additional superstructure were observed at room temperature for Cl covered surfaces. They found [69] that an ordered Cl LEED pattern could be only observed after heating a Cl saturated surface at temperatures of up to 650°C for periods of 5 to 30 minutes. The resulting LEED pattern

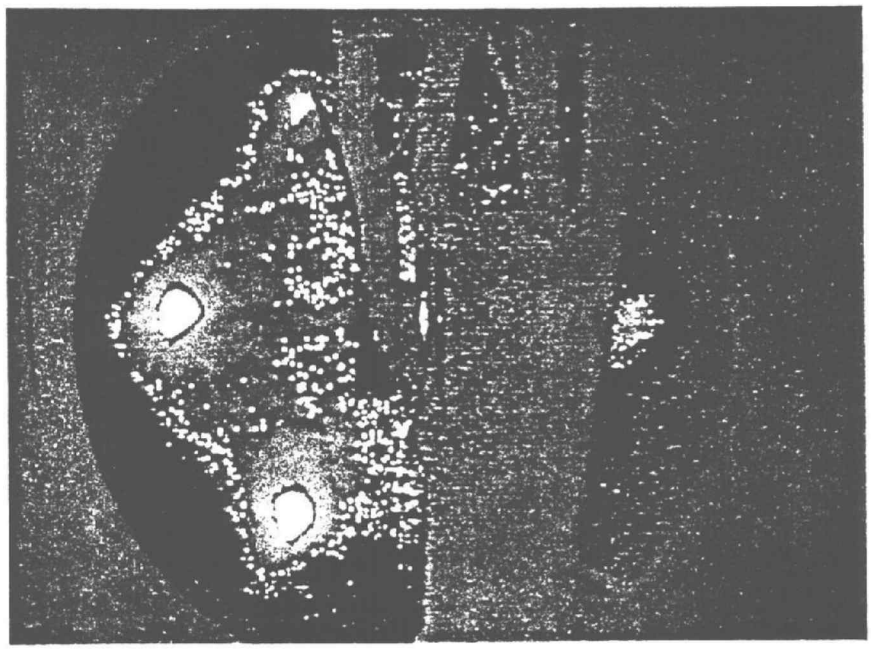

(a)

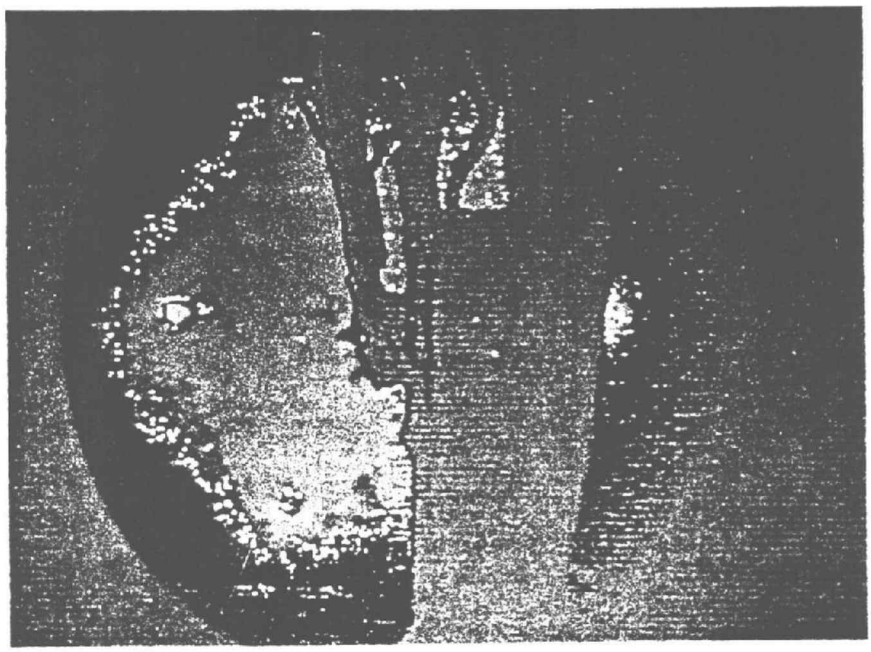

(b)

Figure 6.4 Diffuse LEED patterns of Ti(0001) surface taken at normal incidence (78 eV, 5 μA, 173 K) (a) clean, (b) with 20% monolayer of chlorine.

was interpreted as being due to a coincidence structure of chlorine on the Ti(0001) surface. This result indicated that the chlorine observed on Ti(0001) surface at low coverage & at room temperature is disordered. The employment of another technique which can solve for the disordered Cl arrangement is required. DLEED was chosen for this reason.

C. Intensity correction for the DLEED pattern

In order to measure the experimental diffuse intensities due to adsorbates, it is necessary to remove the intensity contribution of scattering from crystal imperfections and from thermal diffuse scattering. As described earlier in chapter II.C, contributions from surface defects on the substrate can be cancelled by simple subtraction of the diffuse intensity map of the clean surface. The intensity maps of total signal, substrate signal and diffuse scattering intensities as measured at 78 eV, are shown in Figures 6.5, 6.6, and 6.7 respectively. In this study, all adsorbate intensity data and the resulting Y functions are obtained by subtracting the intensity maps of the clean surfaces from those of chlorine covered surfaces. From the original 180x360 pixel grid, taken from the screen window, all the possible intensities with k-space values less than 1.0, were

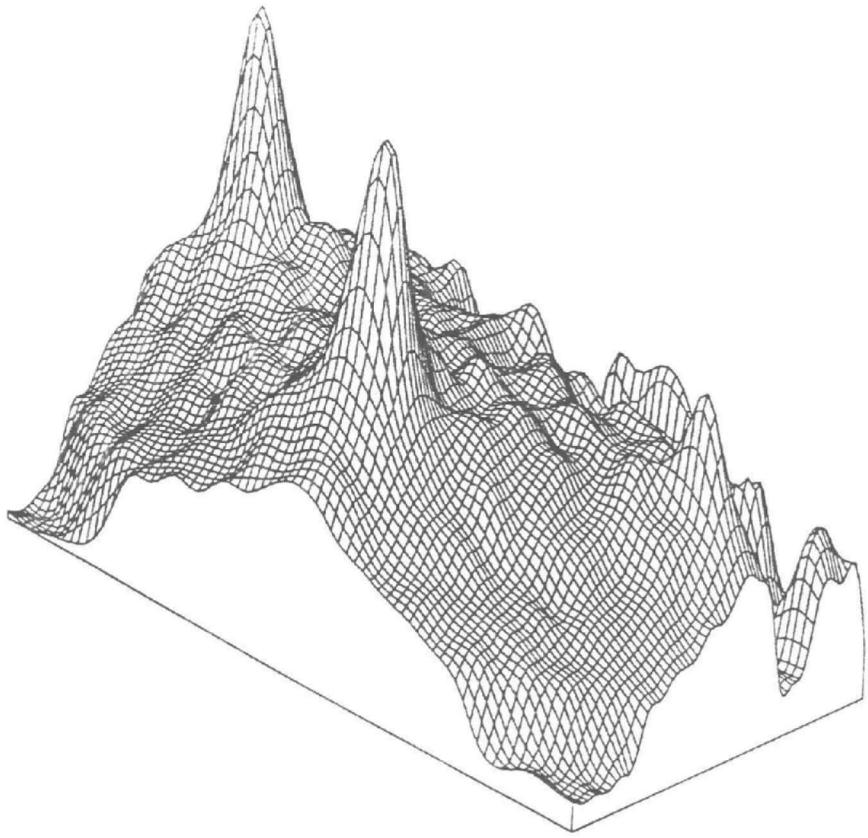

Figure 6.5 Total experimental intensities measured at normal incidence (20% Cl monolayer, 173 K, 78 eV)

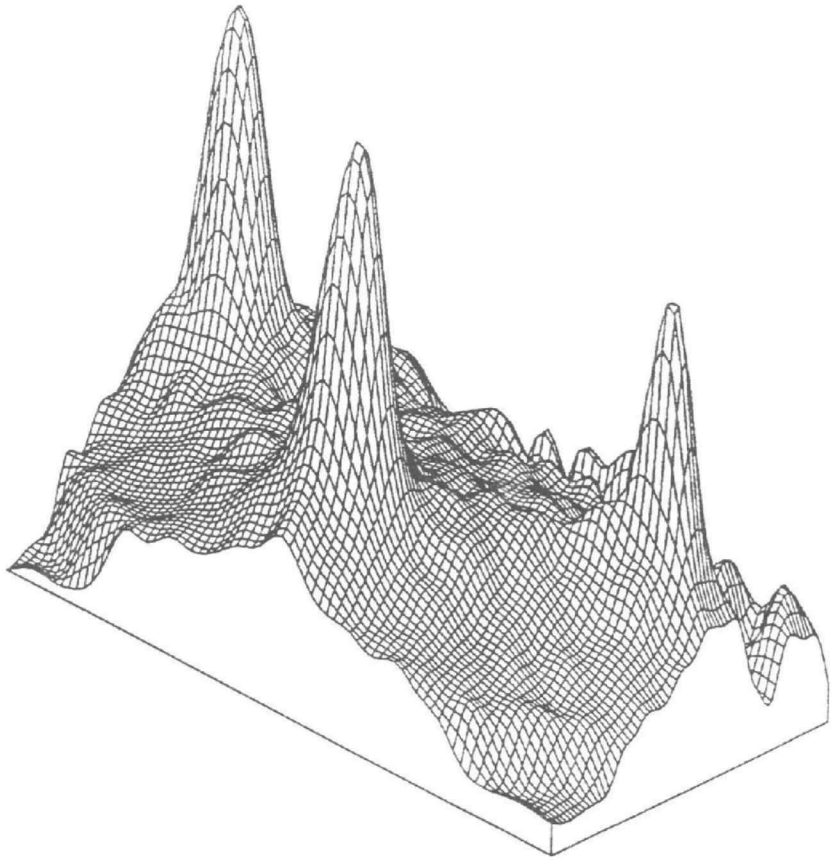

Figure 6.6 Intensity map of the clean surface measured at normal incidence (78 eV, 173 K).

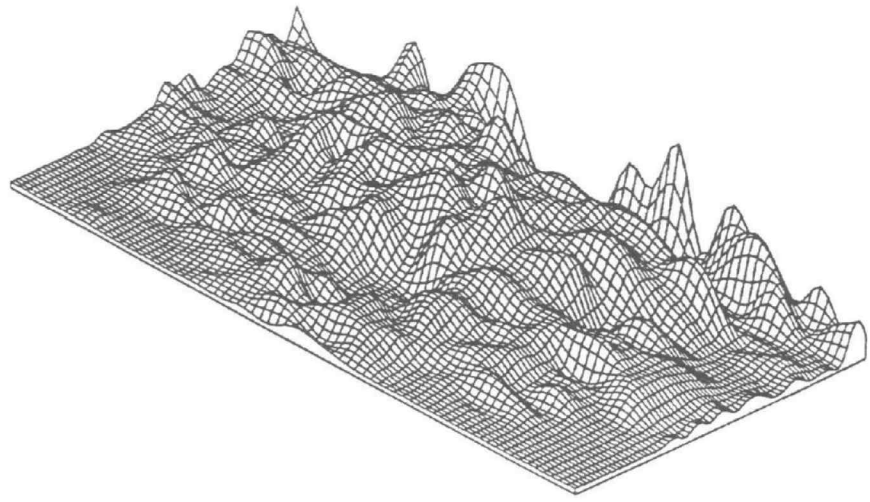

Figure 6.7 Diffuse intensity map after subtraction of clean surface intensity (20% Cl monolayer, 78 eV, 173 K).

collected. Choosing this size window, which was a quarter of the unit grid in k-space, produced a handy grid size that retained the useful part of the data.

D. Construction of Y-functions

For a 20% chlorine coverage monolayer, the phonon corrected Y-functions are calculated from the diffuse intensities measured at two neighboring energies, 78/82 and 90/94 eV, with respect to the Fermi energy. The energy differences are close enough for a derivative approximation. Figure 6.8 shows two intensity maps measured at 78 and 82 eV, respectively, and the constructed Y-function from these neighboring energies. From the maps, it may be noted that the diffuse intensities vary considerably with energy. These variations are more significant for the subtracted maps, allowing the resulting Y-function to retain the structural information needed for theory-experiment comparison. The same procedure was applied to the experimental intensities measured at 90 and the resulting Y-function is shown in Figure 6.9.

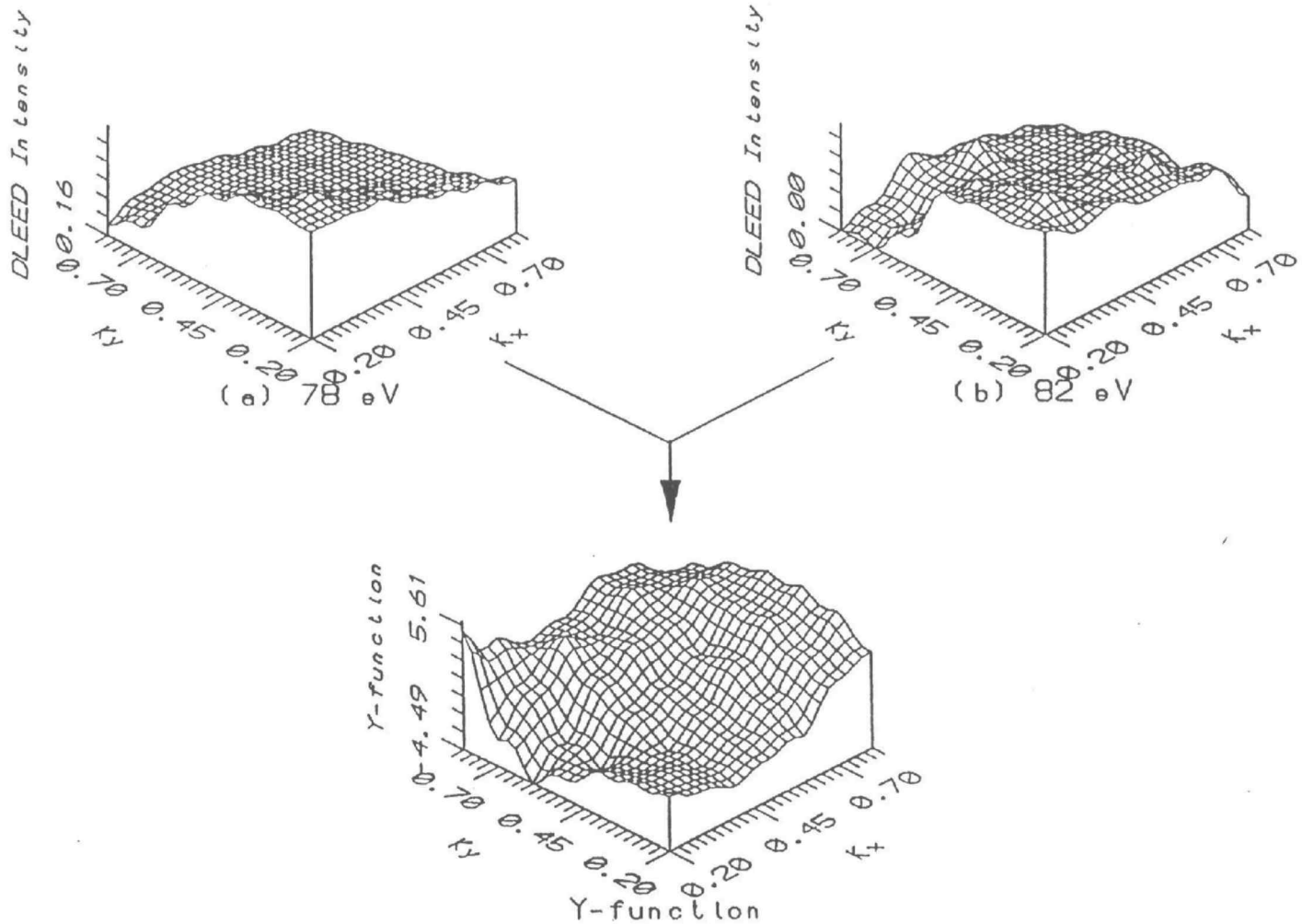

Figure 6.8 Construction of Y-function from two intensity maps measured neighboring energies: (a) 78 eV, (b) 82 eV, (c) Y-function

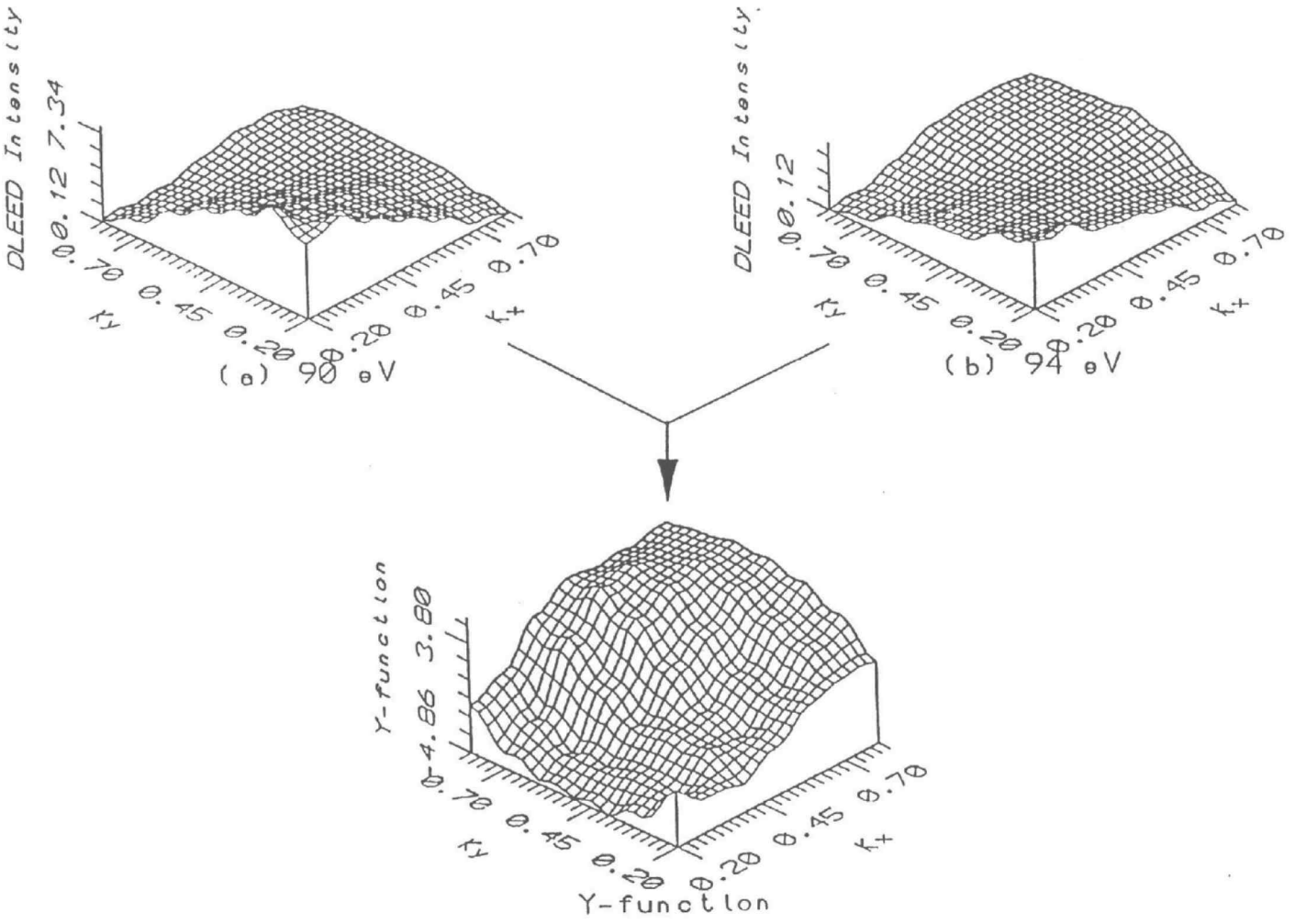

Figure 6.9 Construction of Y-function from two intensity maps measured neighboring energies: a) 90 eV, (b) 94 eV, (c) Y-function

E. Comparison with theory

1. Possible adsorption sites

For comparison with experiment, it was assumed that chlorine would probably adsorb on 4 different possible sites on the Ti(0001) surface. These are on top, bridge, 3-fold hollow with no atom under (3fn), and 3-fold hollow with an atom under (3fa) sites. The relative site adsorption positions are demonstrated in Figure 6.10. The atomic radius x,y and z coordinate values of Ti and Cl atoms are given in Å units in the figure. The distances between the first Ti layers and the chlorine adsorbates were varied within a reasonable range about the values obtained from hard sphere models. For each of the 4 different adsorption sites, theoretical diffuse intensities and Y-functions were calculated from 11 to 18 Ti-Cl distances, in a range of 2.15 Å to 3.43 Å in 0.05 Å increments for each of the corresponding geometries. It was assumed that the symmetry of the substrate is not distorted by adsorption of 20% of a monolayer of chlorine and that no reconstruction occurs.

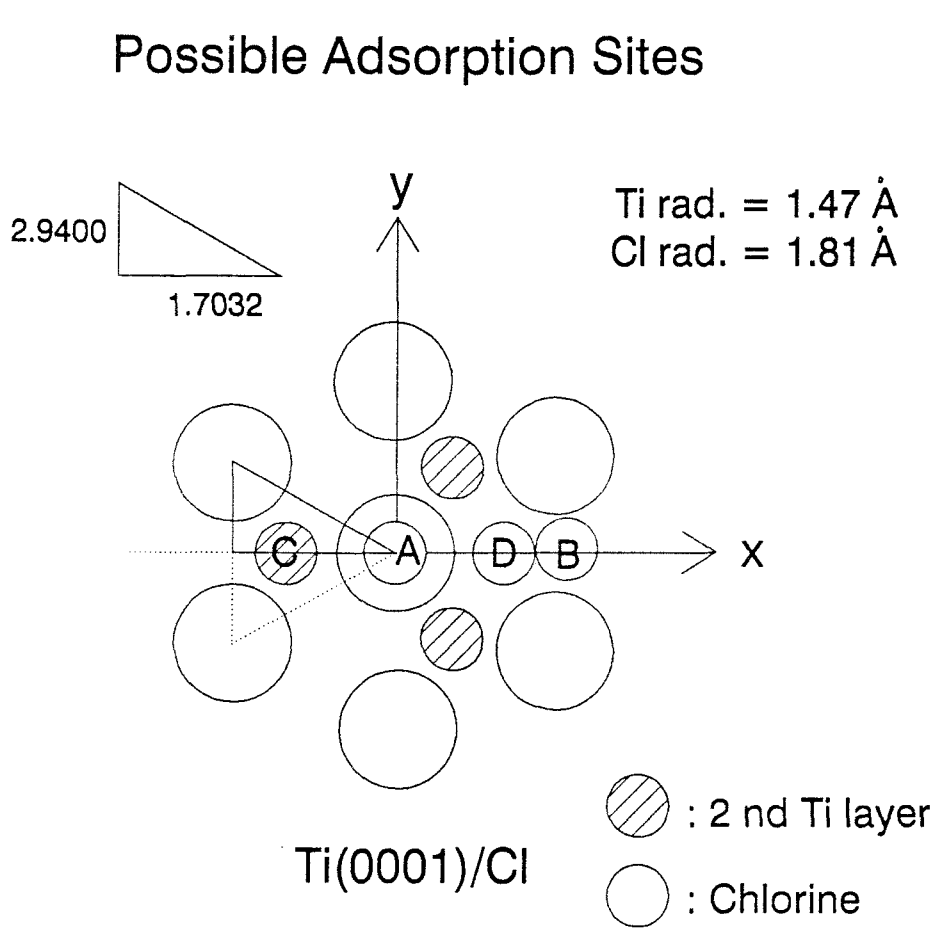

A = Ontop (0, 0, 3.28) Å

B = Bridged (2.5548, 0, 2.932) Å

C = 3-fold hollow (-1.7032, 0, 2.8056) Å
atom under

D = 3-fold hollow (1.7032, 0, 2.8056) Å
nothing under

Figure 6.10 Possible adsorption sites of chlorine atoms on Ti(0001) surface.

2. Calculated Y-functions from 78/82 eV

For the calculation of the diffuse intensities at the energies of 78 and 82 eV, the values of the vertical distance of the chlorine atom to the first Ti layer (d_{Ti-Cl}) was varied in steps of 0.05 Å i.e. from 2.93 to 3.43 Å for the on-top site, from 2.63 to 3.08 Å for the 2-fold bridge site, from 2.3 to 2.95 Å for the 3-fold hollow site with atom under, and from 2.4 to 3.4 Å for the other 3-fold hollow site with no atom under.

A previous study [75] showed that the (0001) face of a hcp metal has two possible terminations and that the surface is composed of equal mixtures of domains of the individual terminations. Therefore, in this study two separate calculations were carried out for each termination (called A and B terminations). The calculated intensity values were averaged and subsequently used to calculate the Y-functions for comparison with experimental data.

All the possible intensities with k-space values less than 2.0, forming a (10 x 10) grid, were calculated. Following interpolation, the original grid was reduced to the size of the experimental data range. This procedure permitted comparison of experimental intensities by application of the same scales of intensity. Thus the smooth nature of the data allowed for a confident interpolation.

As mentioned earlier, the real part of the optical potential experienced by an electron that enters a solid the so called "inner potential"(V_{or}) is a priori unknown quantity. In the calculations this was set to a reasonable value of -10 eV, but it is possible that this value may be in error by up to several eV. The result of such an error (ΔV_{or}) would be that the experimental data taken at V eV should be compared with a calculation performed at (V + ΔV_{or}) eV rather than at V eV itself. To avoid this theoretical problem, several sets of calculations using neighboring energies for a given experimental energy were carried out. The best fit between the experimental data and the theoretical calculations was determined. This corresponds to the lowest value of R_p. The minimum R_p-factors obtained for each adsorption site for each different energy pair are shown in the Figure 6.11. It is apparent that the theoretical data calculated for the same energy (78/82 eV) as the experimental data provides the best agreement.

A quasi three dimensional plot of the theoretical Y-functions with the minimum R_p-factor for the cases of four different adsorption sites are shown in Figures 6.12, 6.13, 6.14, and 6.15. It appears to the eye that the calculated Y-functions for the 3-fold hollow with atom under and bridge site have the most structural similarities with the experimental Y-function.

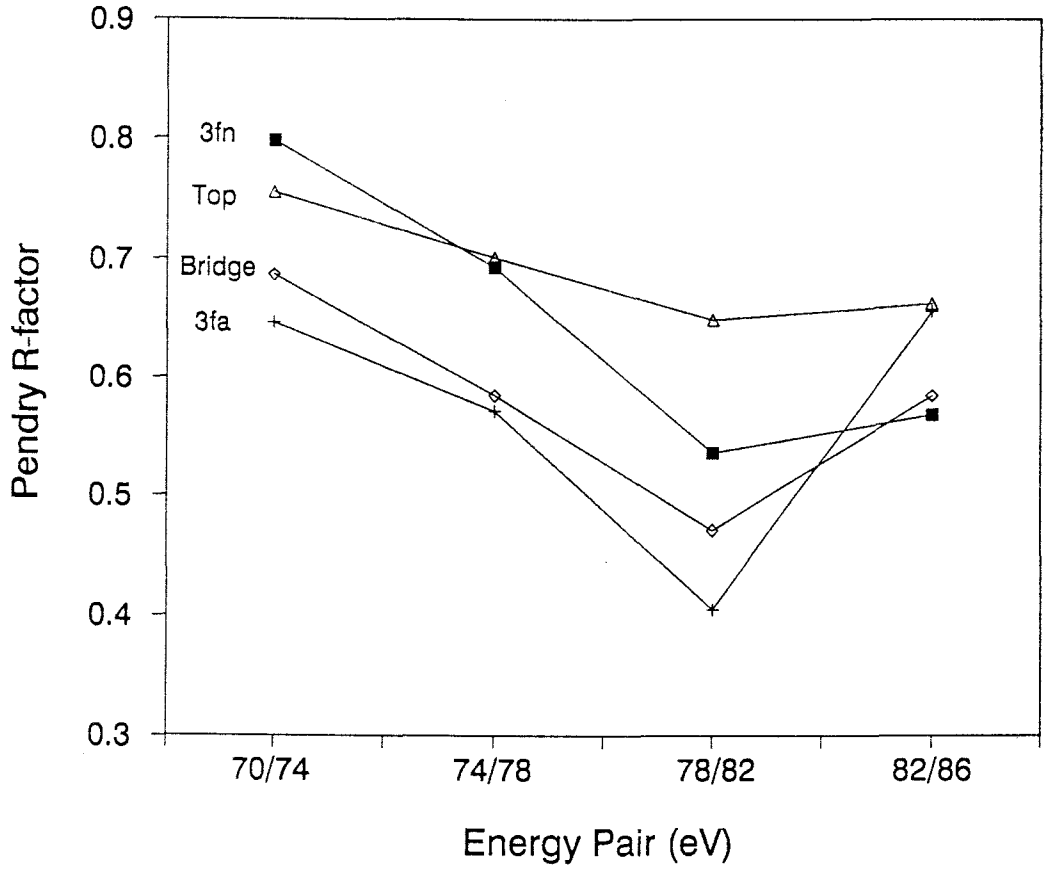

Figure 6.11 Comparison of the calculated Y-functions with different energy pairs and the experimental Y-function measured at 78/82 eV.

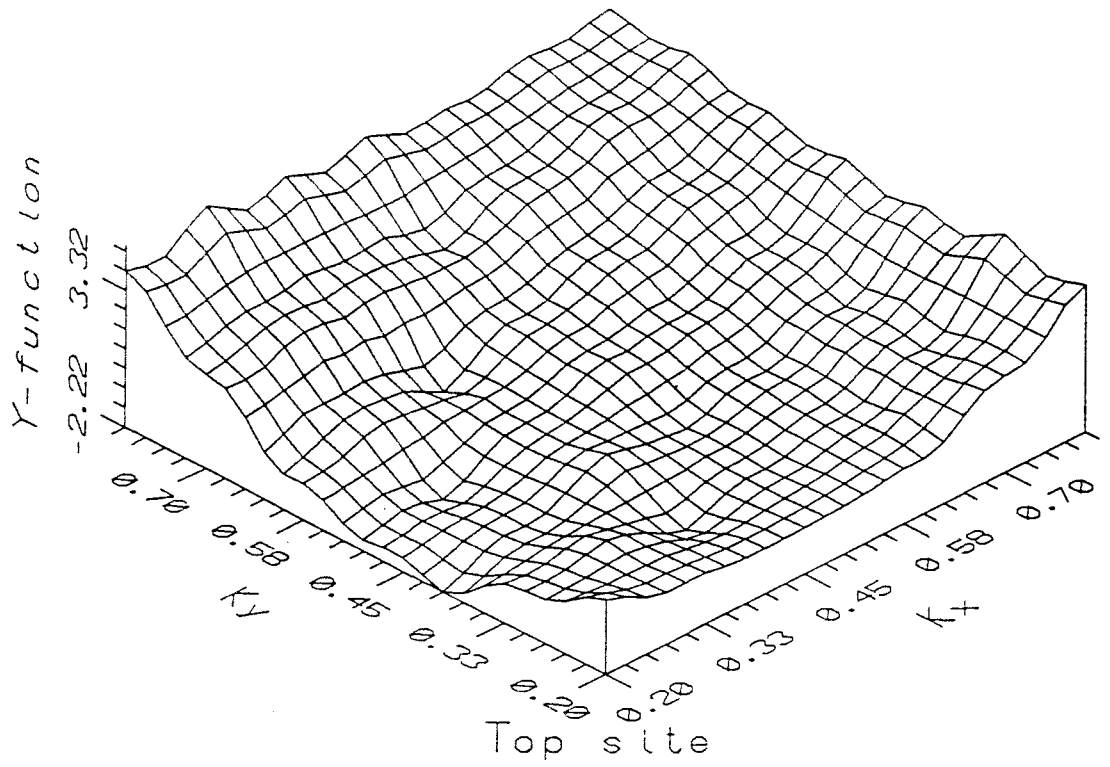

Figure 6.12 Calculated Y-function for the Cl in on-top position at the parameters for the best fit, d_{Ti-Cl}= 3.13 Å, at 78/82 eV.

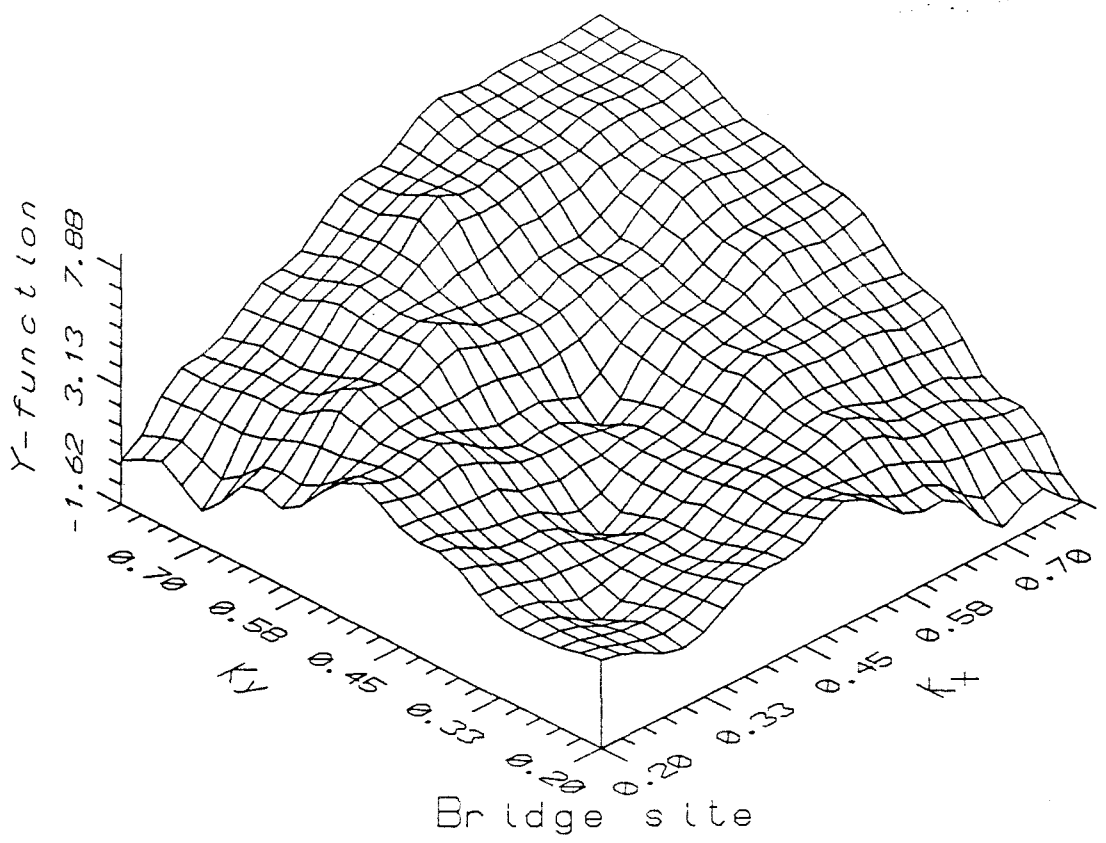

Figure 6.13 Calculated Y-function for the Cl in bridged site at the parameters for the best fit, d_{Ti-Cl} = 2.90 Å, 78/82 eV.

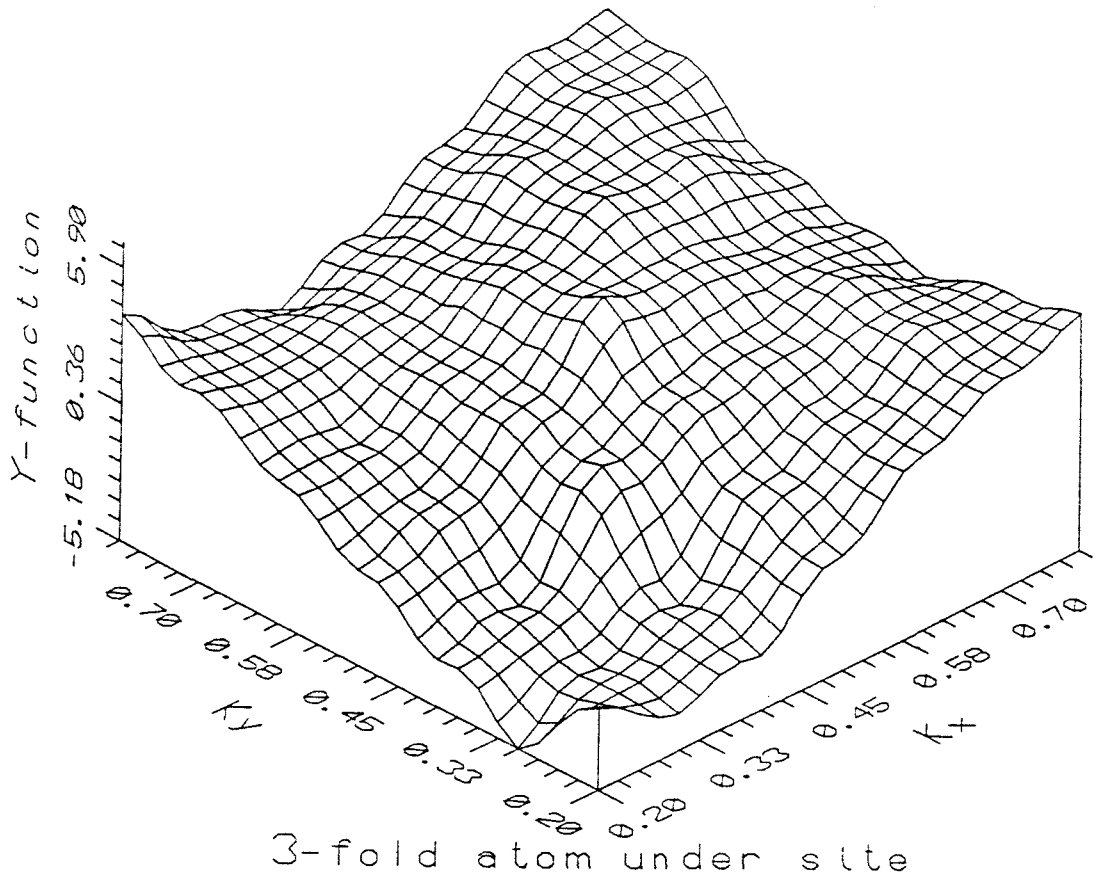

Figure 6.14 Calculated Y-function for the Cl in 3-fold atom under site at the parameters for the best fit, d_{Tl-Cl}= 2.45 Å, at 78/82 eV.

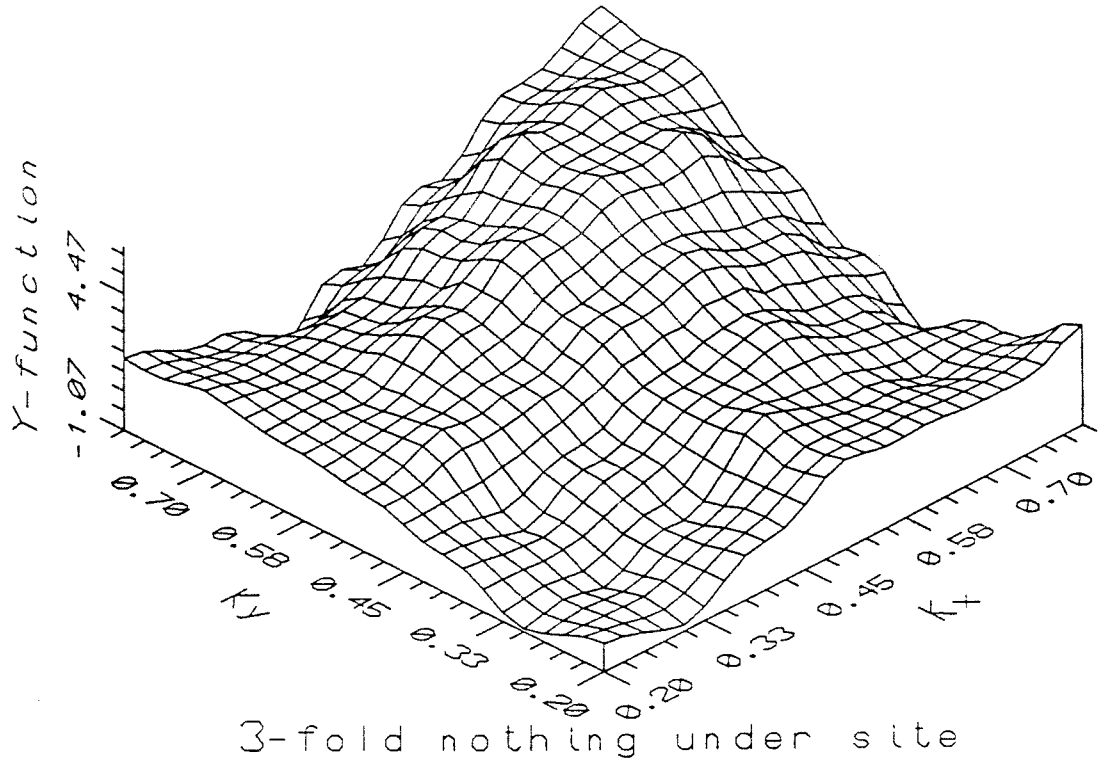

Figure 6.15 Calculated Y-function for the Cl in 3-fold with no atom under site at the parameter for the best fit, d_{Ti-Cl} = 2.4 Å, at 78/82 eV.

3. R_p-factor analysis of the 78/82 eV pair

Detailed analysis for the different adsorption geometries were made using the Pendry R-factor (R_p) between the experimental and calculated Y-functions. The objective in this analysis is to discriminate between sites and provide an unequivocal determination of structural parameters. The geometry yielding the minimum Pendry R-factor was found by going through many cycles of calculations for the different sites. The results of this analysis for 4 different adsorption sites are shown in Figure 6.16 and are gathered in Table 6.1. The R_p-factors for the on-top, bridge and 3fa sites show clear minima. The 3fa sites is favoured slightly over the bridge, but the on-top site has consistently higher R_p-factors and seems to be discriminated against in this set of data. The experimental 3fa site appeared to be indistinguishable from that of the calculated 3fa site in this data set.

In order to check the possibility of different coexisting adsorption sites or, if possible, to reveal the ratio of the relative occupation of coexisting adsorption sites, many mixtures of 3fa and bridge site occupations, from 100% bridge to 100% 3fa, were tested. This is achieved by the addition of the intensities from the desired sites scaled with respect to site occupancy. The dependence on the site mix is illustrated in Figure 6.17

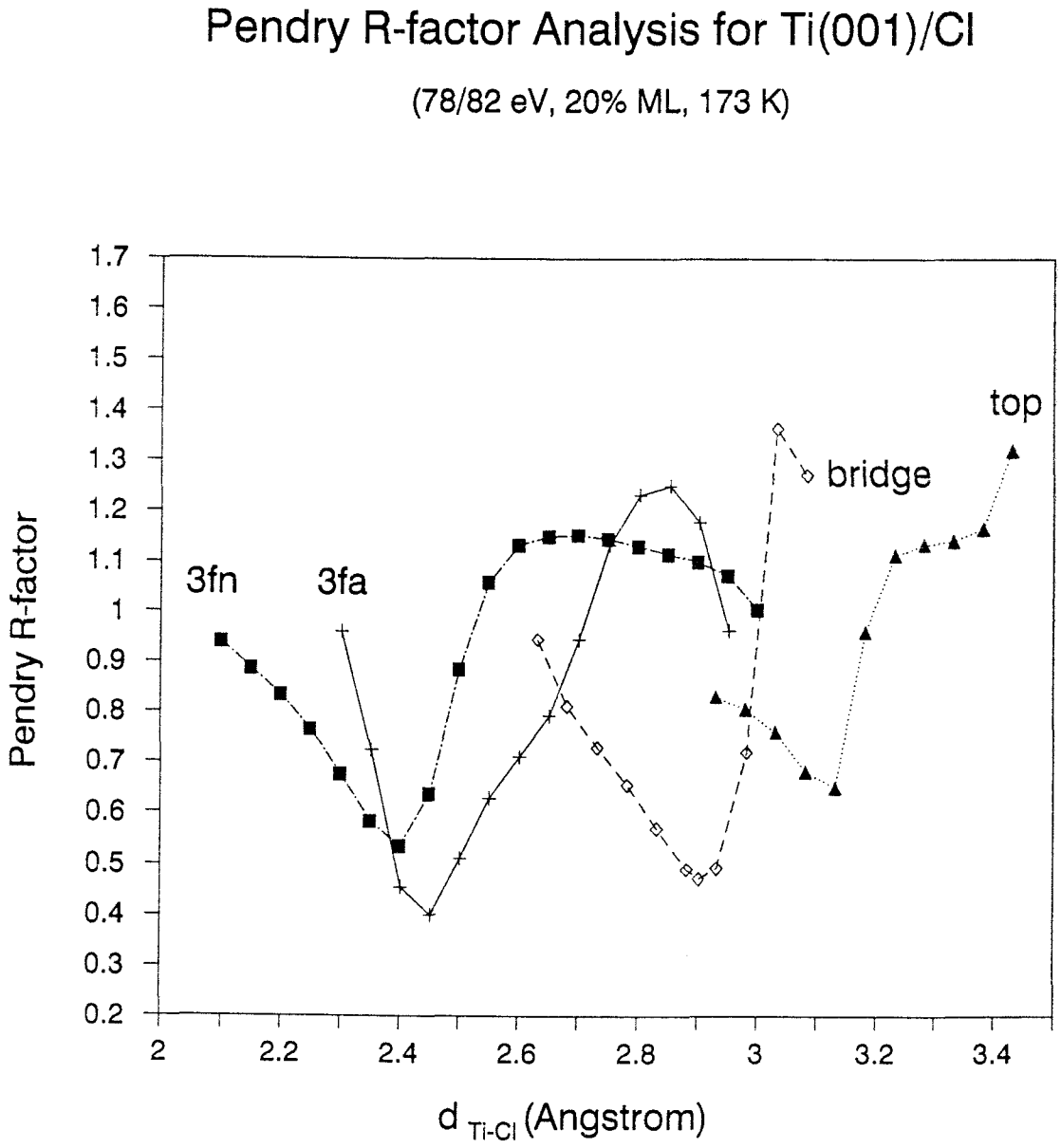

Figure 6.16 Pendry R-factor analysis of experimental data (78/82 eV,20% ML, 173K) and theoretical calculations for the four different adsorption sites.

Table 6.1 The interlayer spacings between the chlorine atoms and the first layer of titanium atoms for four different adsorption sites at the minimum Pendry R-factors and the evaluated surface bond lengths. The diffuse LEED intensities were measured at 78 and 82 eV for the disordered chlorine on Ti(0001) surface (20% ML, 173K).

Sites	$d_{min}^{(Ti-Cl)}$ (Å)	R_p^{min}	d_{Ti-Cl} (Å)
3fa	2.45	0.405	2.98
3fn	2.40	0.536	2.94
bridge	2.90	0.471	3.25
On-top	3.13	0.649	3.13

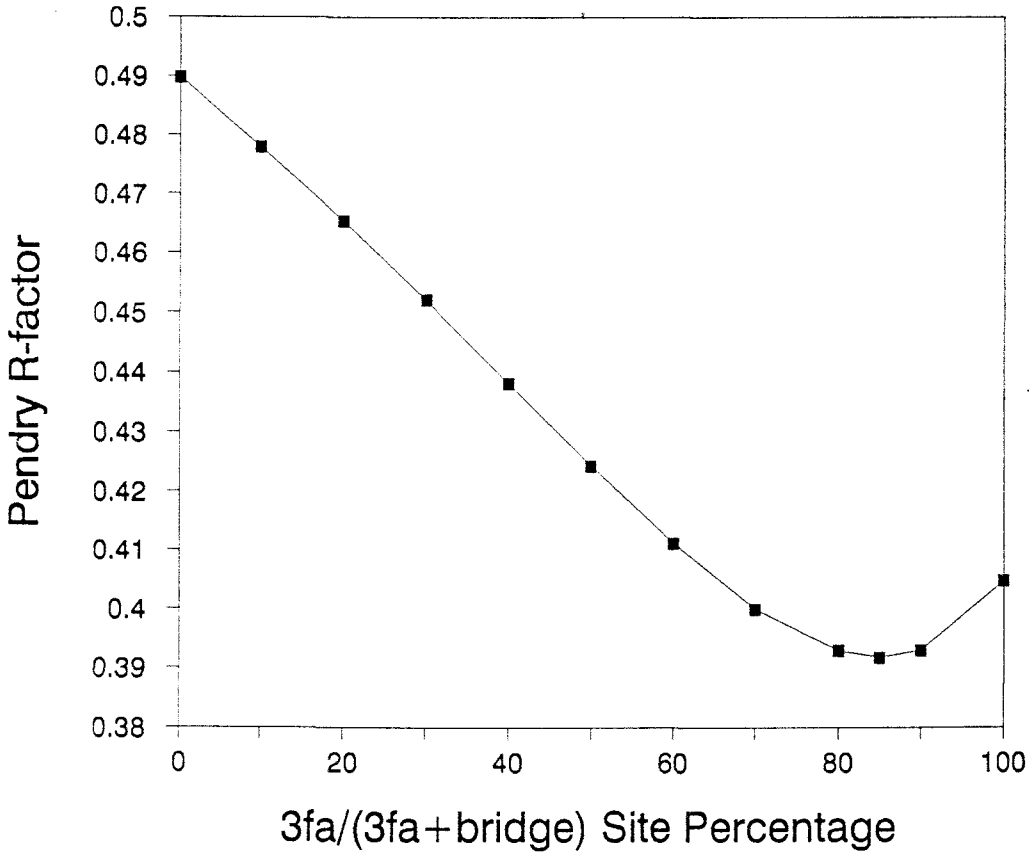

Figure 6.17 Pendry R-factor analysis of 3fa-site percentage occupation vs bridge-site.

with the above assumption for the interlayer spacings. A reasonably sharp minimum is visible near 85% 3fa site and 15% bridge-site occupation. On the other hand, a test of many mixtures of 3fa and 3fn site occupations, which has the next lowest R_p-factor did not show a minimum, but a simple arithmeticly averaged distribution.

4. Data analysis at other conditions

Another set of calculations were carried out for the 90/94 eV energy pair using the same calculation procedure as for the 78/82 eV data set. The three dimensional plots of the theoretical Y-functions with the minimum R_p-factor for the cases of 4 different adsorption sites are shown in Figures 6.18, 6.19, 6.20, and 6.21. The results of Pendry R-factor analysis of the 90/94 eV data set are shown in Figure 6.20 and are gathered in Table 6.2. It is clear that only the 3fn site has a clear minima. The 3fa site showed a range of low R_p factors at the same interlayer spacing as for the 78/82 eV data although it unfortunately did not show a sharp minima. The bridge and on-top sites did not show reasonable minima, having consistantly higher R-factors. We also attempted to analyze experimental data for different chlorine coverages (10 and 40% of a monolayer). For 10% of a monolayer, the diffuse intensities were not large enough to analyze after the

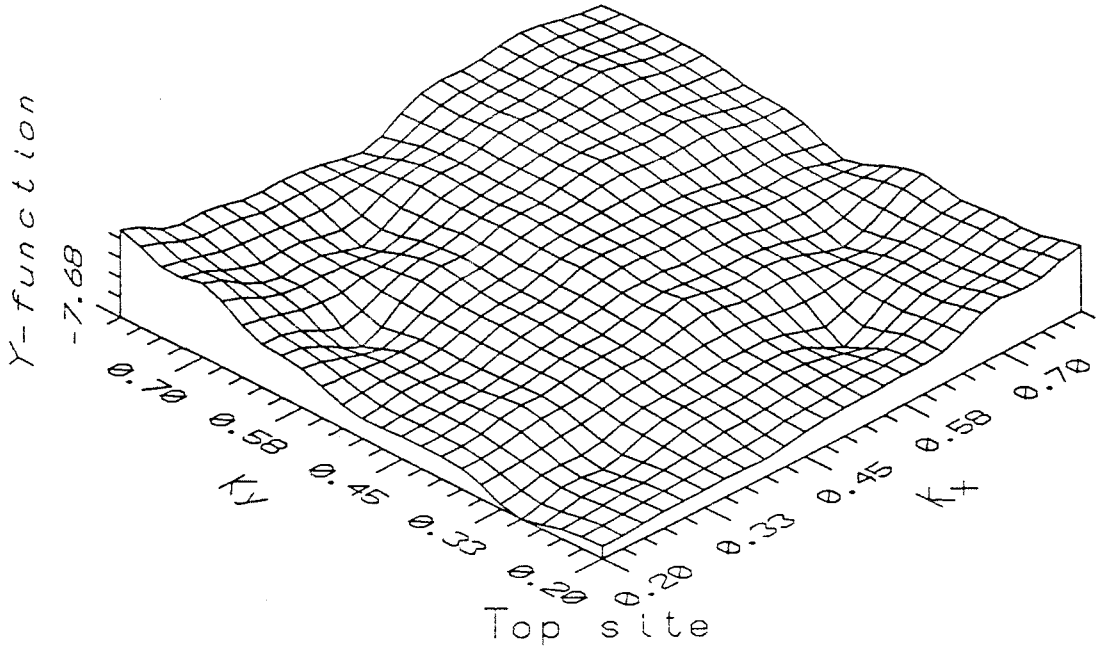

Figure 6.18 Calculated Y-function for the Cl in on-top site at the parameters for the best fit, d_{Ti-Cl}= 3.23 Å, at 90/94 eV.

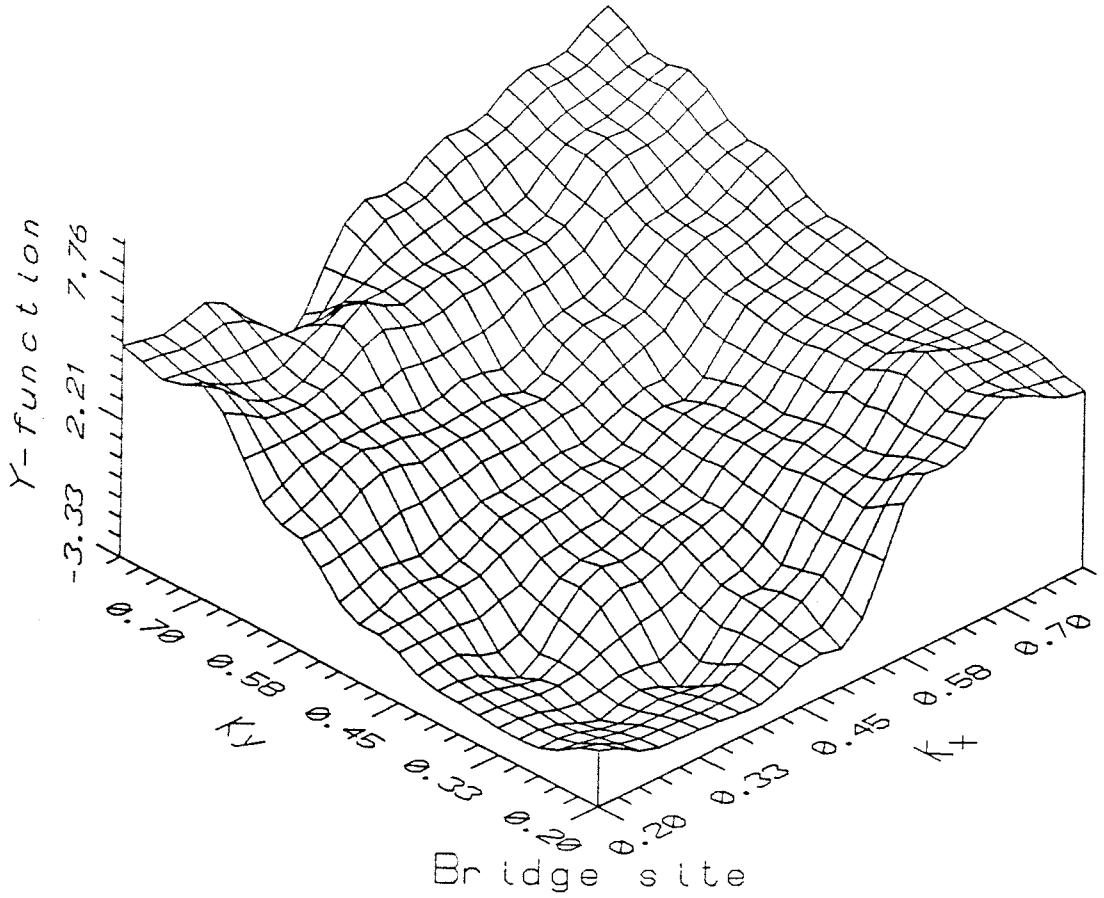

Figure 6.19 Calculated Y-function for the Cl in bridge site at the parameters for the best fit, d_{Ti-Cl}= 3.13 Å, 90/94 eV.

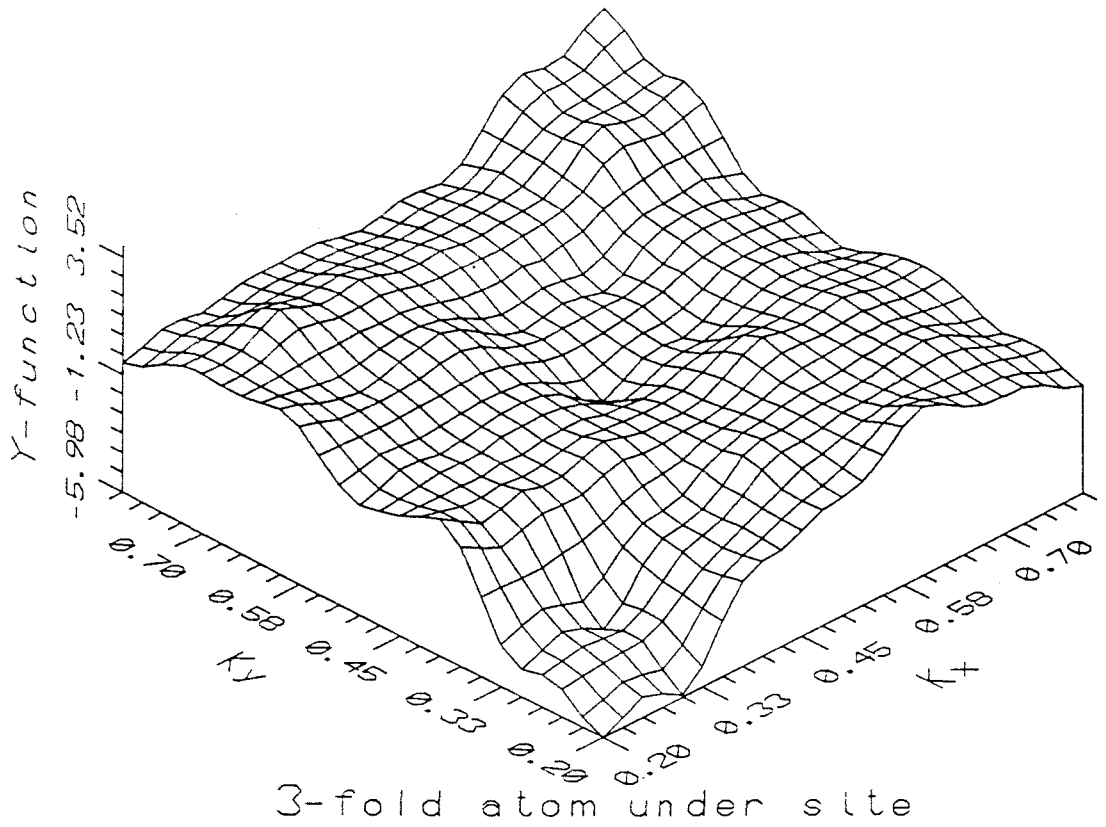

Figure 6.20 Calculated Y-function for the Cl in 3-fold atom under site at the parameters for the best fit, d_{Ti-Cl} = 2.4 Å, at 90/94 eV.

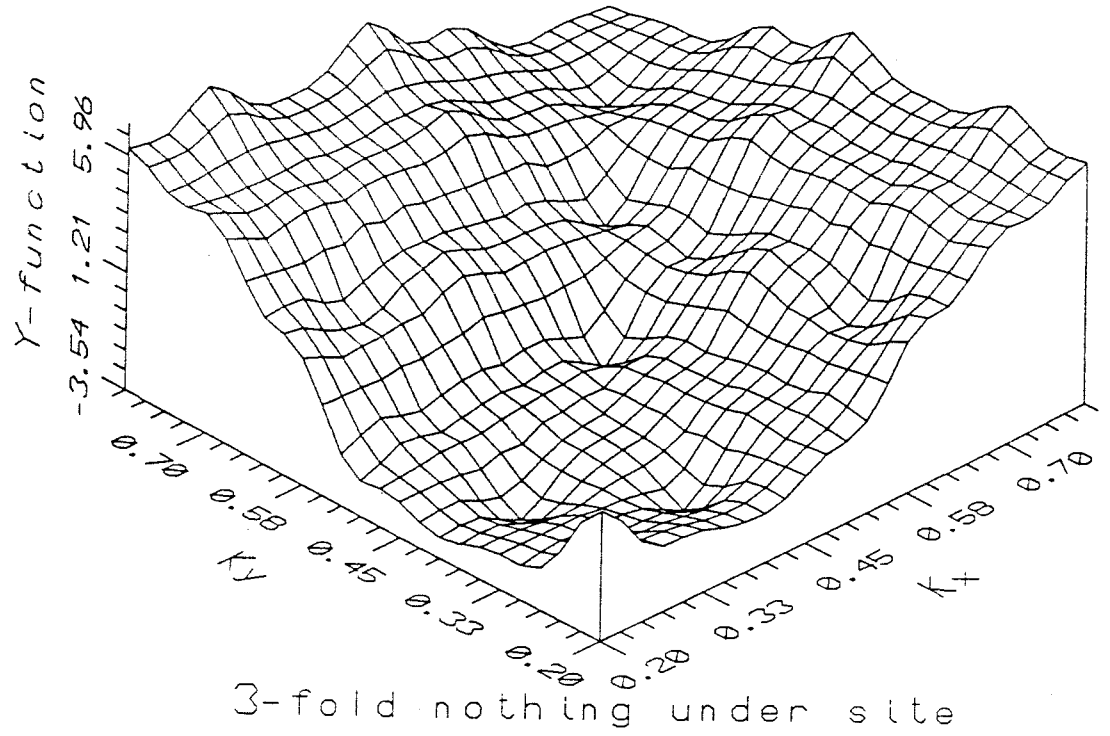

Figure 6.21 Calculated Y-function for the Cl in 3-fold with no atom under site at the parameters for the best fit, d_{Ti-Cl}= 2.55 Å, at 90/94 eV.

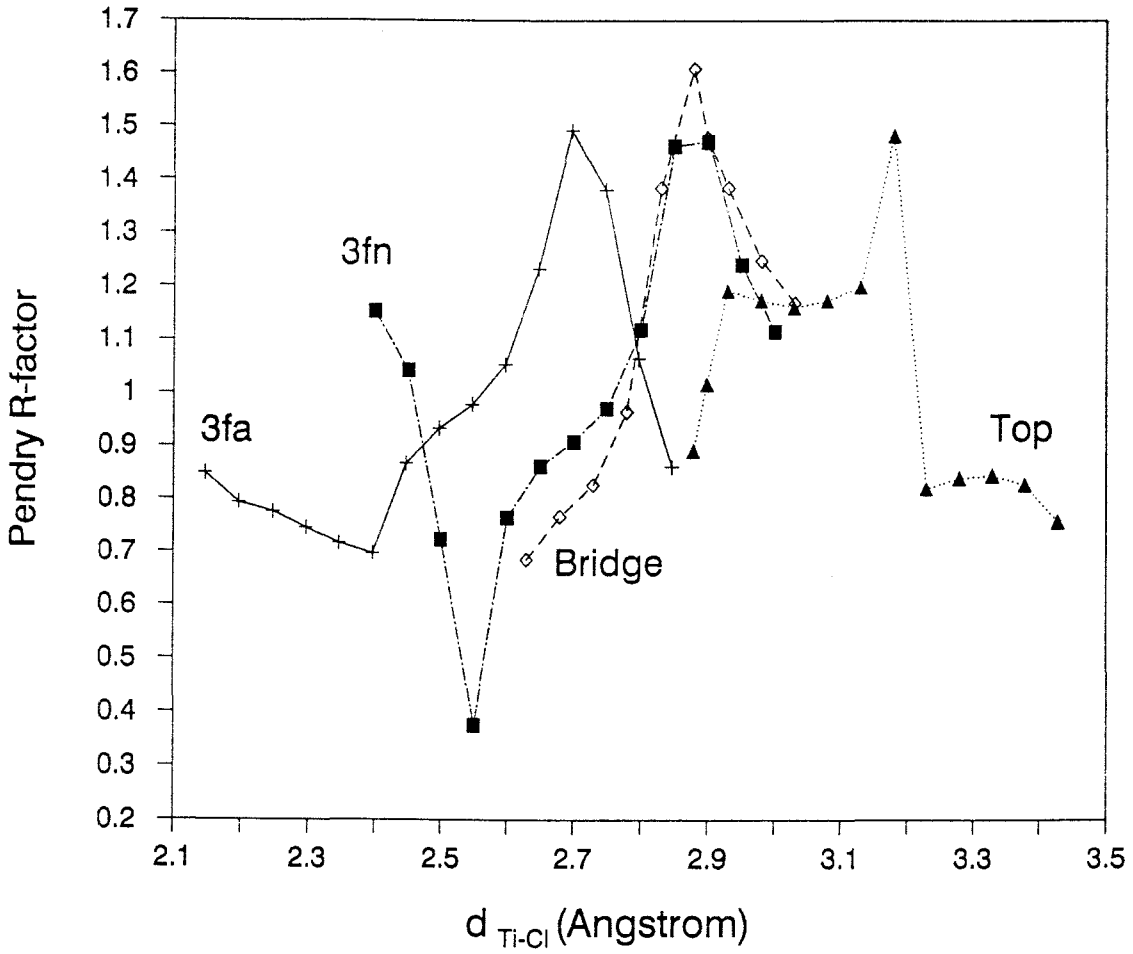

Figure 6.22 Pendry R-factor analysis of experimental data taken at 90/94 eV (20% monolayer, 173K) and theoretical calculations for four different adsorption sites.

Table 6.2 The interlayer spacings between the chlorine atoms and the first layer of Titanium atoms for four different adsorption sites at the minimum Pendry R-factors and the evaluated surface bond lengths. Data were measured at 90 and 94 eV for the disordered chlorine on Ti(0001) surface (20% ML, 173 K).

Sites	d_{min} (Å)	$R_{p^{min}}$	d_{Ti-Cl} (Å)
3fa	2.4	0.732	2.94
3fn	2.55	0.376	3.06
bridge	—	—	— *
on-top	—	—	— *

* no minimum observed.

background contributions were subtracted; for 40% of a monolayer partial ordering due to adsorbate-adsorbate interactions disturbed the analysis.

5. Conclusions from DLEED experiments

From the above results it was concluded that chlorine probably adsorbs on the 3-fold hollow sites, and possibly partly on the bridge sites, of a Ti(0001) surface at interlayer spacings of 2.48 ± 0.07 Å and 2.90 Å respectively. Based on these interlayer spacings, a site mix of about 85% 3-fold and 15% bridge sites was favoured by the Pendry R-factor analysis. The best R_P-factor value of 0.39 obtained here is not as good as that found for the O/W(100) structure analysis [28], 0.13, obtained with Pendry's program, but much better than that found in the CO/Pt(111) structure analysis [52], 0.55, which employed the same method, namely,the beam set neglect method.

We can speculate that the reason why the fit is not so good as for oxygen on tungsten is a result of the low diffuse LEED intensities which were very difficult to analyze. This might be partly explained due to the low Debye temperature (θ_D) of titanium metal (θ_D= 270 K) [76], which contribute to the high levels of phonon background. The cancellation of the phonon background may not be as good for Ti as for the case of tungsten with θ_D= 405

[76].

6. A theoretical approach to the surface bond length

There have been some recent theoretical approaches to understand trends in structural information for atomic adsorption on metal surfaces. A literature review [77] discusses some approaches for assessing the near neighbor X-M interatomic distances when main group (X) atoms are chemisorbed on crystallographically well-defined surfaces of metals(M). The idea of utilizing bond order-bond length relations of the type used by Pauling, in combination with the Schomaker-Stevenson scheme (PSS approach) [78], often worked very well for estimating surface X-M bond lengths although a few distances showed some substantial discrepancies between predicted and experimental values.

Another approach for predicting surface bond distances is to use bond valence-bond length relations deduced from a computer analysis of solid state structures [79]. A recent application to O-M interatomic distances at surfaces, which remained a problem in the PSS approach, in most cases when expressions given by Brown and Altermatt (BA method) were used. A recent paper [81] demonstrated the accuracy of the BA method by comparing data obtained from surface crystallography experiments

with both the BA and PSS methods. The BA approach was found to be good for assessing the general reliability of a particular surface structure.

The Brown-Altermatt method uses the expression:

$$r = r_o - 0.85 \log S \qquad (6\text{-}1)$$

for a particular interatomic distance r. In this case R dependes on valence S, where r_o is the corresponding distance for a bond of unit valence in a suitable solid. The X-M bond lengths can be calculated using the equation (6-1), for a given r_o. The use of equation (6-1) requires the assumption that the sum of bond valencies for each X atom equals the atomic valence *v*. In the case when X adsorbs on a metallic surface with *n* equivalent neighboring M atoms, the bond valence equals *v/n*.

In order to predict the Ti-Cl surface bond length we need a good reference compound in order to determine the unit valence bond distance r_o. Since we anticipate that the oxidation state of the Ti atoms coordinated to an adsorbed Cl atom is small, we require a reference material with a low oxidation state for Ti. Thus $TiCl_4$ (Ti-Cl = 2.18 Å [ref. 82]) is not a suitable choice. A number of solid state X-ray derived values for low valency Ti compounds are gathered in Table 6.3.

The Ti-Cl distance in the organometallic compounds

Table 6.3 Ti-Cl bond lengths from X-ray structure for low valent Ti compounds.

Compounds	Ti-Cl (Å)	Reference
$Cp_2TiCl_2TiCp_2$	2.54	[83]
$(C_2H_5)_2TiCl_2Al(C_2H_5)_2$	2.5	[84]
$(CH_3)_6C_6Ti(Cl_2AlCl_2)_2$	2.62	[85]
$(C_8H_8TiCl)_4$	2.56	[86]
	2.61	
$TiCl_2(s)$	2.53	[87]

C_p = cyclopentadienyl

averages close to 2.58 Å. The simple binary compound $TiCl_2$ has a Ti-Cl distance of 2.53 Å. We choose this latter value as our reference r_o since this compound is closest in general structure to our surface situation. $TiCl_2$ crystalizes in an hexagonal structure [87] (a= 3.56 Å, c = 5.87 Å) of the CdI_2 type. This structure is shown in Figure 6.23(a) and the unit cell in Figure 6.23(b).

Using r_o=2.53 Å as our reference Ti-Cl single bond distance we can predict the surface Ti-Cl bond lengths for our possible adsorption sites by applying the BA equation 6-1.

Table 6.4 compares the predicted and experimentally determined bond lengths for the 3-fold and bridge sites. The agreement between the predicted and measured 3-fold Ti-Cl bond lengths is extremely good, probably fortuitously so. Our experimental value for the Ti-Cl bond length in the bridge site is much longer than that predicted from equation 6-1. However, the bridge site is less favoured than the 3-fold sites in the 78/82 eV data (see Figures 6.16 and 6.17) and has no minimum in the 90/94 eV data set. Hence, it is perhaps not suprising that the prediction in this case is not fulfilled. We could regard the strong agreement between the predicted and measured data for the 3-fold site as further evidence that this is the majority adsorption site for Cl on Ti(0001) at low coverages.

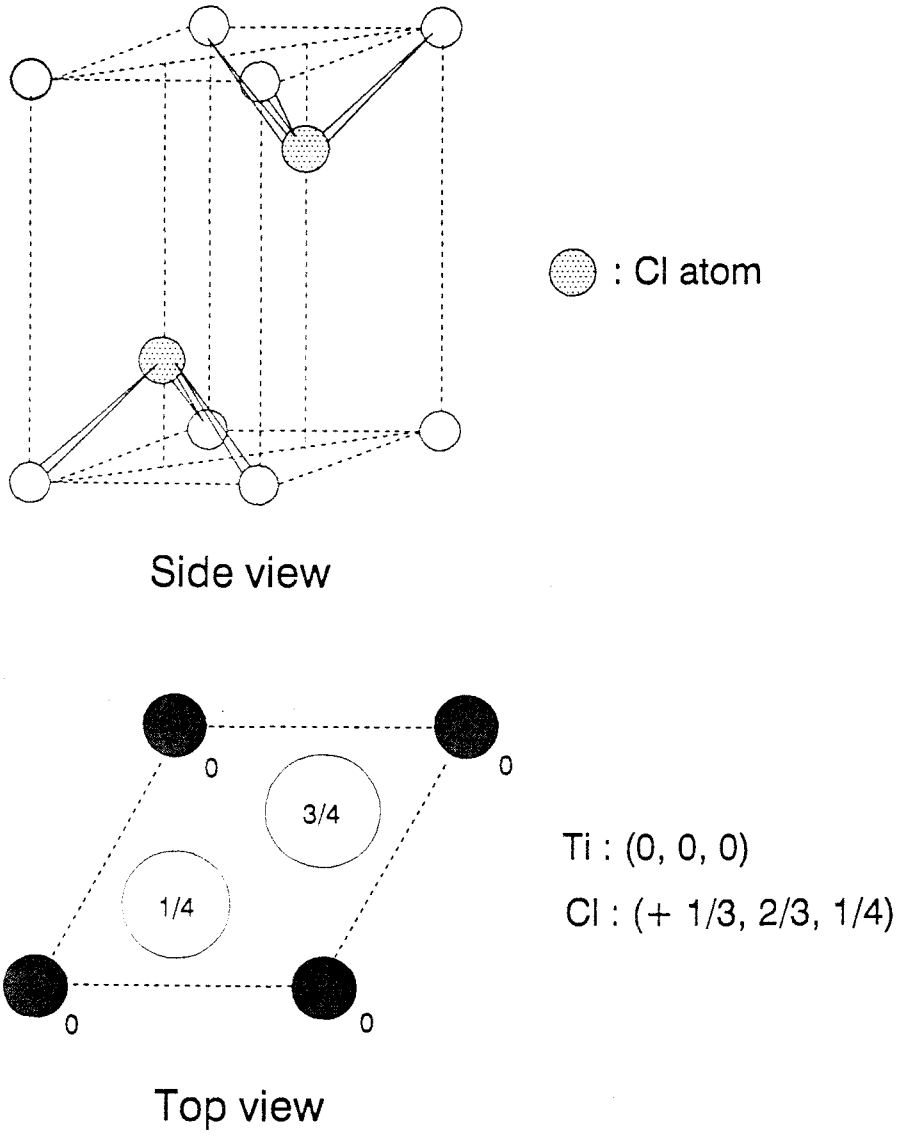

Figure 6.23 (a) The crystal structure (CdI_2-type) of $TiCl_2$ [87]; shaded circle represent Cl atoms. (b) hexagonal unit cell. Ti at (0, 0, 0); Cl at (± 1/3, 2/3, 1/4)

Table 6.4 Comparison of Ti-Cl interatomic distances predicted by BA method and the values obtained DLEED method.

unit = (Å)

Sites	BA	DLEED
3-fold	2.94	2.96 ± 0.04

With this in mind it is interesting to view the $TiCl_2$ crystal structure that we used as a reference for the BA calculation in a surface framework. A section through the $TiCl_2$ unit cell at c/2 (Figure 6.23) would result in a surface that has a local structure with a Cl atom adsorbed in a 3-fold site 2.94 Å from Ti atoms arranged in a hexagonal mesh. This is exactly the structure that we have found in our DLEED experiments, within experimental error, for the Cl-Ti(0001) surface, a surface where the Ti atoms are also hexagonally arranged (see Figure 6.10).

It is interesting to see how our results compare with surface crystallographic data from other M-Cl systems. Unfortunately these are relatively few in number. The results of these investigations and the predicted M-Cl bond lengths using equation 6-1 are presented in Table 6.5.

Our proposed adsorption site for Cl on Ti(0001) in the highest symmetry site is in keeping with the behavior of Cl on all the faces shown in Table 6.5. The Ti-Cl bond length is longer than would be expected from the atomic radius of Ti (1.47 Å) relative to the radii of Cu (1.28 Å and Ag (1.44 Å). The correspondence between the predicted and measured values varies from very good for Ti, Cu(100), Ag(100) to relatively poor for Ag(110). Given the sensitivity of equation 6-1 to the value chosen for r_o, perhaps we should expect its predictions to be no more

Table 6.5 Comparison of surface M-Cl bond lengths in Å and predictions from equation 6-1, using reference bond lengths for Cu-Cl and Ag-Cl from [82].

Metal M	Face	Adsorption site	Predicted	Measured	Reference
Ag	100	4F	2.62	2.67	88
				2.69	89
	110	2F	2.36	2.56	90
	111	3F	2.51	2.70	91
Cu	100	4F	2.35	2.37	92
				2.39	93
	111	3F	2.24	2.39	94
Ti	0001	3F	2.94	2.96	This work

more than a general guide to an expected bond length. The excellent agreement for our Ti(0001)-Cl result probably reflects the close similarity to the reference compound used to predict the surface crystallography.

VII. CONCLUSIONS

The titanium/chlorine surface is intimately connected with Ziegler-Natta catalysis. It has been impossible to study the surface structure of $TiCl_3$ by application of standard surface sensitive techniques. Moreover, earlier model studies in this laboratory have indicated that Cl_2 adsorption on Ti(0001) surface is disordered. Thus new experiments under UHV conditions have been undertaken in order to provide understanding of the atomic structure of titanium/chlorine surfaces. These include the preparation and characterization of $TiCl_3$ crystals, the development of a new technique (Diffuse LEED), and the use of this Diffuse LEED technique for the structural determination of disordered chlorine on Ti(0001) surface.

The growth of $TiCl_3$ single crystals as a real catalyst of the Ziegler-Natta type require the development of a number of special handling techniques accommodated to the friable and water-sensitive crystals. A gradient furnace, designed specially for crystal growth was used to produce good quality crystals. A Pyrex glass cell was prepared and used for $TiCl_3$ vacuum deposition and gold-plating. In addition the fragility of the $TiCl_3$ crystal required the use of special mounting methods. A thin indium film was sandwiched between a gold-plated $TiCl_3$ crystal and a molybdenum plate, and then attached to the

sample holder. This provided a useful means to move and then install the sample crystal within the UHV chamber. Ar ion sputtering was used to make the $TiCl_x$ surface accessible to the surface sensitive tools installed in the UHV chamber. The Auger spectra of the various $TiCl_3$ crystals indicate that the overall procedure was successful. However, for reason of the lack of ordered structures, LEED was not able to reveal useful information about the surface structure of the $TiCl_3$ crystal. Though the $TiCl_3$ crystal surfaces were saturated with a chlorine flux and annealed, they remained disordered. It is possible that the ion bombardment damage was not successfully removed. These results indicate that studies of the real catalyst in UHV condition remain limited by evident physical handicaps. The failure of the application of regular LEED technique on the real catalyst requires the employment and development of alternative techniques sensitive to the disordered surface.

Simulated model surfaces constitute an alternative candidate for the study of Ziegler-Natta surface processes, that is, chlorine layer on a Ti(0001) surface. The DLEED technique for structural determination has been applied to the disordered, low coverage phase of chlorine on Ti(0001). The solid state electrochemical source, used as an internal chlorine source, has indicated an advantage in its ability to provide high dosing level without a

corresponding increase in background pressure.

It was shown that a TV computer method using an image intensifying camera was a useful way to collect the weak diffuse intensities from disordered adsorbates on an ordered surface. The Y-function was employed for the theory-experiment comparison and proved to be good for this purpose. A computer program was developed for a Personal Computer which provided various functions to successfully manipulate the measured diffuse intensities without the aid of Supercomputer or VAX.

The Pendry R-factor analysis of Y-functions using the 78/82-eV data set favored the 3-fold hollow and bridge adsorption sites with spacing of d_{3fa}=2.45 Å and d_{bri}=2.90 Å respectively. The comparison of fits for the other energy set (90/94 eV) was less clear cut but showed similar preferences. A site mix of 85% 3fa and 15% bridge sites was most strongly favored by the Pendry R-factor analysis, having a value of R_P=0.39. This degree of agreement is not as high as in some DLEED studies e.g. W(100)/O (R_P=0.13) [28] but better than others e.g. Pt(111)/CO (R_P=0.55) [52]. We attribute the difficulty in fitting to the weak DLEED signal due possibly to interference from the phonon structure of titanium. The Ti-Cl bond length of 2.96 Å in the 3F site agrees very well with predictions using a recently developed method [80].

REFERENCES

[1] R.B. Seymour, "Polymer Chemistry", Marcel Dekker, Inc., New York and Basle, 1988

[2] G. Natta, J. Polymer Sci., 16 (1955) 143

[3] N.G. Gaylord and H.F. Mark, "Linear and Stereoregular Addition Polymers", Interscience, New York, 1959

[4] Y.V. Kissin, "Isospecific Polymerization of Olefins" Polymers/Properties and Applications, 9 (Springer-Verlog, New York Inc., (1985) pp 2-5

[5] E.J. Arlman, J. Catalysis, 3 (1964) 89

[6] E.J. Arlman and P. Cossee J. Catalysis, 3 (1964) 99

[7] O. Novaro, S. Chow, and P. Magnouat, J. Catalysis, 41 (1976) 91

[8] G. Odian, "Principles of Polymerization", Wiley Interscience, New York, 1981

[9] G. Natta, P. Corradini and Allegra, J. Polymer Sci., 51 (1961) 399

[10] J. Boor, Jr., Macromol. Rev., 2 (1967) 115

[11] J. Boor Jr., "Ziegler-Natta Catalysts and Polymerization", Academic Press, New York, 1979

[12] F.W. Billmeyer, "Textbook of Polymer Science", Wiley Interscience, New York, 1984

[13] J.C.W. Chien, "Coordination Polymerization", Academic Press, 1975

[14] A.D. Gavant in "Catalysis Vol. I", Specialist Periodical Report, The Chemical Society, London, 1977, ch.7

[15] F.J. Karol, Catal. Rev. Sci. Eng., 26 (1985) 255

[16] M. Furuta, J. Polym. Sci. Polm. Phy. Ed., 19 (1981) 135

[17] C. Mousty-Desbuquoit, J. Riga and J.J. Verbist, J. Chem. Phys., 79 (1983) 26

[18] I.H. Khan, Surf. Sci., 48 (1975) 537

[19] T. Smith, J. Electrochem. Soc., 114 (1972) 1398

[20] J.R. Anderson and N. Thompson, Surf. Sci., 28 (1971) 84

[21] M.P. Cox, J.S. Ford, R.M. Lambert and R.H. Prince, Surf Sci., 129 (1983) 375

[22] J.B. Pendry, "Low Energy Electron Diffraction", (Academic Press, London, 1974)

[23] K. Heinz, Progr. Surf. Sci., 145 (1984) 33

[24] P.M. Marcus and F. Jona, "Determination of Surface Structure by LEED", (Plenum, New York, 1984)

[25] P.R. Watson, S.M. Mokler and J.Mischenko III, J. Vac. Sci. Technol., A6(3) (1988) 671

[26] J.B. Pendry and D.K. Saldin, Surf. Sci., 145 (1984) 33

[27] D.K. Saldin, J.B. Pendry, M.A. Van Hove and G.A. Somorjai, Phys. Rev., B 31 (1985) 1216

[28] K. Heinz, K. Muller, W. Popp and H. Lindner, Surf. Sci., 173 (1986) 366

[29] C.T. Davisson and L.H. Germer, Phys. Rev., 30 (1927) 705

[30] L.J. Clarke, "Surface Crystallography", John Wiley & Sons, 1984

[31] D.P. Woodruff and T.A. Delchar, "Modern Technique of Surface Science", Cambridge University Press, 1986 P.24

[32] A. Zangwill, "Physics at Surfaces", Cambridge University Press, 1989 pp. 37-40

[33] M.A. Van Hove, R. Lin and G.A. Somorjai, Phy. Rev. Lett. 51 (1983) 778

[34] J.B. Pendry and D.K. Saldin, Surf. Sci., 145 (1984) 239

[35] J.B. Pendry, "The Structure of Surfaces", Springer Ser. Surf. Sci. 2, M.A. Van Hove and S.Y. Tong, eds. Springer, Berlin (1985) p.124

[36] P.H. Citrin, P. Eisenberger and R.C. Hewitt, Surf. Sci., 89 (1979) 28

[37] J. Stohr, R. Jaeger and S. Brennan, Surf. Sci., 117 (1982) 503

[38] D.K. Saldin, J.B. Pendry, M.A. Van Hove, and G.A. Somorjai, Phy. Rev. B 31 (1985) 1216

[39] H. Ibach and S. Lehwald, Surf. Sci. 176 (1986) 629

[40] P.L. de Andres, P.J. Rous and J.B. Pendry, Surf. Sci., 193 (1988) 1

[41] J.B. Pendry, J. Phy. C. 13 (1980) 937

[42] K. Heinz, D.K. Saldin and J.B. Pendry, Phy. Rev. Lett., 55 (1985) 2312

[43] K. Heinz and K. Muller, in "Structural Studies of Surfaces", edited by G. Hohler, Springer Tracts in Modern Physics, Vol. 91 (Springer, New York, 1982), P.1

[44] P. Heilmann, E. Lang, K. Heinz, and K. Muller, in "Determination of Surface Structure by LEED", edited by P.M. Marcus and F. Jona, Plenum, New York, 1984

[45] H. Ibach and S. Lehwald, Surf. Sci., 176 (1986) 629

[46] U. Clarke, P. Bayer, H. Hloch and K. Heinz, (1988) to be published

[47] P.L. Andres, P.J. Rous and J.B. Pendry, Surf. Sci., 193 (1988) 1

[48] P.J. Rous, J.B. Pendry, D.K. Saldin, K. Heinz, K. Muller and Bickel, Phy. Rev. Letters, 57 (1986) 2951

[49] P.J. Rous, Ph.D. Thesis, Imperial College, London, 1986

[50] G. Illing, D. Heskett, E.W. Plummer, H.J. Freund, J. Somers, Th. Lindner, A.H. Bradshaw, U. Buskotte, M. Neumann, U. Starke, K. Heinz, P.L. De Andres, D. Saldin and J.B. Pendry, Surf. Sci., 206 (1988) 1

[51] P. Piercy, P.A. Heilmann, G. Michalk and D. Menzel, Surf. Sci., 219 (1989) 189

[52] G.S. Blackman, D.F. Ogletree, M.A. Van Hove and G.A. Somorjai, Phys. Rev. Lett., 61 (1988) 2352

[53] M.A. Van Hove, R.F. Lin and G.A. Somorjai, Phy. Rev. Lett., 51 (1983) 778

[54] W.R. Carradine,Jr., and H.F. Rase, J. Appl. Polymer Sci., 15 (1971) 889

[55] J.H. Moore, C.C. Davies and M.A. Coplan, "Building Scientific Apparatus", Addison-Wesley, Massachusetts (1983)

[56] E. Preuss, "Laue Atlas", John Wiley & Sons, New York, London, Toronto

[57] E.A. Wood, "Crystal Orientation Manual", Columbia University Press, New York and London (1963)

[58] E. Preuss, 1973

[59] "Metal Handbook", 1948 Edition (American Society for Metals, Cleveland, Ohio 1948) pp. 159-162

[60] P. Nylen, E. Sunderland, "Modern Surface Coatings", (Interscience Publishers, a division of John Wiley & Sons, Ltd., London (1965) pp. 611-612

[61] H.D. Shih, F. Jona, D.W. Jepsen and P.M. Marcus, J. Phy. C.: Solid State Phys., 9 (1976) 1405

[62] H.L. Davis and J.R. Noonan, J. Vac. Sci. Technol., 20 (1982) 842

[63] N.D. Spencer, P.J. Goddard, , J. Vac. Sci. Technol., A1 (1983) 1554

[64] Reference [34], P.1

[65] D.K. Saldin, J.B. Pendry, Computer Phys. Communication 42 (1986) 399

[66] D.K. Saldin, J.B. Pendry, Computer Phys. Communication 46 (1987) 129

[67] P.A. Lee and J.B. Pendry, Phys. Rev., B11 (1975) 1279

[68] M.A. Van Hove in "Chemistry and Physics of Solid Surfaces VII", Eds. R.F. Howe and R. Vanselow, Springer-verlag (Heidelberg) (1988), p.513

[69] M.A. Van Hove and S.Y. Tong, "Surface Crystallography by LEED" Springer, Heidelberg (1979)

[70] B. Lau, B.J. Mrstik, S.Y. Tong, and M.A. Van Hove (Unpublished)

[71] D. Norman, Daresbury Lab., England, Private Communication

[72] T. Smith, J. Electrochem. Soc., 119 (1972) 1398

[73] M. Grunze and P.A. Dowben, Appl. Surf. Sci., 10 (1982) 209

[74] P.R. Watson, S.M. Mokler and J. Mischenko III, J. Vac. Sci. Technol. A, 6 No.3, (1988) 671

[75] H.L. Davis and D.M. Zehner, J. Vac. Sci. Technol., 17(1), 1980

[76] K.A. Gschneider, Solid State Phys., 16 (1964) 384

[77] K.A.R. Mitchell Surf. Sci., 149 (1985) 93

[78] L. Pauling, "The Nature of the Chemical Bond", Cornell University Press, Ithaca, New York, 1960

[79] I.D. Brown, In "Structure and Bonding in Crystals" Vol. 2 Edited by M. O'Keefe and A. Navrotsky, Academic Press, New York, 1981, P.1

[80] I.D. Brown and D. Altermatt, Acta Crystallgr., B 41 (1985) 244

[81] K.A.R. Mitchell, S.A. Schlatter, and R.N.S. Sodhi, Can. J. Chem., 64 (1986) 1435

[82] G.M. Lamble, R.S. Brooks, J.C. Campuzano, D.A. King and D. Norman, Phys. Rev., B 36 (1987) 1796

[83] R. Jungst, D. Sekutowski, J. Davis, M. Luly and G. Stuckey, Inorg. Chem., 16 (1977) 1695

[84] G. Natta, P. Corradini and I.W. Bassi, J. Amer. Chem. Soc., 80 (1958) 755

[85] U. Thewalt and F. Osterle, J. Organomet. Chem., 172 (1979) 317

[86] H.R. Van Der Waal, F. Overzet, H.O. Van Oven, J.L. De Boer, H.J. De Liefale Meijer and F.Jellinek, J.Organomet. Chem., 92 (1978) 329

[87] N.C. Baenziger and R.E. Rundle, Acta Cryst., 1 (1948) 274

[88] E. Zanazzi, F. Jona, D.W. Jepsen and P.M. Marcus, Phys. Rev., B14 (1976) 432

[89] G.M. Lamble, R.S. Brooks, J-C. Campuzano, D.A. King and D. Norman, Phys. Rev., B36 (1987) 1796

[90] D.J. Holmes, N. Panagoitides, R. Dus, D. Norman, G.M. Lamble, C.J. Banes, F. Della Valle and D.A. King, J. Vac. Sci. Technol., A5 (1987) 703

[91] G. Lamble, R.S. Brooks, S. Ferrer, D.A. King and D. Norman, Phys. Rev., B34 (1986) 2975

[92] F. Jona, D.Westphal, A. Goldman and P.M. Marcus, J. Phys. C., 16 (1983) 3001

[93] P.H. Citrin, D.R. Hamann, L.F. Mattheiss and J.E. Rowe, Phys. Rev. Lett. 49 (1982) 1712

[94] M.D. Crapper, C.E. Riley, P.J.J. Sweeney, C.F. McConville, D.P. Woodruff and R.G. Jones, Surf. Sci., 182 (1987) 182

[95] G.E. Coates, M.L.H. Green, and K. Wade, "Organometallic compounds", Methuen, (1967) p. 323, 328

[96] F.L. Cotton and G. Wilkinson "Advanced Inorganic Chemistry", 4th ed., John Wiley & Sons, pp. 696-704 1980

[97] M.F.C. Ladd and R.A. Palmer, "Structure Determination by X-ray Crystallography", Plenum Press, New York and London, 1985

[98] R.P.H. Gasser, "An Introduction to Chemisorption and Catalysis by Metals" Clarendon Press, Oxford 1985 pp. 53-55

[99] L. Davis, N. MacDonald, P. Palmberg, G. Raich and R. Weber, "PHI Handbook of Auger Spectroscopy" 2nd Ed., Physical Electronic Industries, (1976)

[100] J.B. Pendry, "Low Energy Electron Diffraction", Academic Press, New York (1974)

APPENDICES

APPENDIX 1. Plotting program of the simulated Laué pattern

```
SCREEN 0: CLS
PRINT "*************************************************************************"
PRINT "*                                                                       *"
PRINT "*                        PROGRAM : PLOTTER                              *"
PRINT "*                                                                       *"
PRINT "*                   PLOTTING OF THE LAUE PATTERN                        *"
PRINT "*                                                                       *"
PRINT "*                        ( JUNE  27  1988 )                             *"
PRINT "*                                                                       *"
PRINT "*************************************************************************"
    PRINT
10  PRINT
    INPUT "Enter the name of the input file "; X$
    PRINT
30 'INPUT "Enter the number of the data set "; N
   'PRINT
    OPEN "I", #1, X$
50  'INPUT "Enter the Name of the output file "; Y$
70  'OPEN "O", #2, Y$
    INPUT "Do you want to see the Graph of the LAUE Pattern (Y/N)"; Q$
    IF Q$ = "Y" OR Q$ = "y" THEN 100 ELSE 200
100 INPUT "Enter the number of the data set "; N
   'OPEN "I", #1, X$
    PRINT
    CLS
    SCREEN 2
    CIRCLE (320, 100), 215
120 FOR I = 1 TO N
        INPUT #1, A1, A2, A3, A4, A5, A6
        IF A6 < 200 THEN R = 2
        IF (200 <= A6 AND A6 < 500) THEN R = 4
        IF (500 <= A6 AND A6 < 2300) THEN R = 6
        IF A6 >= 2300 THEN R = 8
        CIRCLE (2 * A4 + 320, A5 + 100), R
    NEXT
    CLOSE (1)
    CLOSE (2)
200 PRINT
    INPUT "Do you want to plot the LAUE Pattern (Y/N) "; Q2$
    IF Q2$ = "Y" OR Q2$ = "y" THEN 250 ELSE END
    'PLOTTING PROGRAM FOR THE HP PLOTTER BASED ON THE CALCULATED DATA SETS
    '*************************************************************************"
    PRINT
250 INPUT "Enter the name of the input file "; X$
   'OPEN "I", #1, X$
    PRINT
    INPUT "Enter the number of LAUE Spots which you want to plot"; N
    CLS
    OPEN "COM1:9600,S,7,1,RS,CS65535,DS,CD" FOR RANDOM AS #3
    PRINT #3, "IN;SP1;"
   'PRINT #3, "PA6050,4000;CI3000,5;"
    PRINT #3, "SP2;"
300 FOR I = 1 TO N
        INPUT #1, A1, A2, A3, A4, A5, A6
        IF A6 < 200 THEN R = 2
```

```
        IF (200 <= A6 AND A6 < 500) THEN R = 4
        IF (500 <= A6 AND A6 < 2300) THEN R = 6
        IF A6 > 2300 THEN R = 8
        'CONVERSIONS OF THE COORDINATES FOR PLOTTING
        X = (A4 + 100) * 28 + 3200
        Y = (A5 + 100) * 30 + 850
        R = 2 * SQR(A6)
        'PLOTTING OF LAUE SPOTS
        PRINT A1, A2, A3, X, Y, R
        FOR I = 2 TO N
            IF (A1 = N * (A1) AND A2 = N * (A2) AND A3 = N * (A3)) THEN READ DUM
            IF R < 5.2 THEN READ DUMMY
            GOTO 440
            'SORTING PROGRAM
            ********************************************************************
            DIM ARRAY(N)
                FOR J = 2 TO N
                A = ARRAY(J)
                    FOR I = J - 1 TO I STEP -1
                    IF (ARRAY(I) <= A) THEN GOTO 430
                    ARRAY(I + 1) = ARR(I)
                    NEXT I
                I = 0
430         ARRAY(I + 1) = A
                NEXT J
440         PRINT
            PRINT #3, "PA", X, ",", Y, ";CI", R, ",10;"
            ' FILLING PROGRAM FOR THE PLOTTED LAUE SPOTS
            '*******************************************************************
450         PRINT #3, "PT.7;FT1;"
            IF R > 90 THEN PRINT #3, "WG-95,270,360;"
            IF (45 <= R AND R < 90) THEN PRINT #3, "WG-45,270,360;"
            IF (33 <= R AND R < 45) THEN PRINT #3, "WG-33,90,360;"
            IF (30 <= R AND R < 33) THEN PRINT #3, "WG-30,90,360;"
            IF (24 <= R AND R < 30) THEN PRINT #3, "WG-25,90,360;"
            IF (18 <= R AND R < 24) THEN PRINT #3, "WG-18,90,360;"
            IF (10 <= R AND R < 18) THEN PRINT #3, "WG-10,90,360;"
            IF (5.2 <= R AND R < 10) THEN PRINT #3, "WG-6,90,360;"
            IF R < 5.2 THEN 500
            ' LABELING MILLER INDICES ON EACH LAUE SPOTS
            '*******************************************************************
500         X1 = X - 320
            Y1 = Y + 120
            PRINT #3, "PA", X1, ",", Y1, ";"
            PRINT #3, "SR0.5,0.7;"
           ' CRITERIA FOR THE LABELING SIZES OF MILLER INDICES
           ' IF R = 120 THEN PRINT #3, "SR1,1.5;LB400" + CHR$(3)
           ' IF R = 30 THEN 550
           ' IF R = 60 THEN 560
           ' IF R = 90 THEN 570
           ' IF R = 120 THEN 580
550        ' PRINT #3, "SR .4, .5;"; LB; ";A1;A2;A3;CHR$(3)"
560        ' PRINT #3, "SR .6, .8;"; LB; ";A1;A2;A3;CHR$(3)"
570        ' PRINT #3, "SR .8, 1;"; LB; ";A1;A2;A3;CHR$(3)"
           ' PRINT #3, "SR 1,1.3;"; LB; ";A1;A2;A3;CHR$(3)"
            PRINT #3, "LB"; A1; A2; A3; CHR$(3);
        NEXT
650 NEXT
    'DRAWING THE OUTSIDE BOX
    '*******************************************************************"
```

```
700 PRINT #3, "SP1;PA100,350;XT;PD100,7620;XT;"
    PRINT #3, "PA100,7620;YT;PD10000,7620;YT;"
    PRINT #3, "PA10000,7620;XT;PD10000,350;XT;"
    PRINT #3, "PA10000,350;YT;PD100,350;YT;"
    'LABELING TEXTS FOR THE LAUE PATTERN
    '*************************************************************************"
    'LABELING TEXT WHICH WILL BE IN THE TOP SPACE
    PRINT "NOW YOU WANT TO ENTER ALL THE VALUES AND PARAMETERS FOR YOUR LAUE PAT
    PRINT
    PRINT #3, "SI"
800 PRINT #3, "SP2;PU 300,7450;"
    DIM X$(80)
    PRINT #3, "LBLAUE REFLECTION DIAGRAM : TRIKLIN TEST," + CHR$(3)
    INPUT "ENTER THE SIZE OF FILM DISTANCE (CM)", X$(1)
    PRINT #3, "PA 3350,7450;"
    PRINT #3, "LB", X$(1), CHR$(3)
    PRINT #3, "PU 5100,7450;"
    PRINT #3, "LBCM FILM DISTANCE" + CHR$(3)
    PRINT #3, "PU 300,7250;"
    PRINT #3, "LBLAUE PATTERN IN REFLECTION OF THE" + CHR$(3)
    PRINT #3, "PU 50,7050;"
    INPUT "ENTER THE MILLER INDEX (h  k  l)"; X$(2)
    PRINT #3, "PA -850,7050;"
    PRINT #3, "LB", X$(2), CHR$(3)
    PRINT #3, "PU 300,7050;"
    PRINT #3, "LB(       ) PLANE NORMAL" + CHR$(3)
    PRINT #3, "PU 300,6850;"
    PRINT #3, "LBTHE CRYSTAL AXES ARE (ANGSTR.):" + CHR$(3)
    PRINT #3, "PU 300,6650;"
    PRINT #3, "LBA= " + CHR$(3)
    INPUT "ENTER THE VALUE OF LATTICE PARAMETER (A) "; X$(3)
    PRINT #3, "PA -500,6650;"
    PRINT #3, "LB", X$(3), CHR$(3)
    PRINT #3, "PU 300,6450;"
    PRINT #3, "LBB= " + CHR$(3)
    INPUT "ENTER THE VALUE OF LATTICE PARAMETER (B) "; X$(4)
    PRINT #3, "PA -500,6450;"
    PRINT #3, "LB", X$(4), CHR$(3)
    PRINT #3, "PU 300,6250;"
    PRINT #3, "LBC= " + CHR$(3)
    INPUT "ENTER THE VALUE OF LATTICE PARAMETER (C) "; X$(5)
    PRINT #3, "PA -500,6250;"
    PRINT #3, "LB", X$(5), CHR$(3)
    PRINT #3, "PU 300,6050;"
    PRINT #3, "LBTHE CRYSTAL ANGLES ARE (DEGR.):" + CHR$(3)
    PRINT #3, "PU 300,5850;"
    PRINT #3, "LBALPHA = " + CHR$(3)
    INPUT "ENTER THE VALUE OF CRYSTAL ANGLE (ALPHA)"; X$(6)
    PRINT #3, "PU 0,5850;"
    PRINT #3, "LB", X$(6), CHR$(3)
    PRINT #3, "PU 300,5650;"
    PRINT #3, "LBBETA  = " + CHR$(3)
    INPUT "ENTER THE VALUE OF CRYSTAL ANGLE (BETA)"; X$(7)
    PRINT #3, "PU 0,5650;"
    PRINT #3, "LB", X$(7), CHR$(3)
    PRINT #3, "PU 300,5450;"
    PRINT #3, "LBGAMMA = " + CHR$(3)
    INPUT "ENTER THE VALUE OF CRYSTAL ANGLE (GAMMA)"; X$(8)
    PRINT #3, "PU 0,5450;"
    PRINT #3, "LB", X$(8), CHR$(3)
```

```
    INPUT "ENTER THE NAME OF CRYSTAL TYPE (e.g. DIAMOND)"; X$(10)
    PRINT #3, "PU 880,650;"
    PRINT #3, "LB", X$(10), CHR$(3)
    PRINT #3, "PU 300,450;"
    PRINT #3, "LBTHE THREE MILLER INDICES ARE IN THE RANGE OF +-" + CHR$(3)
1000 PRINT #3, "SP0;"
    END
```

APPENDIX 2. Manipulating program for the image processing

```
'*************************************************************************
'*   PROGRAM : IMAGE MANIPULATER                                         *
'*   THIS PROGRAM IS WRITTEN FOR THE ARITHMETIC MANIPULATIONS BETWEEN    *
'*   IMAGES. IF YOU WANT TO ADD,SUBTRACT OR DIVIDE DATA, YOU NEED TO ENTER *
'*   TWO INPUT FILES AND ONE OUTPUT FILE                                 *
'*************************************************************************
    CLS
    PRINT
    PRINT "*************** PROGRAM : IMAGE MANIPULATER ******************"
    PRINT
    PRINT "OPTIONS:"
    PRINT
    PRINT "<M> DATA ADDITION, SUBTRACTION, DIVISION OR EXPL Y-FUNCTION"
    PRINT "<B> SCALAR ADDITION, SUBTRACTION DIVISION OR MULTIPLICATION"
    PRINT "<C> DATA CONVERSION FOR 3-D PLOT (SURFER)"
    PRINT "<D> DATA FILTERING FOLLOWED BY SQUEEZING"
    PRINT "<E> DATA SMOOTHING AND SLOW SQUEEZING"
    PRINT "<Y> Y-FUNCTION FROM SORTED DATA(THEORETICAL)"
    PRINT "<S> DATA SAMPLING (N*N)"
    PRINT "<K> CONVERSION OF COORDINATES TO K-SPACE"
    PRINT "<I> K-SPACE VALUE ADJUSTING FOR R-FACTOR ANALYSIS"
    PRINT "<A> DATA ADDITION FOLLOWED BY AVERAGING"
    PRINT "<R> PENDRY R-FACTOR CALCULATION"
    PRINT
    INPUT "WHICH FUNCTION DO YOU WANT TO TRY "; Q$
    IF Q$ = "M" OR Q$ = "m" THEN GOTO 200
    IF Q$ = "B" OR Q$ = "b" THEN GOTO 700
    IF Q$ = "C" OR Q$ = "c" THEN GOTO 1200
    IF Q$ = "D" OR Q$ = "d" THEN GOTO 1300
    IF Q$ = "E" OR Q$ = "e" THEN GOTO 1500
    IF Q$ = "Y" OR Q$ = "y" THEN GOTO 1550
    IF Q$ = "S" OR Q$ = "s" THEN GOTO 1800
    IF Q$ = "K" OR Q$ = "k" THEN GOTO 2700
    IF Q$ = "I" OR Q$ = "i" THEN GOTO 3500
    IF Q$ = "A" OR Q$ = "a" THEN GOTO 3800
    IF Q$ = "R" OR Q$ = "r" THEN GOTO 3900
    '----------------------------------------
    '-   SUBROUTINE 1 : IMAGE MANIPULATION   -
    '----------------------------------------
    'MAIN STRUCTURE FOR IMAGE ADDITION, SUBTRACTION AND DIVISION ***********
200 PRINT
    INPUT "ENTER INPUT FILE NAME 1:"; AA$

    INPUT "ENTER INPUT FILE NAME 2:"; BB$
    INPUT "ENTER OUTPUT FILE NAME 3:"; CC$
    INPUT "ENTER THE Vor VALUE (ev)"; Vor
    OPEN AA$ FOR INPUT AS #1
    OPEN BB$ FOR INPUT AS #2
    OPEN CC$ FOR OUTPUT AS #3
    'RESERVE THE CONDITIONS FOR DATA ***********************************
       'INPUT #1, I1
       'INPUT #2, I2
       'PRINT #3, I1, "/", I2
       'PRINT #3, I2,
        K = 1
```

```
      DO UNTIL K > 5
         INPUT #1, I1
         INPUT #2, I2
         PRINT #3, I2
         K = K + 1
      LOOP
   PRINT
   CLS
   PRINT "*****************************************************"
   PRINT "*                 <A> DATA ADDITION                 *"
   PRINT "*                 <S> DATA SUBTRACTION              *"
   PRINT "*                 <D> DATA DIVISION                 *"
   PRINT "*                 <Y> EXPERIMENTAL Y-FUNCTION       *"
   PRINT "*                 <Q> QUIT                          *"
   PRINT "*****************************************************"
   PRINT
   PRINT "SELECT ONE OPTION (USE CAPITAL LETTER) ?";
   GOSUB 290: J = INSTR("ASDYQ", A$): PRINT
   ON J GOTO 300, 400, 500, 600, 3000
290 A$ = INKEY$: IF A$ = "" THEN GOTO 290 ELSE PRINT A$; : RETURN
300  PRINT
    'SUBROUTINE 1-1 : DATA ADDITION***********************************
    DO UNTIL EOF(1) OR EOF(2)
       INPUT #1, I1
       INPUT #2, I2
       A = I1 + I2
       PRINT #3, USING "###"; A
       K = K + 1
    LOOP
    PRINT "ALL DONE ... ADDED.DAT CREATED"
    GOTO 4000
    '*****************************************************************
400  PRINT
    'SUBROUTINE 1-2 : DATA SUBTRACTION********************************
    DO UNTIL EOF(1) OR EOF(2)
       INPUT #1, I1
       INPUT #2, I2
       S = I1 - I2
       PRINT #3, USING "###"; S
       K = K + 1
    LOOP
    PRINT "ALL DONE ... SUBTRACTED.DAT CREATED"
    GOTO 4000
    '*****************************************************************
500  PRINT
    'SUBROUTINE 1-3 : DATA DIVISION **********************************
    DO UNTIL EOF(1) OR EOF(2)
       INPUT #1, I1
       INPUT #2, I2
       D = I1 / I2
       IF I1 = 0 THEN D = 0!
       IF I2 = 0 THEN I2 = 1
       PRINT #3, USING "###.##"; D
       K = K + 1
    LOOP
    PRINT "ALL DONE ... DIVIDED.DAT CREATED"
    GOTO 4000
    '*****************************************************************
600  PRINT
    'SUBROUTINE 1-4 : EXPERIMENTAL Y-FUNCTION ************************
```

```
      'CALAULATE THE EXPERIMENTAL Y-FUNCTION FROM THE PIXEL VALUES
      INPUT "ENTER THE ESTEP VALUE(E2-E1)"; ESTEP
      PRINT
      DO UNTIL EOF(1) OR EOF(2)
         INPUT #1, I1
         INPUT #2, I2
               I21 = I2 - I1
               IF I21 = 0 THEN Y = 0!
               IF I1 = 0 THEN I1 = 1
               L = I21 / (ESTEP * (I1 + I2) / 2)
               J = (L ^ 2) * Vor ^ 2
               Y = 100 * L / (1 + J)
         PRINT #3, USING "###.##"; Y
         K = K + 1
      LOOP
      PRINT "ALL DONE ... EXPERIMENTAL Y-FUNCTION CREATED"
      GOTO 4000
      '*****************************************************************
700   PRINT
      '----------------------------------------
      '-   SUBROUTINE 2: SCALAR MANIPULATION   -
      '----------------------------------------
      'MAIN STRUCTURE FOR SCALAR ADDITION, SUBTRACTION, DIVISION
      'AND MULTIPLICATION OF DATA
      INPUT "ENTER INPUT FILE NAME 1:"; A$
750   INPUT "ENTER THE ARITHMETIC FACTOR(AF)"; AF
      INPUT "ENTER OUTPUT FILE NAME 2:"; B$
      OPEN A$ FOR INPUT AS #1
      OPEN B$ FOR OUTPUT AS #2
           K = 1
           DO UNTIL K > 5
              INPUT #1, I1
              PRINT #2, I1
              K = K + 1
           LOOP
       PRINT
       CLS
       PRINT "*********************************************************"
       PRINT "*                <A> SCALAR ADDITION                    *"
       PRINT "*                <S> SCALAR SUBTRACTION                 *"
       PRINT "*                <D> SCALAR DIVISION                    *"
       PRINT "*                <M> SCALAR MULTIPLICATION              *"
       PRINT "*                <Q> QUIT                               *"
       PRINT "*********************************************************"
       PRINT
       PRINT "SELECT ONE OPTION (USE CAPITAL LETTER) ?";
       GOSUB 790: J = INSTR("ASDMQ", A$): PRINT
       ON J GOTO 800, 900, 1000, 1100, 3000
790    A$ = INKEY$: IF A$ = "" THEN GOTO 790 ELSE PRINT A$; : RETURN
800    PRINT
       'SUBROUTINE 2-1 : SCALAR ADDITION ******************************
       DO UNTIL EOF(1)
          INPUT #1, I1
          A = I1 + AF
          A = A * 100
          PRINT #2, USING "###.#"; A
          K = K + 1
       LOOP
       PRINT "ALL DONE ... ADDED.DAT CREATED"
       GOTO 4000
```

```
      '*****************************************************************
900   PRINT
      'SUBROUTINE 2-2 : SCALAR SUBTRACTION ****************************
      DO UNTIL EOF(1)
         INPUT #1, I1
         S = I1 - AF
         PRINT #2, USING "###.###"; S
         K = K + 1
      LOOP
      PRINT "ALL DONE ... SUBTRACTED.DAT CREATED"
      GOTO 4000
      '*****************************************************************
1000  PRINT
      'SUBROUTINE 2-3 : SCALAR DIVISION *******************************
      DO UNTIL EOF(1)
         INPUT #1, I1
         D = I1 / AF
         IF I1 = 0 THEN D = 0!
         IF AF = 0 THEN GOTO 750
         PRINT #2, USING "###.##"; D
         K = K + 1
      LOOP
      PRINT "ALL DONE ... DIVIDED.DAT CREATED"
      GOTO 4000
      '*****************************************************************
1100  PRINT
      'SUBROUTINE 2-4 : SCALAR MULTIPLICATION *************************
      DO UNTIL EOF(1)
         INPUT #1, I1
         M = I1 * AF
         PRINT #2, USING "###.##"; M
         K = K + 1
      LOOP
      PRINT "ALL DONE ... MULTIPLIED.DAT CREATED"
      GOTO 4000
      '*****************************************************************
1200  PRINT
      '-------------------------------------------------------------
      '-   SUBROUTINE 3 : DATA CONVERSION FOR 3-D PLOT(SURFER)    -
      '-------------------------------------------------------------
      INPUT "ENTER INPUT FILE NAME 1:"; A$
      INPUT "ENTER OUTPUT FILE NAME 2:"; B$
      INPUT "ENTER THE XSIZE OF WINDOW"; XSIZE
      INPUT "ENTER THE YSIZE OF WINDOW"; YSIZE
      OPEN A$ FOR INPUT AS #1
      OPEN B$ FOR OUTPUT AS #2
      'DUMMY READ SET
      'FOR K = 1 TO 5
          'INPUT #1, DUMMY
      'NEXT K
      'GET DESIRED VALUE
      INPUT #1, I1
      INPUT #1, I2
      INPUT #1, I3
      INPUT #1, I4
      INPUT #1, I5
      PRINT #2, I1, I2, I3, I4, I5
      Y = 1
      DO UNTIL Y > YSIZE
         X = 1
```

```
      DO UNTIL X > XSIZE
         INPUT #1, I
         PRINT #2, X, Y, I
         X = X + 1
      LOOP
      Y = Y + 1
   LOOP
   PRINT
   PRINT "ALL DONE ... CONVERTED.DAT FOR 3-D PLOT CREATED"
   GOTO 4000
   '*****************************************************************
1300 PRINT
   '-------------------------------------
   '-   SUBROUTINE 4 : DATA SMOOTHING   -
   '-------------------------------------
   'SUBROUTINE 4-1 : DATA FILTERING FOLLOWED BY SQUEEZING **********
   INPUT "ENTER INPUT FILE NAME 1:"; A$
   INPUT "ENTER OUTPUT FILE NAME 2:"; B$
   INPUT "ENTER THE COLUMN SIZE(COLSIZE)"; COLSIZE
   OPEN A$ FOR INPUT AS #1
   OPEN B$ FOR OUTPUT AS #2
   'DUMMY READ SET
   FOR K = 1 TO 5
       INPUT #1, A(K)
       PRINT #2, A(K)
   NEXT K
   'GET DESIRED VALUE
   DO UNTIL EOF(1)
      K = 1
      'STORE THE DATA OF THE FIRST ROW IN A(400)
      DO UNTIL K > COLSIZE OR EOF(1)
         A(K) = VAL(INPUT$(3, #1))
         K = K + 1
      LOOP
      K = 1
      DO UNTIL K > COLSIZE OR EOF(1)
         PIX1 = VAL(INPUT$(3, #1))
         PIX2 = VAL(INPUT$(3, #1))
         AK = A(K) + A(K + 1)
         PX = PIX1 + PIX2
         SPX = (AK + PX) / 4
         PRINT #2, USING "###"; SPX
        K = K + 2
      LOOP
   LOOP
   PRINT
   PRINT "ALL DONE ... SMOOTHED AND SQUEEZED.DAT CREATED"
   GOTO 4000
   '*****************************************************************
1500 PRINT
   'SUBROUTINE 4-2 : DATA SMOOTHING FOLLOWED BY SLOW SQUEEZE *******
   DIM B(1 TO 400)
   DIM C(1 TO 400)
   INPUT "ENTER INPUT FILE NAME 1:"; A$
   INPUT "ENTER OUTPUT FILE NAME 2:"; B$
   INPUT "ENTER THE COLUMN SIZE(COLSIZE)"; COLSIZE
   OPEN A$ FOR INPUT AS #1
   OPEN B$ FOR OUTPUT AS #2
   'HEADER INFORMATION
   FOR K = 1 TO 5
```

```
        INPUT #1, A(K)
        PRINT #2, A(K)
    NEXT K
    'GET DESIRED VALUE
    DO UNTIL EOF(1)
       K = 1
       'STORE THE DATA OF THE FIRST ROW IN A(400)
       FOR I = 1 TO COLSIZE
           A(I) = VAL(INPUT$(3, #1))
       NEXT I
       FOR J = 1 TO COLSIZE
           B(J) = VAL(INPUT$(3, #1))
       NEXT J
       'SMOOTH AND SLOW SQUEEZE IMAGE WINDOW
       DO UNTIL K > COLSIZE OR EOF(1)
           FOR J = 1 TO COLSIZE
               AI = A(I) + A(I + 1)
               BJ = B(J) + B(J + 1)
               CIJ = (AI + BJ) / 4
               PRINT #2, USING "###"; CIJ
           NEXT J
           FOR J = 1 TO COLSIZE
               A(I) = B(J)
           NEXT J
           FOR J = 1 TO COLSIZE OR NOT EOF(1)
               B(J) = VAL(INPUT$(3, #1))
           NEXT J
       LOOP
    LOOP
    PRINT
    PRINT "ALL DONE ..."
    GOTO 4000
    '*****************************************************************
    '-----------------------------------------------
    '-   SUBROUTINE 6 : THEORETICAL Y-FUNCTION    -
    '-----------------------------------------------
1550 CLS
    PRINT "************************************************************"
    PRINT "*              <A> Y-FUNCTION FROM 2 ENERGIES              *"
    PRINT "*              <B> Y-FUNCTION FROM 3 ENERGIES              *"
    PRINT "************************************************************"
    PRINT
    PRINT "SELECT ONE OPTION (USE CAPITAL LETTER) ?";
    GOSUB 1590: J = INSTR("AB", A$): PRINT
    ON J GOTO 1600, 1700
1590 A$ = INKEY$: IF A$ = "" THEN GOTO 1590 ELSE PRINT A$; : RETURN
1600 PRINT
    INPUT "ENTER INPUT FILE NAME 1:"; A$
    INPUT "ENTER INPUT FILE NAME 2:"; B$
    INPUT "ENTER OUTPUT FILE NAME 3:"; C$
    INPUT "ENTER THE ESTEP VALUE(E2-E1)"; ESTEP
    INPUT "ENTER THE Vor VALUE(eV)"; Vor
    OPEN A$ FOR INPUT AS #1
    OPEN B$ FOR INPUT AS #2
    OPEN C$ FOR OUTPUT AS #3
    'WRITE THE TEXT TO THE OUTPUT FILE
    'DIM STRING1 AS STRING
    'STRING1 = "THEORETICAL Y-FUNCTION DATA FOR TI(001)/CL"
    'PRINT #3, STRING1
    'RESERVE THE CONDITION FOR DATA
```

```
        INPUT #1, DUMMY
        INPUT #2, DUMMY
        'PRINT #3, X2
        'CALCULATE Y-FUNCTION FROM 2 DATA FILES
        K = 1
        DO UNTIL EOF(1) OR EOF(2)
           INPUT #1, X1, Y1, I1
           INPUT #2, X2, Y2, I2
                     I21 = I2 - I1
                     IF I21 = 0 THEN Z = 0!
                     I12 = I1 + I2
                     IF I12 = 0 THEN I12 = 1! * E - 10
                     'IF I1 = 0 THEN I1 = 1
                     L = I21 / (ESTEP * I12 / 2)
                     J = (L ^ 2) * (Vor ^ 2)
                     Z = 100 * L / (1 + J)
                     'X2 = (X1 + X2) / 2
                     'Y2 = (Y1 + Y2) / 2
           PRINT #3, X2, Y2, Z
           K = K + 1
        LOOP
        PRINT
        PRINT "ALL DONE ... THEORETICAL Y-FUNCTION(2 ENERGIES) CREATED"
        GOTO 4000
        '*************************************************************
1700    PRINT
        INPUT "ENTER INPUT FILE NAME 1:"; A$
        INPUT "ENTER INPUT FILE NAME 2:"; B$
        INPUT "ENTER INPUT FILE NAME 3:"; C$
        INPUT "ENTER OUTPUT FILE NAME 4:"; D$
        INPUT "ENTER ESTEP VALUE(E2-E1)"; ESTEP
        INPUT "ENTER THE Vor VALUE (eV)"; Vor
        OPEN A$ FOR INPUT AS #1
        OPEN B$ FOR INPUT AS #2
        OPEN C$ FOR INPUT AS #3
        OPEN D$ FOR OUTPUT AS #4
        'WRITE THE TEXT TO THE OUTPUT FILE*********************************
        DIM STRING2 AS STRING
        STRING2 = "THEORETICAL Y-FUNCTION DATA FOR TI(001)/S"
        PRINT #4, STRING2
        'RESERVE THE CONDITION FOR DATA************************************
        INPUT #1, X1
        INPUT #2, X2
        INPUT #3, X3
        PRINT #4, X2
        'CALCULATE Y-FUNCTION FROM 3 DATA FILES****************************
        K = 1
        DO UNTIL EOF(1) OR EOF(2)
           INPUT #1, X1, Y1, I1
           INPUT #2, X2, Y2, I2
           INPUT #3, X3, Y3, I3
                     I31 = I3 - I1
                     IF I31 = 0 THEN Z = 0!
                     IF I2 = 0 THEN I2 = 1! * E - 10
                     'IF I1 = 0 THEN I1 = 1
                     L = I31 / (2 * ESTEP * I2)
                     J = (L ^ 2) * (Vor ^ 2)
                     Z = 100 * L / (1 + J)
           PRINT #4, X2, Y2, Z
           K = K + 1
```

```
      LOOP
      PRINT
      PRINT "ALL DONE ... THEORETICAL Y-FUNCTION(3 ENERGIES) CREATED"
      GOTO 4000
      '*****************************************************************
1800  PRINT
      '-----------------------------------
      '-   SUBROUTINE 5 : DATA SAMPLING   -
      '-----------------------------------
      'SAMPLING 1 DATA FROM (N*N) MATRIX
      'MAIN STRUCTURE FOR DATA SAMPLING
      DIM D(1 TO 1000)
      INPUT "ENTER INPUT FILE NAME 1:"; A$
      INPUT "ENTER OUTPUT FILE NAME 2:"; B$
      INPUT "ENTER THE COLUMN SIZE(COLSIZE)"; COLSIZE
      OPEN A$ FOR INPUT AS #1
      OPEN B$ FOR OUTPUT AS #2
      'HEADER INFORMATION
      FOR K = 1 TO 5
          INPUT #1, D(K)
          PRINT #2, D(K)
      NEXT K
      PRINT
      CLS
      PRINT "*************************************************************"
      PRINT "*                    <A> (2*2) SAMPLING                     *"
      PRINT "*                    <B> (3*3) SAMPLING                     *"
      PRINT "*                    <C> (3*3)-SAMPLING                     *"
      PRINT "*                    <D> DATA REWRITING                     *"
      PRINT "*                    <E> (4*4) SAMPLING                     *"
      PRINT "*                    <F> (5*5) SAMPLING                     *"
      PRINT "*                    <G> (6*6) SAMPLING                     *"
      PRINT "*************************************************************"
      PRINT
      PRINT "SELECT ONE OPTION (USE CAPITAL LETTER) ?";
      GOSUB 1900: J = INSTR("ABCDEFG", A$): PRINT
      ON J GOTO 2000, 2100, 2200, 2300, 2400, 2500, 2600
1900  A$ = INKEY$: IF A$ = "" THEN GOTO 1900 ELSE PRINT A$; : RETURN
2000  PRINT
      'SUBROUTINE 5-1 : (2*2) SAMPLING *********************************
      K = 1
      DO UNTIL EOF(1)
         K = 1
         DO UNTIL K > COLSIZE OR EOF(1)
            INPUT #1, DUMMY
            K = K + 1
         LOOP
         K = 1
         DO UNTIL K > COLSIZE OR EOF(1)
            INPUT #1, D(K)
            INPUT #1, D(K + 1)
            PRINT #2, D(K + 1)
            K = K + 2
         LOOP
      LOOP
      PRINT "ALL DONE ... (2*2) SAMPLED.DAT CREATED"
      GOTO 4000
      '*****************************************************************
2100  PRINT
      'SUBROUTINE 5-2 : (3*3) SAMPLING *********************************
```

```
      K = 1
      DO UNTIL EOF(1)
         K = 1
         DO UNTIL K > COLSIZE OR EOF(1)
            INPUT #1, DUMMY
            'D(K) = VAL(INPUT$(3, #1))
            'D(K) = DUMMY
            K = K + 1
         LOOP
         K = 1
         DO UNTIL K > COLSIZE - 1 OR EOF(1)
            INPUT #1, DUMMY
            INPUT #1, D(K + 1)
            INPUT #1, DUMMY
            PRINT #2, D(K + 1)
            K = K + 3
         LOOP
            'INPUT #1, DUMMY
         K = 1
         DO UNTIL K > COLSIZE OR EOF(1)
            INPUT #1, DUMMY
            K = K + 1
         LOOP
      LOOP
      PRINT "ALL DONE ... (3*3) SAMPLED.DAT CREATED"
      GOTO 4000
      '*****************************************************************
2200  PRINT
      'ANOTHER (3*3)-SAMPLING FOR (9*9) SAMPLING WITH PARALELL WRITING
      K = 1
      DO UNTIL EOF(1)
         K = 1
         DO UNTIL K > COLSIZE OR EOF(1)
            INPUT #1, DUMMY
            K = K + 1
         LOOP
         K = 1
         DO UNTIL K > COLSIZE OR EOF(1)
            INPUT #1, DUMMY
            INPUT #1, D(K)
            INPUT #1, DUMMY
            PRINT #2, D(K)
            K = K + 3
         LOOP
         K = 1
         DO UNTIL K > COLSIZE OR EOF(1)
            INPUT #1, DUMMY
            K = K + 1
         LOOP
      LOOP
      PRINT "ALL DONE ... (9*9)SAMPLED.DAT CREATED"
      GOTO 4000
      '*****************************************************************
2300  PRINT
      'SUBROUTINE 5-3 : REWRITING DATA IN PARALELL ********************
      K = 1
      DO UNTIL EOF(1)
         K = 1
         DO UNTIL K > COLSIZE OR EOF(1)
            INPUT #1, D(K)
```

```
            K = K + 1
         LOOP
         PRINT #2, USING "## "; D(1); D(2); D(3); D(4); D(5); D(6); D(7); D(8);
      LOOP
      PRINT "ALL DONE ... REARRANGED.DAT CREATED"
      GOTO 4000
      '*****************************************************************
2400  PRINT
      'SUROUTINE 5-3 : SAMPLING 1 DATA FROM (4*4) MATRIX **************
      K = 1
      DO UNTIL EOF(1)
         K = 1
         DO UNTIL K > COLSIZE
            INPUT #1, DUMMY
            K = K + 1
         LOOP
         K = 1
         DO UNTIL K > COLSIZE
            INPUT #1, D(K)
            INPUT #1, D(K + 1)
            INPUT #1, D(K + 2)
            INPUT #1, D(K + 3)
            PRINT #2, D(K + 1)
            K = K + 4
         LOOP
         K = 1
         DO UNTIL K > 2 * COLSIZE
            INPUT #1, DUMMY
            K = K + 1
         LOOP
      LOOP
      PRINT "ALL DONE ... (4*4) SAMPLED.DAT CREATED"
      GOTO 4000
      '*****************************************************************
2500  PRINT
      'SUBROUTINE 5-4 : (5*5) SAMPLING ********************************
      K = 1
      DO UNTIL EOF(1)
         K = 1
         DO UNTIL K > 2 * COLSIZE OR EOF(1)
            INPUT #1, DUMMY
            K = K + 1
         LOOP
         K = 1
         DO UNTIL K > COLSIZE OR EOF(1)
            INPUT #1, DUMMY
            INPUT #1, DUMMY
            INPUT #1, D(K + 2)
            INPUT #1, DUMMY
            INPUT #1, DUMMY
            PRINT #2, DUMMY
            K = K + 5
         LOOP
         K = 1
         DO UNTIL 2 * COLSIZE OR EOF(1)
            INPUT #1, DUMMY
            K = K + 1
         LOOP
      LOOP
      PRINT "ALL DONE ... (5*5) SAMPLED.DAT CREATED"
```

```
        GOTO 4000
        '*****************************************************************
2600    PRINT
        'SUBROUTINE 5-5 : (6*6) SAMPLING ********************************
        K = 1
        DO UNTIL EOF(1)
           K = 1
           DO UNTIL K > 2 * COLSIZE OR EOF(1)
              INPUT #1, DUMMY
              K = K + 1
           LOOP
           K = 1
           DO UNTIL K > COLSIZE OR EOF(1)
              INPUT #1, DUMMY
              INPUT #1, DUMMY
              INPUT #1, D(K + 2)
              INPUT #1, DUMMY
              INPUT #1, DUMMY
              INPUT #1, DUMMY
              PRINT #2, DUMMY
              K = K + 6
           LOOP
           K = 1
           DO UNTIL K > 3 * COLSIZE OR EOF(1)
              INPUT #1, DUMMY
              K = K + 1
           LOOP
        LOOP
        PRINT "ALL DONE ... (6*6) SAMPLED.DAT CREATED"
        GOTO 4000
        '*****************************************************************
        PRINT
        '-------------------------------------------------------------'
        '-   SUBROUTINE 7 : CONVERSION OF COORDINATES TO K-SPACE    -'
        '-------------------------------------------------------------'
2700    PRINT
        INPUT "ENTER INPUT FILE NAME 1:"; A$
        INPUT "ENTER OUTPUT FILE NAME 2:"; B$
        OPEN A$ FOR INPUT AS #1
        OPEN B$ FOR OUTPUT AS #2
        'WRITE THE TEXT TO THE OUTPUT FILE
        'DIM STRING3 AS STRING
        'STRING3 = "CONVERTED K-SPACE VALUES FROM X,Y COORDINATES"
        'PRINT #2, STRING3
        'RESERVE THE CONDITION (ENERGY,CURRENT,COVERAGE,XSIZE,YSIZE)
        'READ DUMMY SET
        FOR K = 1 TO 5
            INPUT #1, DUMMY
        NEXT K
        'CONVERT CARTESIAN COORDINATES TO K-SPACE
        CLS
        PRINT "***********************************************"
        PRINT "*                  <A>  74 eV                 *"
        PRINT "*                  <B>  76 eV                 *"
        PRINT "*                  <C>  78 eV                 *"
        PRINT "*                  <D>  80 eV                 *"
        PRINT "*                  <E>  86 eV                 *"
        PRINT "*                  <F>  90 eV                 *"
        PRINT "*                  <G>  94 eV                 *"
        PRINT "***********************************************"
```

```
        PRINT
        PRINT "SELECT ONE OPTION (USE CAPITAL LETTER) ?";
        GOSUB 2750: J = INSTR("ABCDEFG", A$): PRINT
        ON J GOTO 2800, 2850, 2900, 2950, 3000, 3050, 3100
2750    A$ = INKEY$: IF A$ = "" THEN GOTO 2750 ELSE PRINT A$; : RETURN
        '*****************************************************************
2800    'CONVERSION COEFFICIENTS AND COORDINATE VALUE FOR (0,0)POINT
        'FOR THE CLEAN TI(001)SURFACE ( 74eV )
              A = .001963
              B = .042445
              C = -.04516
              D = -.02244
              Xoo = 27.31
              Yoo = 27.24
        GOTO 3200
2850    '*****************************************************************
        'CONVERSION COEFFICIENTS AND COORDINATE VALUES FOR 76eV
              A = .0449
              B = .0216
              C = -.4424
              D = .01972
              Xoo = 27.42
              Yoo = 28.91
        GOTO 3200
        '*****************************************************************
2900    'CONVERSION COEFFICIENTS AND COORDINATE VALUES FOR 78eV
              A = -.0004502
              B = .02852
              C = -.03112
              D = -.0149
              Xoo = 41.99
              Yoo = 43.76
        GOTO 3200
        '*****************************************************************
2950    'CONVERSION COEFFICIENTS AND COORDINATE VALUES FOR 80eV
              A = .04624
              B = .02233
              C = -.0454
              D = -.020265
              Xoo = 27.49
              Yoo = 28.54
        GOTO 3200
        '*****************************************************************
3000    'CONVERSION COEFFICIENTS AND COORDINATE VALUES FOR 86eV
              A = -.0002604
              B = .02955
              C = -.03512
              D = -.01631
              Xoo = 41.81
              Yoo = 43.88
        GOTO 3200
        '*****************************************************************
3050    'CONVERSION COEFFICIENTS AND COORDINATE VALUES FOR 90eV
              A = -.001055
              B = .02991
              C = -.03083
              D = -.01733
              Xoo = 42.16
              Yoo = 44.13
        GOTO 3200
```

```
      '*****************************************************************
3100  'CONVERSION COEFFICIENTS AND COORDINATE VALUES FOR 94eV
            A = -.001332
            B = .03071
            C = -.03412
            D = -.01607
            Xoo = 39.31
            Yoo = 44.38
      '*****************************************************************
3200  'CONVERT CARTESIAN COORDINATES TO K-SPACE
      PRINT
      INPUT "WHICH PART DO YOU WANT TO SORT OUT "; Q$
      IF Q$ = "P" OR Q$ = "p" THEN GOTO 3250
      IF Q$ = "N" OR Q$ = "n" THEN GOTO 3350
3250  'POSITIVE REGION (0.1<Kx<1.0)
      K = 1
      DO UNTIL EOF(1)
         INPUT #1, X1, Y1, I1
            Xm = X1 - Xoo
            Ym = Y1 - Yoo
            Kx = A * Xm + B * Ym
            Ky = C * Xm + D * Ym
            IF Kx > 1.1 OR Kx < -.1 THEN GOTO 3300
            IF Ky > 1.1 OR Ky < -.1 THEN GOTO 3300
         PRINT #2, Kx, Ky, I1
         K = K + 1
3300  LOOP
      PRINT
      PRINT "ALL DONE ... CONVERTED K-SPACE.DAT CREATED"
      GOTO 4000
3350  'NEGATIVE REGION (-0.1<Kx<-1.0)
      K = 1
      DO UNTIL EOF(1)
         INPUT #1, X1, Y1, I1
            Xm = X1 - Xoo
            Ym = Y1 - Yoo
            Kx = A * Xm + B * Ym
            Ky = C * Xm + D * Ym
            IF Kx > -.09 OR Kx < -1! THEN GOTO 3400
            IF Ky > 1! OR Ky < .09 THEN GOTO 3400
         PRINT #2, Kx, Ky, I1
         K = K + 1
3400  LOOP
      PRINT
      PRINT "ALL-DONE ... CONVERTED K-SPACE VALUES ARE CREATED"
      GOTO 4000
      '-----------------------------------------------------------------
      '-   SUBROUTINE 8 : K-SPACE VALUE ADJUSTING FOR R-FACTOR ANALYSIS   -
      '-----------------------------------------------------------------
      'THIS SUBROUTINE IS WRITTEN FOR THE ADJUSTMENT OF EXPERIMENTAL
      'K-SPACE VALUES TO THE CORRESPONDING THEORETICAL K-SPACE VALUES
3500  PRINT
      INPUT "ENTER INPUT FILE (THEO DATA) NAME 1:"; A$
      INPUT "ENTER INPUT FILE (EXPL DATA) NAME 2:"; B$
      INPUT "ENTER OUTPUT FILE NAME 3:"; C$
      INPUT "ENTER THE Z VALUE(RADIUS FOR K-SPACE POINT)"; Z
      OPEN A$ FOR INPUT AS #1
      OPEN C$ FOR OUTPUT AS #3
      Z2 = Z ^ 2
      'WRITE THE TEXT TO THE OUTPUT FILE
```

```
        'DIM STRING4 AS STRING
        'STRING4 = "ADJUSTED EXPERIMENTAL K-SPACE VALUES FOR *****YK.DAT FILE"
        'PRINT #3, STRING4
        'IGNORE THE CONDITION
        'INPUT #1, DUMMY
        'READ IN THE THEORETICAL DATA SET (Kx, Ky, Y-FUNCTION)
        K = 1
        DO UNTIL EOF(1)
           INPUT #1, X1, Y1, I1
           'PRINT #3, X1, Y1, I1 (FOR CHECKING THEORETICAL DATA)
           OPEN B$ FOR INPUT AS #2
           'SET THE INITIAL VALUE
           SUM = 0
           COUNT = 0
           'FIND OUT THE GROUP OF EXPERIMENTAL DATA SET CLOSE
                 'TO THE THEORETICAL DATA
           'SUM THE EXPERIMANTAL DATA IN A CIRCLE WITH RADIUS Z
           'COMPUTE THE AVERAGE VALUE OF Y-FUNCTION AND KEEP IT
           DO UNTIL EOF(2)
              INPUT #2, X2, Y2, I2
              A = (X1 - X2) ^ 2 + (Y1 - Y2) ^ 2
              IF A < Z2 THEN SUM = SUM + I2
              IF A < Z2 THEN COUNT = COUNT + 1
              IF A > Z2 THEN GOTO 3700
              'PRINT #3, COUNT, X2, Y2, SUM (FOR CHEKING SUMMING PROCESS)
3700       LOOP
           AVE = 0
           IF COUNT > 0 THEN AVE = SUM / COUNT
           PRINT #3, X1, Y1, AVE
           CLOSE #2
           K = K + 1
        LOOP
        PRINT
        PRINT "ALL DONE ... ADJUSTED K-SPACE DATA CREATED"
        GOTO 4000
        '------------------------------------------------------------
        '-   SUBROUTINE 9 : DATA ADDITION FOLLOWED BY AVERAGING    -
        '------------------------------------------------------------
3800    PRINT
        'THIS SUBROUTINE ADDS CALCULATED DLEED INTENSITIES FOR 2 DIFFERENT
        'STACKINGS (A & B) AND TAKE THE AVERAGED VALUE
        INPUT "ENTER INPUT FILE NAME 1:"; A$
        INPUT "ENTER INPUT FILE NAME 2:"; B$
        INPUT "ENTER OUTPUT FILE NAME 3:"; C$
        INPUT "ENTER THE RATIO OF INTENSITY 1 (I1)"; A
        INPUT "ENTER THE RATIO OF INTENSITY 2 (I2)"; B
        OPEN A$ FOR INPUT AS #1
        OPEN B$ FOR INPUT AS #2
        OPEN C$ FOR OUTPUT AS #3
        'RESERVE THE CONDITION FOR DATA
        INPUT #1, I1
        INPUT #2, I2
        PRINT #3, I1
        'READ IN DATA SET FROM 2 INPUT FILES AND AVERAGE
        K = 1
        DO UNTIL EOF(1) OR EOF(2)
             INPUT #1, X1, Y1, I1
             INPUT #2, X2, Y2, I2
             I1 = A * I1
             I2 = B * I2
```

```
            AVE = I1 + I2
            'AVE = (I1 + I2) / 2
            PRINT #3, X2, Y2, AVE
            K = K + 1
        LOOP
        PRINT
        PRINT "ALL DONE ... AVERAGED DATA CREATED"
        GOTO 4000
        '-------------------------------------------------
        '-   SUBROUTINE 10 : PENDRY R-FACTOR CALCULATION   -
        '-------------------------------------------------
        'FUNCTION : CALCULATES PENDRY R-FACTOR
3900    PRINT
        INPUT "ENTER INPUT FILE (EXPL Y-FN) NAME 2:"; A$
        INPUT "ENTER INPUT FILE (THEO Y-FN) NAME 2:"; B$
        'INPUT "ENTER OUTPUT FILE NAME 3:"; C$
        PRINT
        OPEN A$ FOR INPUT AS #1
        OPEN B$ FOR INPUT AS #2
        'OPEN C$ FOR OUTPUT AS #3
        'SET THE INITIAL VALUE
            D = 0!
            U = 0!
        'READ IN EXPERIMENTAL AND THEORETICAL Y-FUNCTION DATA
        K = 1
        DO UNTIL EOF(1) OR EOF(2)
            INPUT #1, X1, Y1, EY1
            INPUT #2, X2, Y2, TY2
            U = U + (TY2 - EY1) * (TY2 - EY1)
            D = D + (EY1 * EY1) + (TY2 * TY2)
            K = K + 1
        LOOP
        'CALCULATE R-FACTOR
        RF = U / D
        'PRINT #3, USING "#.#####"; RF
        PRINT "R-FACTOR ="; RF
4000    CLOSE #1, #2, #3, #4
4100    PRINT
        PRINT "END"
        END
```

APPENDIX 3. Chlorine phase shifts

E(H)	d0	d1	d2	d3	d4	d5	d6
0.2	8.205515	4.057908	0.018549	0.000261	0	0	0
0.4	7.821054	4.546708	0.104015	0.003088	0.000011	0	0
0.6	7.577601	4.636401	0.278235	0.012339	0.000264	0	0
0.8	7.398892	4.617791	0.524498	0.031488	0.00134	0	0
1	7.25904	4.571559	0.78196	0.062384	0.004114	0	0
1.2	7.145089	4.5206	0.995732	0.104819	0.009467	0	0
1.4	7.049255	4.471969	1.15414	0.156581	0.018196	0.000527	0
1.6	6.96636	4.427529	1.269876	0.214102	0.030724	0.001821	0
1.8	6.892859	4.38715	1.357637	0.27346	0.047094	0.004184	0
2	6.826357	4.350131	1.427525	0.331319	0.066947	0.007906	0
2.2	6.765231	4.315668	1.485415	0.385534	0.089604	0.013191	0
2.4	6.708421	4.283097	1.534464	0.435148	0.114192	0.020175	0.000762
2.6	6.655225	4.252	1.576424	0.480111	0.139807	0.028823	0.002178
2.8	6.605215	4.222119	1.612419	0.520916	0.165581	0.039032	0.004286
3	6.558075	4.193331	1.64331	0.558222	0.190855	0.050569	0.007206
3.2	6.513581	4.165635	1.669917	0.592679	0.215197	0.063155	0.010977
3.4	6.471568	4.13907	1.692986	0.624804	0.238365	0.076459	0.015616
3.6	6.431838	4.113653	1.713197	0.654946	0.260278	0.090185	0.021093
3.8	6.394232	4.0894	1.731156	0.683275	0.281018	0.104031	0.027354
4	6.358576	4.0663	1.747345	0.70993	0.300714	0.117777	0.034276
4.2	6.324689	4.044313	1.76214	0.734932	0.319507	0.131223	0.041734
4.4	6.29241	4.02336	1.775805	0.75833	0.337543	0.144296	0.049614
4.6	6.261548	4.003365	1.788503	0.780171	0.354943	0.15691	0.057765
4.8	6.231982	3.984236	1.800345	0.800504	0.371783	0.169073	0.066049
5	6.203566	3.96588	1.811392	0.819449	0.38813	0.180805	0.074372
5.5	6.136829	3.922797	1.835773	0.861514	0.426795	0.208614	0.094799
6	6.07529	3.882946	1.855916	0.897644	0.462117	0.234854	0.114127
6.5	6.018205	3.845791	1.872514	0.92953	0.493914	0.259966	0.132296
7	5.965127	3.811113	1.886459	0.958182	0.522411	0.284014	0.149644
7.5	5.915738	3.778824	1.898518	0.984034	0.548102	0.306716	0.166475
8	5.869629	3.748769	1.909159	1.007307	0.571601	0.327907	0.182947
8.5	5.826399	3.720695	1.918568	1.028208	0.593395	0.347532	0.198991